ABSTRACT

BUSCHE, BRADLEY JAMES. Compatibilization of Polystyrene/Poly(dimethylsiloxane) using Star Polymers Containing a γ-Cyclodextrin Core and Polystyrene Arms. (Under the direction of C. Maurice Balik and Alan E. Tonelli.)

Star polymers containing a γ-cyclodextrin (CD) core and polystyrene (PS) arms (CD-star) were successfully synthesized by atom transfer radical polymerization. These stars are the first of their kind containing a γ-CD core. CD-stars made with twelve PS arms proved to be soluble in typical PS solvents. Control over CD-star arm length was achieved, as shown by nuclear magnetic resonance (NMR) and gel permeation chromatography (GPC) analysis.

Rapidly stirred blends of polydimethylsiloxane (PDMS) and PS prepared in chloroform with and without CD-star formed an emulsion. Adding CD-star to these turbid solutions resulted in clearing, whereas control solutions *without* CD-star remained turbid. Post-stirring, these clear solutions demonstrated excellent temporal stability illustrating their successful compatibilization. Characterization of these clear solutions by 2D-NMR revealed that CD-stars were threaded onto PDMS. This complexation formed a hybrid slip-ring copolymer with PDMS as the backbone and CD-star PS arms effectively acting as the grafts. Solution characterization *via* capillary viscometery, dynamic light scattering, and GPC showed traits similar to traditional graft copolymers.

Films were made from the blended solutions by spin or solution casting. Spun-cast films prepared from compatibilized solutions exhibited homogeneous nanophase morphology, whereas non-compatibilized solutions displayed heterogeneous microphase morphology. Atomic force microscopy and scanning electron microscopy analyses of these films revealed PDMS phase domains measuring 50nm or less. However, solution cast films with subsequent compression molding showed macroscopic phase segregation for samples *with or without* CD-star. Significant loss of PDMS was observed during processing. Compositional analysis conducted by ^{1}H-NMR revealed ~80% PDMS retention for films with CD-star, whereas only ~20% retention was observed for films without CD-star. This larger PDMS retention for samples with CD-star results from the anchoring of PDMS chains which

threaded through CD-stars. Differential scanning calorimetry and dynamic mechanical analysis characterization point to partial compatibilization, as determined from the glass-transition temperatures of the homopolymers shifting toward each other. Solution-cast film characterization by thermal gravimetric analysis confirmed the PDMS thermal degradation decreased with increased CD-star complexation.

Compatibilization of Polystyrene/Poly(dimethylsiloxane) Blends Using Star Polymers Containing a γ-Cyclodextrin Core and Polystyrene Arms

by
Bradley James Busche

A dissertation submitted to the Graduate Faculty of
North Carolina State University
in partial fulfillment of the
requirements for the Degree of
Doctor of Philosophy

Materials Science and Engineering

Raleigh, North Carolina

2009

APPROVED BY:

_____	_____
Keith Dawes	Richard J. Spontak
_____	_____
C. Maurice Balik, Co-chair	Alan E. Tonelli, Co-Chair

DEDICATION

This work is dedicated to God, my extremely supportive and patient wife, my always encouraging parents, my inspirational brother, as well as all my family and friends. Thank you!

BIOGRAPHY

Brad was born and raised in Olympia, Washington. He attended the University of Washington in Seattle earning a Bachelor of Science in Ceramic Engineering. During his undergraduate career he was exposed to the "Nylon rope-trick" which presented a world of polymer curiosities, which consequently, influenced his future studies in polymers. As an undergraduate student, he was awarded summer research Fellowships at Pacific Northwest National Laboratories (PNNL) in Richland, Washington. His knowledge in organic synthesis and interfacial interactions was seeded under the mentorship of Dr. Glen E. Fryxell at PNNL. Brad's involvement in interfacial and materials chemistry during his time at PNNL fueled his yearning to further understand material properties.

Due to these influential research experiences, he applied to graduate school to pursue a Doctorate degree. In the Fall of 2003 he accepted an opportunity to study polymers in the Department of Materials Science and Engineering at North Carolina State University (NCSU), Raleigh, under the direction of Dr. C. Maurice Balik and Dr. Alan E. Tonelli. While at NCSU, he performed research related to improving polymer properties with cyclodextrins and, as a result, became the relative topic of his dissertation.

ACKNOWEDGMENTS

I sincerely thank Professors C. Maurice Balik and Alan E. Tonelli for their excellent mentorship and guidance during my time in graduate school. It was due to their curiosity and passion for polymers that resulted in me fully enjoying my time under their direction. I truly appreciate all they have done for me. I would also like to thank Dr. Keith Dawes for his organic synthesis/polymerization mentorship and for his willingness to be on my committee. I also thank Dr. Richard Spontak for his instruction in polymer blends and for agreeing to be on my committee.

Furthermore I would like to thank my past group members Dr. Marcus Hunt, Dr. Tamer Uyar, Drs. Cristian and Mariana Rusa, Dr. Jennifer Ayres, John Osborne, and Jacob Majikes for their help and insightful conversations, not to mention laughs. Also I wish to thank my current group members Jaewook Seok, Brandon Williamson, Anushree Mohan, Gerry Antony, and Marc Moore for their help and valuable conversations. I extend my appreciation to Andy Newell for his help in SEM imaging, and Ka “Wingo” Wong for his help in conducting EDX. I thank Evren Ozcam for his time in conducting nanoindentation. I especially thank Dr. Hanna Gracz for her invaluable help in performing ROESY NMR. Finally I would like to thank Ms. Birgit Andersen for her characterization help spanning my time at NCSU as well as Dr. Keith Beck for his help in performing GPC measurements.

For my final acknowledgements, I wish to recognize my past mentors. First I would like to thank Dr. Miqin Zhang at The University of Washington who gave me my first research opportunity and position in her biomaterials laboratory. I especially would like to thank “the one who dances with molecules” Dr. Glen E. Fryxell of Pacific Northwest National Laboratories (PNNL) for his excellent mentorship and for transferring some of his organic synthesis knowledge to me. Additionally I wish to thank Dr. R. Shane Addleman, also of PNNL, who has shared many words of wisdom and insightful knowledge with me over the past years.

TABLE OF CONTENTS

LIST OF TABLES

LIST OF FIGURES

COMPATIBILIZATION OF POLYSTYRENE/POLY(DIMETHYLSILOXANE) BLENDS USING STAR POLYMERS CONTAINING A γ-CYCLODEXTRIN CORE AND POLYSTYRENE ARMS

1. INTRODUCTION

1.1. Properties of Cyclodextrins

Cyclodextrins are natural cyclic oligosaccharides first discovered and purified in 1891.[1] Three types of cyclodextrins (CDs) exist in nature and only differ by the number of glucopyranose units found within the cyclodextrin ring. These three are referred to as α-cyclodextrin, β-cyclodextrin, and γ-cyclodextrin, which have 6, 7, and 8 glucopyranose units in their ring, respectively. The physical structure of cyclodextrin is a torus shaped molecule that has a hydrophilic exterior with a relative hydrophobic core as illustrated in Figure 1.1. It is the cyclodextrin core that gives these molecules their interesting properties.

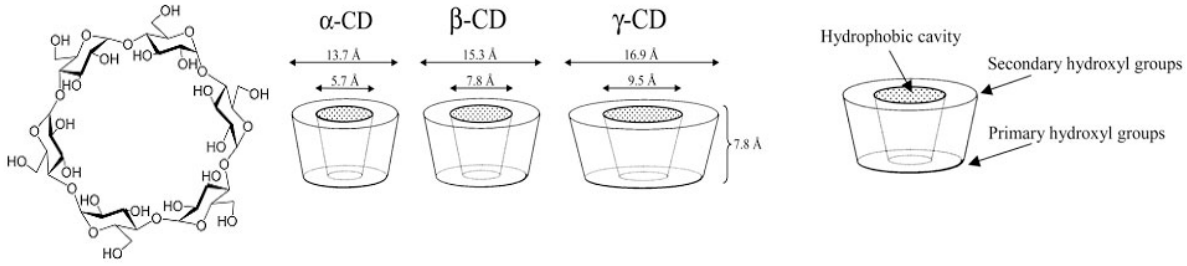

FIGURE 1.1. Dimensions and physical properties of cyclodextrins. After reference [2].

Due to the many hydroxyls on CDs, their solubility in water is generally very high. Table 1.1 shows the properties of CDs and their solubilities in water. It is noticed that α-CD and γ-CD have excellent solubilities in water, but β-CD is found to have a much lower solubility. Tchoreloff *et al.* report that low solubility for β-CD is a consequence of the odd symmetry of the molecule.[3] It is known that all three CDs exist in solution in the form of large aggregates through strong hydrogen bonds.[3, 4] Therefore, favorable hydrogen bonding between the

structure of water and α-CD or γ-CD is found and of which both have been shown to contain even-symmetry. However, since β-CD has odd-symmetry, then no such favorable overlap with the structure of water exists resulting in a lower solubility in water.[3]

TABLE 1.1. Properties of cyclodextrins.

Property	α-CD	β-CD	γ-CD
glucopyranose units†	6	7	8
molecular weight (g/mol)†	972	1135	1297
solubility in water (g/L)‡	145	20	220
outer diameter (Å)§	13.7	15.3	16.9
inner diameter (Å)§	5.7	7.8	9.5
height of torus (Å)§	7.8	7.8	7.8

† After reference [5]. ‡ After reference [3]. § After reference [2].

Cyclodexrins in the solid state can take the form of different crystal structures as seen in Figure 1.2. Both α-CD and β-CD are observed to form all three crystal structures, whereas γ-CD has been observed to develop into only the cage and channel type structures.[6] Water is known to play an important role in the stability of these structures. In the cage structure the numbers of water molecules complexed to each CD for α-CD, β-CD, and γ-CD are 6, 8, and 14, respectively.[6] These water molecules are found inside *and* outside the CD cavity. Hunt *et al.* studied the water adsorption for both α-CD and γ-CD, and their role in crystal structure transformation.[7, 8] They report that the CD channel structure becomes unstable and transforms to the cage structure when exposed to increasing amounts of humidity. Therefore this points to specific CD crystal structures being dependent on the number of stabilizing hydrate interactions produced.

FIGURE 1.2. Common crystal structures of cyclodextrins. After reference [9].

1.2. Cyclodextrin Inclusion Complexes

1.2.1. Small Molecule/Cyclodextrin Inclusion Complexes

The hydrophobic cavity of CDs enables these molecules to play host to various molecular guests. This interaction can result in increased aqueous solubility for guest molecules that commonly only experience low solubility. This apparent increase in solubility for the guest is a consequence of the CD hydroxyl groups, which promote excellent solubilization in aqueous environments. For example, this interaction can be seen in Figure 1.3 between CD and toluene in water. This figure illustrates how the toluene guest resides in the CD host. Establishment of an equilibrium that favors inclusion of a guest is created if a lower energy state is experienced by toluene within the CD cavity, rather than in the aqueous environment.

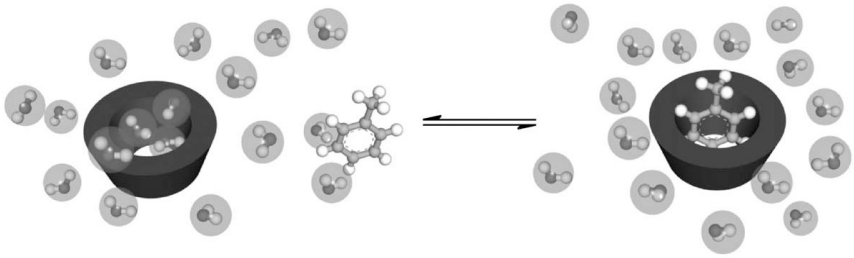

FIGURE 1.3. Host-guest complexation of cyclodextrin and toluene in an aqueous environment. After reference [10].

Many guest molecules have been discovered to include into CD, leading to many applications being proposed to take advantage of this interaction.[11] It is well documented that CDs have very low toxicity and are thus well-suited as food flavor stabilizers or delivery vehicles.[12] One anticipated application is within the area of pharmaceuticals.[1, 13-15] Since the human body is an aqueous-based environment, beneficial drugs that have low solubility in water can be administered at higher doses due to the increased solubility *via* the CD cavity. However, it should be noted that drug guests need to be of a size and shape complementary to the CD cavity for full or partial inclusion to occur.[16]

Besides pharmaceuticals, textile applications are seen as a promising application for CDs and are predicted to be involved in a lucrative revolution for this industry.[1] For instance, when CDs were used in textiles for dyeing, Savarino and coworkers saw a four to ten fold improvement in the color uniformity for Nylon 66 and Nylon 6 when CD was used as the dye delivery vehicle.[17-19] Commonly, inclusion of dyes into CD results in increased stability and fluorescence of the dyes.[20, 21] After laundering in the presence of CDs, the surfactant remaining on the fiber is largely reduced, which can benefit the final dyeing and finishing processes in the textile industry.[22] Furthermore, CDs can act as scent delivery vehicles to either introduce and retain perfumes in garments, or as time-release agents.[23] On the other hand, instead of perfumes, if small molecules designed for insect repellants, antistatic, antistain, antibiotics,[24, 25] or flame retardents[26] were used, then the functionality of the garment is increased further.[23]

CDs have also been suggested for use in environmental protection and remediation.[1] It has been shown that CDs are effective in tertiary oil recovery operations, which they remove oil left within the soil and rocks after an oil well has been initially pumped.[27] Water purification and soil remediation of toxins,[28-30] pesticides,[30-33] or herbicides is another environmentally promising use of CDs. Again this is a consequence of their high solubility in water and

ability to trap apolar guests. These applications are just a few of the practical ideas for which CDs can be successfully used.

1.2.2. Polymer/Cyclodextrin Inclusion Complexes

Cyclodextrins not only form inclusion complexes with small molecules but also complex with macomolecules as well. Polymer/cyclodextrin inclusion-compounds (CD-ICs) are very interesting due to the induced confinement of the polymer chain while threaded into the CD-core. A typical procedure for making CD-ICs is shown in Figure 1.4. This illustration displays the characteristic channel structure that CD-ICs adopt. Confinement of the polymer chains in the CD channel serves to order them in the direction of the tube axis. This threaded complex is generally referred to as a polyrotaxane and has been found to occur with several polymers.[34, 35] After CD-ICs are formed, CD can be washed away or enzymatically degraded to yield a coalesced polymer structure that possesses a higher degree of ordering than initially seen for the homopolymer itself.[36]

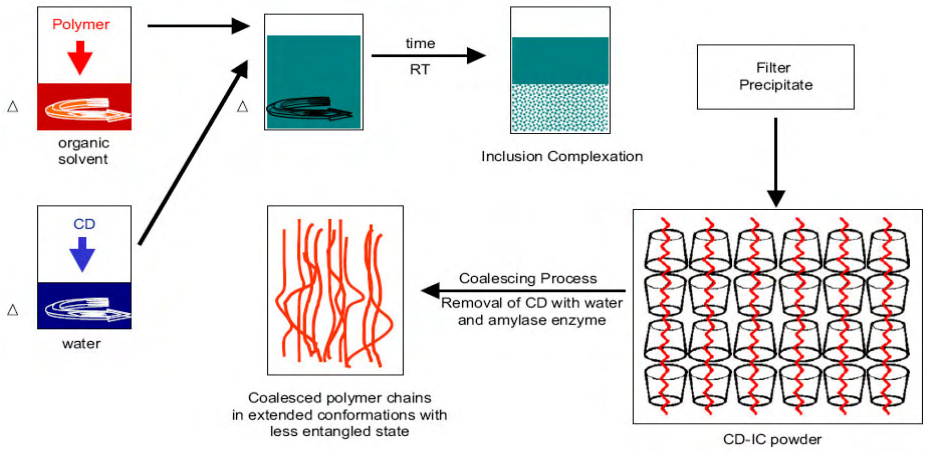

FIGURE 1.4. Procedure for making CD-ICs and the resultant extended polymer structure after coalescence. After reference [37].

Table 1.2 lists many of the polymer/CD-ICs that are known to form and their respective CD host. Polymer abbreviations used throughout this chapter are listed in Table 1.3. As can be

seen, many polymers have been found to thread into γ-CD, while α-CD and β-CD show fewer polymer species threaded. Characterization of the CD-ICs typically involves x-ray diffraction, which identifies the transformation of the CD crystal from the cage to columnar structure.[38-41] Other characterization techniques such as NMR,[42-44] FTIR,[38, 45] DSC,[38, 46] and TGA[38, 45] have all been employed to confirm successful CD-IC complexation. Commonly, if a semicrystalline polymer is used to form a CD-ICs (or coalesced from CD-ICs), the precipitated product can exhibit higher degradation temperatures, increased levels of crystallinity, unusual polymorphs, and higher melting.[37] For amorphous polymers, an increase in the glass transition temperature is characteristically observed.[37]

TABLE 1.2. Polymers that have been found to form CD-ICs.

α-CD (d_{core}=5.7Å)*		β-CD (d_{core}=7.8Å)*		γ-CD (d_{core}=9.5Å)*	
Polymer§	Ref.	Polymer§	Ref.	Polymer§	Ref.
PEO	[43, 47-49]	PPG	[43, 50]	PDMS	[41, 51, 52]
PEO-b-PTHF-b-PEO	[53]	PAni	[54]	PHB	[55]
PCL	[48, 56]	PPy	[57]	i-PP	[58]
Nylon-6	[59]	PT	[60, 61]	PC	[38, 62, 63]
PCL-b-PLLA	[64]	PEO	[65]	PI	[40]
PCL-b-PEO-b-PCL	[66]	PDMS	[51, 52]	PB	[39]
PPO-b-PEO-b-PPO	[46]			PVA	[67]
PCL-b-PPG-b-PCL	[45]			PMMA	[38, 62, 63]
				PET	[68]
				PVC	[69]
				i-PBu	[36]
				PAN	[41]
				PMVE	[43]
				PCL	[55]
				PEN	[68]
				PPG	[43]
				PVAc	[38, 62]
				PCL-b-PPG-b-PCL	[45]
				PCL-b-PEO-b-PCL	[66]
				Silk protein	[70]

* d_{core} = CD-core diameter

§ See Table 1.3 for polymer abbreviation definitions.

TABLE 1.3. Abbreviations and definitions of select polymers.

i-PBu	poly-1-butene	PLLA	poly(L-lactide)
PAN	polyacrylonitrile	PLU	pluronic 105
PAni	polyaniline	PMeDMA	poly(2-(dimethylamino) ethyl methacrylate
PB	polybutadiene		
PBH	poly(R,S-3-hydroxybutyrate)	PMMA	poly(methyl methacrylate)
PBS	poly(butylene succinate)	PMVE	poly(methyl vinyl ether)
PC	polycarbonate	PPG/PPO	poly(propylene glycol)
PCL	poly(ε-caprolactone)	PPy	polypyrrole
PDMS	poly(dimethylsiloxane)	PS	polystyrene
PEG/PEO	poly(ethylene glycol)	PT	polythiophene
PEI	polyethylenimine	PtBA	poly(t-butyl acrylate)
PEN	poly(ethylene 2,6-naphthalate)	PTHF	poly(tetrahydrofuran)
PET	poly(ethylene terephthalate)	PVAc	poly(vinyl acetate)
PI	polyisoprene	PVC	poly(vinyl chloride)
PLA	polylactide		

Proposed applications of CD-ICs span many areas. First, since the dimension of the CD cavity is fixed, then polymers possessing larger cross-sections will not be able to thread into CD. Hunt and coworkers performed conformational modeling to demonstrate that only isotactic PS would thread into γ-CD, excluding syndiotactic PS which has a larger cross-section. This illustrates that CD-ICs may be used to separate polymer chains by their tacticity.[71] Furthermore, polymer molecular weight separations were examined by Rusa and coworkers.[49, 56] They found that higher molecular weight polymers were preferentially formed with CDs. A variation of this effect was also noted by Nepogodiev and Stoddart, who report that as the degree of polymerization for PEG increased, so does the yield of CD-IC, suggesting an increase in CD-IC stability when made with higher molecular weights.[35] Polydispersities of commercial polymers are typically large and could be narrowed by this technique in order to separate lower from higher molecular weight chains.

In addition, polymerizing monomers with CDs in an aqueous environment has been shown to be a viable and environmentally friendly method for making polymers.[10, 60, 61, 72, 73] This is made possible by the monomer being included in the cavity, thereby solublizing it in water. Nanowires have also been shown to be made when a monomer is used in polymerizing a conductive polymer to form the CD-IC, in which the CD acts as an insulator.[54, 60] Therefore if an organic solvent is used for a given common polymerization, this technique may reduce the environmental impact by replacing the solvent with water in making the polymer.

Possibly the most promising application is the use of CD-ICs as nucleation agents in bulk polymers. Since the formed CD-IC aligns the polymer chains, then the aligned chains protruding from the CD complex can aid in nucleation of bulk polymer chains. Dong *et al.* found that by adding 2 wt% CD-IC made with semicrystalline polymers (PCL, PEG, or PBS), of nucleation is enhanced in the crystalline regions of the respective bulk polymers.[74, 75] It was shown by Zhang *et al*. that the storage modulus of PEG films nucleated with PEG-CD-IC increased with increased amounts of CD coverage.[76] In addition they illustrated that films nucleated with PEG-CD-IC could be used as shape memory materials, using the CD-IC as a fixing phase, and achieving a recovery ratio of 97%. Furthermore, Vogel and coworkers successfully demonstrated that PHB melt-spun fibers nucleated by PHB-CD-ICs possessed a higher tensile strength than fibers without PHB-CD-IC.[77] These examples illustrate the effectiveness of using CD-IC to enhance nucleation in bulk polymers.

1.3. Factors Affecting Formation of Cyclodextrin Inclusion Complexes

In forming complexes between guests and CD, a driving force must be present for a guest to be included into a CD host. Several researchers have made calorimetry measurements to find the change in the Gibbs free energy (ΔG), which can be used to quantify the CD interaction with the molecular guest.[11] Contributions that affect ΔG, under isothermal conditions, include variations in enthalpy (ΔH) and entropy (ΔS), as shown in equation 1.1, where *T* describes the absolute temperature. An entropy decrease occurs due to the ordering of the

guest in the CD cavity, therefore making this action unfavorable for complex formation.[43] However, when a guest is included into the CD cavity, the overall ΔS value is slightly positive which stems from the release of a large number of solvent molecules from the CD core.[47] With that said, the dominating interaction is enthalpic for nearly all CD/guest systems polymeric or otherwise.[11, 53, 78] It has also been noted that if the guest is capable of hydrogen bonding, then interactions between the guest and CD hydroxyls may aid to further stabilize it.[11, 79] In general, Lo Nostro and coworkers conclude that the driving force for guest/host complexation lies within the hydrophilic solvent pushing the hydrophobic polymer chain into the hydrophobic CD-core, thereby resulting in stabilization of the entire system.[50]

$$\Delta G = \Delta H - T\Delta S \quad \text{---------- (1.1)}$$

1.3.1. Solvent Effects

The inclusion environment that a guest senses greatly depends on the comparative hydrophobicity of the CD-core to the solvent. Okumura *et al.* report that, in a set of polymers varying from hydrophilic to hydrophobic, CD-IC formation increases with increasing guest hydrophobicity.[43, 52] Solvents that ranged in hydrogen bonding strength were studied by Ceccato et al., who found that the amount of time to thread (t_{th}) PEG slightly increased with decreasing hydrogen bonding strength ($D_2O > H_2O >$ urea).[47] This conclusion was confirmed using the identical solvents with PPG and PLU.[80]

Lo Nostro and coworkers also studied the formation of amine-terminated PPG CD-IC with various salts.[50] They found that anions affect the kinetics of CD-IC formation more than cations, giving larger fluctuations in threading times. The threading times for these environments decreased in the order of $F^- > OH^- > Cl^- > Br^- > I^-$ for anions, whereas for cations $K^+ > NH_4^+ > Na^+ > Ca^{2+} > Li^+$. They conclude that hydrophobic forces in the solution clearly play the dominant role for driving complexation of CD-ICs.

1.3.2. Guest Molecule Size Effects

There are two chain dimensions that have been found to affect the threading of the guest in the CD host: (1) the cross sectional dimension of the chain, and (2) the length (or molecular weight) of the chain. This second type was discussed previously in section 1.2.2, establishing that an increase in chain length promoted improved stability of the CD-IC. With regard to the first dimension, cross-sectional size exclusions can be manipulated by either using a polymer with bulky pendant groups, or in some cases, by changing the polymer tacticity. As stated earlier, molecular modeling has shown that isotactic PS can thread into γ-CD, however syndiotactic PS is found to be too large and is excluded.[71] If a triblock copolymer, such as for α-CD and PCL-b-PPG-b-PCL, is used for CD-IC formation the end blocks of PCL are favored for IC formation, while the midblock of PPG is not, in which case CD-ICs will preferentially form on the end blocks.[45] Likewise if the midblock of a triblock copolymer is preferred to form CD-ICs, such as for α-CD and PPO-b-PEO-b-PPO, then CDs will develop primarily on the PEO.[46] Therefore placement of the CDs can be controlled by the manipulation of the polymer chemical structure. Many researchers have shown that if a polymer which typically forms CD-ICs (eg. PEO) is capped with large bulky groups on the chain end, these endgroups can either prevent CDs from including or trap CDs on the chain.[43]

1.3.3. Temperature Effects

In all solvent cases (D_2O, H_2O, urea), Lo Nostro *et al.* found that both ΔH and ΔS of the complex decrease with increasing temperature.[80] However they note that the enthalpic and enthropic contributions balance resulting in little change in ΔG with temperature.[80] Ikeda and coworkers essentially observed this as well, and found that ΔG decreased slightly with increasing temperature after forming a rotaxane with PEO-b-PTHF-b-PEO.[53]

1.4. Polymers Chemically Modified with Cyclodextrin

Exploitation of CD guest/host interactions for applications that contain polymers is best done by chemically attaching CD to the polymer. Methods for selective chemical attachment of

the CD within polymer backbones and to polymers have been derived.[81] Possible structures that can be obtained from CD attachment are shown in Figure 1.5, and will be individually discussed in the following sections. If the CD is not chemically bonded to the polymer, then leaching of the CD could be a concern when in an aqueous environment.[12]

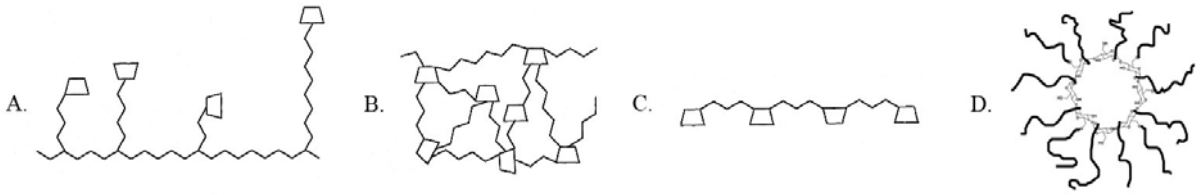

FIGURE 1.5. Possible structures obtained by attaching CD to polymer by (A) grafting, (B) networking, (C) linearly polymerizing, and (D) star formation. Images A-C from reference [79].

1.4.1. Linear Cyclodextrin Polymers

Linear polymers with CD within the backbone chain have been prepared.[79] However these polymers require rigorous synthesis techniques and separation. This is a result of CDs containing 18 to 24 hydroxyl groups which are used for chemical attachment in a linear fashion. Therefore selectively modifying only two hydroxyls on a CD is very challenging. Tian *et al.* linearly synthesized CD to form a macromonomer, however, separation of the linear components was conducted via HPLC in order to ensure its linearity.[82] Cheng *et al.* synthesized a linear β-CD-PEG polymer by selectively functionalizing two primary hydroxyls on the CD with iodine atoms that were positioned across from one another, and they claim ~80% yield for all of the polymers made.[83] They found that this recovered polymer was water soluble and good for use as a drug-delivery vehicle to combat tumor cells. These examples illustrate that CDs can be linearly placed into a polymer chain, but extensive and sophisticated synthetic methods must be employed to do so.

1.4.2. Grafted Cyclodextrin Polymers

Grafting CDs onto polymers presents similar challenges in that there are many reactive hydroxyl groups, thus making crosslinking highly probable. However there are typically two methods which are used: (1) to chemically attach the CD directly onto the surface of a preformed substrate, or (2) to chemically attach CD as a pendant group onto the polymer chain. Lee *et al.* employed method (1) to graft β-CD onto cotton fibers after which it was complexed with an antibacterial guest and observed to give a drastic increase in the antibacterial properties of the material even after ten laundering cycles.[84] Others have done the same with Nylon-6, and again with cotton.[85, 86] In order to accomplish method (2), one pathway to attach CD grafts is to prepare an alternating or random copolymer which contains one monomer that can react with CD while the other will not. This method was used by Renard *et al.* to successfully graft CDs on the copolymer backbone of poly(methyl vinyl ether)-alt-(maleic anhydride) by an esterification reaction.[87] The product was found to be water soluble, which suggests no networking. As for linear CD polymers, grafted CD polymers are possible. However, due to the many hydroxyls on the CD this method becomes challenging to perform.

1.4.3. Networked Cyclodextrin Polymers

Networking can be accomplished either by (1) crosslinking the chains together, or (2) introducing complementary components that can react to make a network. Networks made by method (1) are typically examined as gels. Several researchers have studied the rheological behavior of this type of gel network formed from incorporating CDs.[88, 89] Typically step growth polymerization is employed in networked materials formed by (2). These materials yield insoluble beads that are highly networked.[90-92] A network containing Nylon 610 with methylated-β-CD was synthesized upon which dyeing studies were conducted with a blue dye.[93] This study found that with only 5 mol% CD incorporation a 100% increase in dye uptake was observed. Ogoshi and Chujo used method (2) to build a silica network around an organic polymer having side groups that were included within CD,

thereby forming an inorganic/organic composite.[94] Insoluble networked CD-polymer particulates could be blended with homopolymer to form films or fibers, but uniform distribution of CDs cannot be accomplished to any great degree.

1.4.4. Cyclodextrin Star Polymers

Since this dissertation is primarily concerned with CD-star polymers, an exhaustive literature search reveals that only stars containing cores of α-CD and β-CD were found and have been thus far investigated. Table 1.4 shows the results of this search.

TABLE 1.4. Summary of CD-stars found in literature.

CD core	polymer[§] arm species	# of arms	polymerization method	M_n,star[‡]	PDI[‡]	Ref.
α-CD	PtBA	18	ATRP	not given	not given	[95]
	PEI	6	Step-growth	1,490 (NMR)	not given	[96]
	PEI	5	Step-growth	4,200 (NMR)	not given	[96]
β-CD	PLA	14	ring-opening	12,500 (NMR)	1.7 (DLS)	[97]
	PMeDMA	21	ATRP	669,000	1.49	[98]
	PMeDMA	21	ATRP	26,400	1.15	[98]
	PMMA	21	ATRP	61,200	1.89	[99]
	PMMA	21	ATRP	33,000	1.06	[100]
	PMMA	21	ATRP	162,000	1.13	[100]
	PS	21	ATRP	11,500	1.5	[99]
	PS	7	TEMPO	45,200	1.05	[101]
	PS	21	ATRP	14,200	1.12	[100]
	PS	21	ATRP	53,700	1.41	[100]
	PS	1	NMP	10,860	1.17	[102]
	PS	7	RAFT	21,000	1.75	[103]
	PS	7	RAFT	56,000	1.65	[103]
	PtBA	21	ATRP	18,000	1.1	[95]
	PtBA	21	ATRP	80,000	1.05	[95]
	PtBA	21	ATRP	98,000	1.13	[104]
	PtBA	21	ATRP	147,000	1.12	[104]

§ See Table 1.3 for polymer abbreviation definitions.

‡ Number average molecular weight (M_n) and polydispersity index (PDI) found by GPC using PS standards unless otherwise stated. Other methods are defined as nuclear magnetic resonance (NMR) and dynamic light scattering (DLS).

The synthesis methods used for making the CD-stars involved mostly living polymerizations. In this table, the polymerization routes used to make CD-stars included reverse addition-fragmentation chain transfer (RAFT) polymerization, 2,2,6,6-tetramethylpiperidine-1-oxyl (TEMPO) initiation, nitroxide mediated polymerization (NMP), and atom transfer radical polymerization (ATRP). Use of living polymerization is beneficial due to the fact that termination by coupling is virtually nonexistent, thereby preventing a networked structure from forming. Essentially these CD-stars are observed to be monodisperse having polydispersity indices between 1 and 2, while the number of arms varied from 1 to 21. The advantage of CD-star polymers is in the control of the number and length of star-arms, which results in well-defined structures.

1.5. Compatibilization of Blended Homopolymers

Compatibilization lowers the interfacial energies between blend phases and stabilizes the dispersed phase. This often results in a reduction of the blend domain size in a solid-state film. More often than not, benefits of compatibilization are often seen as an improvment in the resultant mechanical properties of a film. Essentially there are two types of compatibilization: (1) reactive compatibilization and (2) compatibilization by addition of a third component that promotes blending.[105] These two methods will be discussed further in the following sections.

1.5.1. Compatibilization by Reactive Blending

Reactive compatibilization involves *in situ* macromolecular reactions to aid in the stabilization of the dispersive phase. Two common types of reactive blending are described as (1) a heterogeneous reaction that takes place at a melt or solid phase boundary[106, 107], or (2) polymerizing a monomer in the presence of a second polymer[108]. Type (1) reactive blending occurs between the blended polymer interface while being processed or molded. Interfacial reactions between blend components causes either block or graft copolymers to form *in situ*, resulting in compatibilization and stability of the dispersed phase. High-impact polystyrene

(HIPS) is a classic example of type (2) reactive blending. The rubber phase in HIPS material is blended, while free radial polymerization of styrene monomer occurs resulting in graft-coupling of PS to the rubber phase.[109] Both methods typically give an increase in impact toughness as a consequence of improved interfacial bridging.

1.5.2. Compatibilization by Addition of a Compatibilizer

Addition of a third component that serves to bridge the interface and lower interfacial energies is referred to as a compatibilizer. For this type of compatibilizer to be successful the added component needs to be capable of migrating to the interface while being processed. Two types of compatibilizer additives are found: (1) copolymer that contains both blended polymer species, or (2) as a multi-purpose compatibilizer (co-solvent). The quantity of compatibilizer typically added to a blend is between 0.5 - 4 wt% for a copolymer, while 15 - 35 wt% is added for a multi-purpose compatibilizer.[107] The addition of a tailored compatibilizer generally results in an increase in stress transfer and toughness. Figure 1.6 shows the mechanical affects of adding a compatibilizer, in this case CPE, to blends of HDPE/PVC and LDPE/PVC. Clearly when CPE is present in the blends, a drastic increase in toughness occurs.

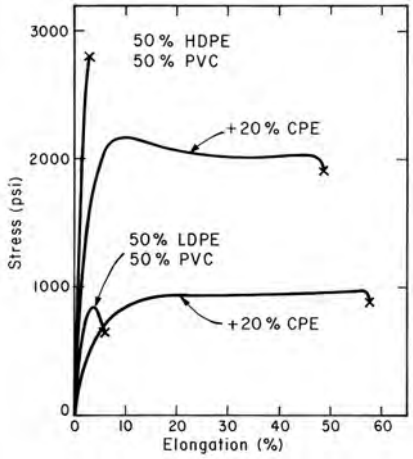

FIGURE 1.6. Stress-Strain curves for blends of low-density or high-density polyethylene (LDPE or HDPE) and poly(vinyl chloride) (PVC) using a compatibilizer of chlorinated polyethylene (CPE). From reference [110].

1.5.3. Compatibilization with Unmodified Cyclodextrins

Compatibilization is also possible by processing with pure CDs. If two immiscible polymers are mixed simultaneously to form a common CD-IC, then an intimate blend between these homopolymers can be obtained. An illustration of this concept can be seen in Figure 1.7. Since the formed ICs are fully covered in a jacket of CD, then the polymer pairs are shielded from each other. This results in the polymer chains having the ability to be intimately blended without being in intimate contact with one another and experiencing repulsive interactions that may increase their phase segregation. When coalescence of the CD-IC blend is performed by washing with warm water, the material produced from the blended polymer pair remains intimately blended.

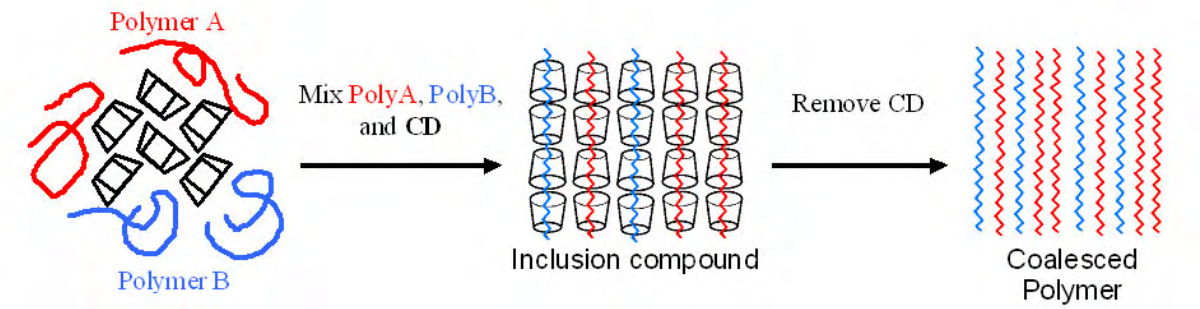

FIGURE 1.7. Intimate blending of two immiscible polymers (Poly-A and Poly-B) and their processing to achieve intimate blends using CDs.

This compatibilization technique was first discovered by Rusa and Tonelli.[111] They found if PCL and PLLA were processed together to form a common CD-IC, and were subsequently coalesced, characteristics identifiable with an intimate blend became evident.[111] The intimate CD-IC mixture that was collected had weight fractions of 55/45 w/w for PCL/PLLA. Glass transition temperatures (T_g) for both homopolymers, as well as the melting temperature of PCL (T_m), were unobservable. The only thermal event observed for this blend was the $T_{m,PLLA}$ at 166 °C. It was also seen that the crystallinity of the PLLA declined from a value

of 56.6% for the pure homopolymer to 5.5% for the coalesced blend. However a physical blend of PCL/PMMA (50/50, w/w) showed all thermal events for both polymers in addition to the PLLA retaining a crystallinity of 41%. Visual evidence of blending can be seen within the micrographs in Figure 1.8, where all films used in this study were examined after annealing for 3 minutes at 200 °C.

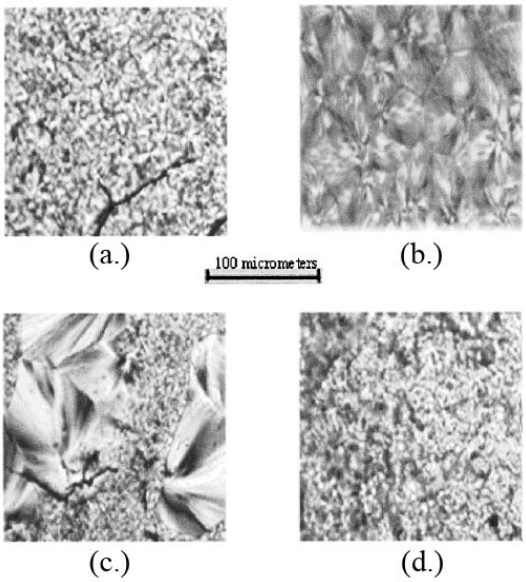

FIGURE 1.8. Polarized optical micrographs of (a.) PLLA, (b.) PCL, (c.) solution cast, and (d.) coalesced PLLA/PCL blends. After reference [111].

Intimate blending *via* CD-ICs of several other polymer pairs have since been found. Similar observations were made with blends of PC/PMMA,[63] PHB/PCL,[55] PET/PEN,[68] PC/PVAc,[62, 112] and PMMA/PVAc.[62] For many of these materials, the final stoichiomentry of the CD-IC blends are different than the initially blended amounts. This is a consequence of the competitive threading of the two polymer into the CDs, in which one may preferentially thread over the other. For example, PC/PVAc was initially mixed at a molar feed ratio of 1:4.5, however the CD-IC molar ratio was found to be 1:1 leading to the conclusion that PC is preferred over PVAc in the CD channels.[62] Therefore it has been successfully shown that coalescence of polymer pairs from CD-ICs can result in intimate blends.

1.5.4. Compatibilization using Cyclodextrin-Stars

Achieving compatibilization of immiscible polymers with CD-stars was conceived as an extension of the research done by Rusa and Tonelli where they use as-received CDs for intimately blending polymers, as described in the previous section. Rather than using excess CD with respect to included polymer (typically CD ~90 wt% of the CD-IC), as performed in that work, our current work uses CD as a minor component (CD-core ~1wt%) in which the majority of mixed material is the blended homopolymers. Therefore an idea was envisioned that uses CDs as a compatibilizer to physically handcuff an incompatible polymer into a polymer matrix. Figure 1.9 illustrates this concept.

To accomplish compatibilization with CD-stars, the star polymer arms (poly-A) that are attached to the CD-core need to be of the same species as the matrix polymer (poly-A). This results in being able to homogeneously blend the CD-star into the polymer matrix *via* the compatibilizing star arms. This is in contrast to blending unmodified CD which forms aggregates in the polymer. Therefore, by adding CD-stars to a blend of poly-A and poly-B, and subsequent threading of poly-B into the CD-stars, poly-B will be anchored and physically blended into the matrix of poly-A.

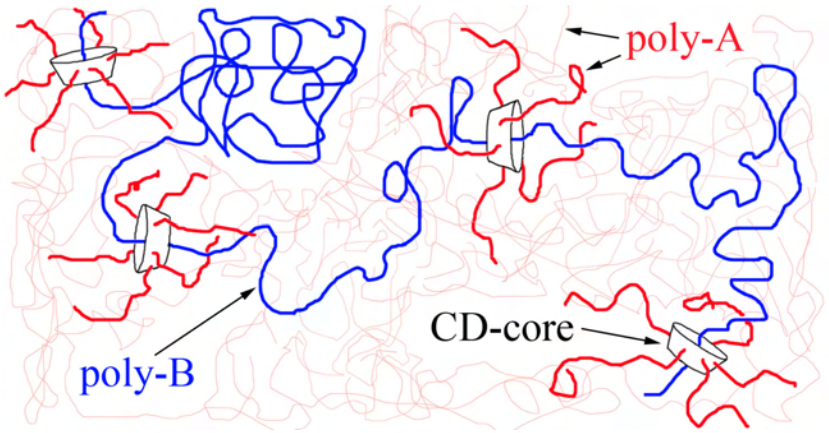

FIGURE 1.9. An illustration of how compatibilization might work with CD-stars.

Compatibilizers of this type have not been realized before. CD-star molecules have the ability to thread and compatibilize many different polymers (refer to Table 1.2) into a given polymer matrix. The primary advantage in using the CD-star compatibilizers, verses block or graft copolymers, is the versatility and ease of blending many polymers without the need to synthesize a new copolymer compatibilizer for each polymer blend. Interestingly, the final CD-star complex is analogous to a graft copolymer in structure and properties. This structure is a result of the threaded polymer (poly-B) creating the "backbone" of the polymer whereas the CD-star core with arms of poly-A making up the hybrid "slip-ring grafts" from poly-B. Therefore it is reasonable to imagine that the resultant properties of the CD-star system will be similar to traditional graft copolymers.

In fact it has been found, and will be discussed in this dissertation, that there are many similarities between the CD-stars and graft copolymers with respect to compatibilization. A brief summary of these findings are 1.) clearing of turbid solutions which possibly indicate unimolecular-micelle formation, 2.) a drastic decrease in blended polymer domain size for spun-cast films, 3.) stabilization of the phase morphology to annealing, 4.) increased retention of blended polymer due to physical constraint incurred by the CD-star slip-ring grafts, and 5.) thermal and mechanical property measurements that suggest compatibilization. These and other results will be discussed in the following chapters.

1.6. Motivation and Organization

As discussed in the previous sections, compatibilizing homopolymer blends produces property modifications by drawing desirable properties from each homopolymer to create a new hybrid composite polymer material. Tailored material property modifications may include, for example, mechanical and electrical properties, surface interactions, or cost and weight reduction. Therefore compatibilization is dependent on the overall interfacial bridging of these phases and the ability of these phases to contribute to the overall properties of the material.

The motivation for this work is to develop a general compatibilizer that can be used with various polymer blends so as to tailor the desired properties found in the homopolymers to the application of interest. As discussed earlier, cyclodextrins have been shown to thread onto many polymers offering a variety of possible blending options. The flexibility of having one compatibilizer additive that can be potentially used for blending several polymers within a given polymer matrix might be more cost effective. If blending occurs with CD-stars, syntheses of special blend-specific compatibilizers are not necessary. This leads to a compatibilizer system that is more advantageous from a cost and convenience standpoint.

Initially one immiscible system will be studied (in this case PS and PDMS), and the processing variables and resultant properties will be explored to determine the principles that are important for accomplishing compatibilization using CD-star molecules. In theory, the principles found for this blend can then be applied to other polymer blends for accomplishing compatibility. Therefore this dissertation will cover the following topics which involve CD-stars for blend compatibilization.

- CD-star synthesis and chemical characterization.
- Solution blending and processing.
- Resultant film morphology found by solution and spin casting.
- Thermal and mechanical properties of blended films.

Lastly, conclusions will be drawn from this work and summarized. These conclusions will include some suggestions for future work that contain some promising investigative avenues.

1.7. References

1. Szejtli, J. *Pure Appl. Chem.* **2004,** 76, (10), 1825-1845.

2. Larsen, K. L. *Journal of Inclusion Phenomena and Macrocyclic Chemistry* **2002,** 43, 1-13.

3. Tchoreloff, P.; Baszkin, A.; Boisonnade, M.-M.; Zhang, P.; Coleman, A. W. *Supermolecular Chemistry* **1995,** 4, 169-171.

4. Coleman, A. W.; Nicolis, I.; Keller, N.; Dalbiez, J. P. *Journal of Inclusion Phenomena and Molecular Recognition in Chemistry* **1992,** 13, 139-143.

5. Martin Del Valle, E. M. *Process Biochemistry* **2004,** 39, (9), 1033-1046.

6. Harata, K. *Chemical Reviews* **1998,** 98, (5), 1803-1828.

7. Hunt, M. A.; Rusa, C. C.; Tonelli, A. E.; Balik, C. M. *Carbohydrate Research* **2004,** 339, (17), 2805-2810.

8. Hunt, M. A.; Rusa, C. C.; Tonelli, A. E.; Balik, C. M. *Carbohydrate Research* **2005,** 340, (9), 1631-1637.

9. Uyar, T. Nanostructuring Polymers with Cyclodextrins. Dissertation, North Carolina State University, Raleigh, NC, 2005.

10. Ritter, H.; Tabatabai, M. *Progress in Polymer Science* **2002,** 27, 1713-1720.

11. Rekharsky, M. V.; Inoue, Y. *Chemical Reviews* **1998,** 98, 1875-1917.

12. Hedges, A. R. *Chemical Reviews* **1998,** 98, 2035-2044.

13. Uekama, K. *Chem. Pharm. Bull.* **2004,** 52, (8), 900-915.

14. Singh, M.; Sharma, R.; Banerjee, U. C. *Biotechnology Advances* **2002,** 20, (5-6), 341-359.

15. Bibby, D. C.; Davies, N. M.; Tucker, I. G. *International Journal of Pharmaceutics* **2000,** 197, 1-11.

16. Chen, W.; Chang, C.-E.; Gilson, M. K. *Biophys. J.* **2004,** 87, (5), 3035-3049.

17. Savarino, P.; Viscardi, G.; Quagliotto, P.; Montoneri, E.; Barni, E. *Dyes and Pigments* **1999,** 42, 143-147.

18. Savarino, P.; Parlati, S.; Buscaino, R.; Piccinini, P.; Barolo, C.; Montoneri, E. *Dyes and Pigments* **2006,** 69, 7-12.

19. Savarino, P.; Parlati, S.; Buscaino, R.; Piccinini, P.; Degani, I.; Barni, E. *Dyes and Pigments* **2004,** 60, 223-232.

20. Park, J. S.; Wilson, J. N.; Hardcastle, K. I.; Bunz, U. H. F.; Srinivasarao, M. *Journal of the American Chemical Society* **2006,** 128, 7714-7715.

21. Liu, Y.; Han, B.-H.; Chen, Y.-T. *Journal of Organic Chemistry* **2000,** 65, 6227-6230.

22. Buschmann, H. J.; Denter, U.; Knittel, D.; Schollmeyer, E. *Journal of the Textile Institute* **1998,** 89, (3), 554-561.

23. Szejtli, J. *Starch-Starke* **2003,** 55, (5), 191-196.

24. Huang, L.; Taylor, H.; Gerber, M.; Orndorff, P. E.; Horton, J. R.; Tonelli, A. *Journal of Applied Polymer Science* **1999,** 74, (4), 937-947.

25. Lu, J.; Hill, M. A.; Hood, M.; Greeson, D. F.; Horton, J. R.; Orndorff, P. E.; Herndon, A. S.; Tonelli, A. E. *Journal of Applied Polymer Science* **2001,** 82, (2), 300-309.

26. Huang, L.; Gerber, M.; Lu, J.; Tonelli, A. E. *Polymer Degradation and Stability* **2001,** 71, (2), 279-284.

27. Leslie, T.; Xiao, H.; Dong, M. *Journal of Petroleum Science and Engineering* **2005,** 46, 225-232.

28. Wang, X.; Brusseau, M. L. *Environ. Sci. Technol.* **1995,** 29, 2632-2635.

29. Hardt, I. H.; Wolf, C.; Gehrcke, B.; Hochmuth, D. H.; Pfaffenberger, B.; Huhnerfuss, H. *Journal of High Resolution Chromatography* **1994,** 17, 859-864.

30. Wang, X.; Brusseau, M. L. *Environ. Sci. Technol.* **1993,** 27, 2821-2825.

31. Sawunyama, P.; Bailey, G. W. *Journal of Molecular Structure (Theochem)* **2001,** 541, (1-3), 119-129.

32. Kamiya, M.; Kameyama, K.; Ishiwata, S. *Chemosphere* **2001,** 42, (3), 251-255.

33. Zeng, Q.; Liao, B.; Luo, Y.; Liu, C.; Tang, H. *Bull. Environ. Contam. Toxicol.* **2003,** 71, 668-674.

34. Araki, J.; Ito, K. *Soft Matter* **2007,** 3, 1456-1473.

35. Nepogodiev, S. A.; Stoddart, J. F. *Chemical Reviews* **1998,** 98, 1959-1976.

36. Rusa, C.; Wei, M.; Bullions, T. A.; Rusa, M.; Gomez, M. A.; Porbeni, F. E.; Wang, X.; Shin, I. D.; Balik, C. M.; White, J. L.; Tonelli, A. E. *Crystal Growth & Design* **2004,** 4, (6), 1431-1441.

37. Tonelli, A. E. *Polymer* **2008,** 49, (7), 1725-1736.

38. Uyar, T.; Rusa, C. C.; Hunt, M. A.; Aslan, E.; Hacaloglu, J.; Tonelli, A. E. *Polymer* **2005,** 46, (13), 4762-4775.

39. Michishita, T.; Okada, M.; Harada, A. *Macromol. Rapid Commun.* **2001,** 22, 763-767.

40. Michishita, T.; Takashima, Y.; Harada, A. *Macromol. Rapid Commun.* **2004,** 25, 1159-1162.

41. Porbeni, F. E.; Edeki, E. M.; Shin, I. D.; Tonelli, A. E. *Polymer* **2001,** 42, (16), 6907-6912.

42. Paik, Y.; Poliks, B.; Rusa, C. C.; Tonelli, A. E.; Schaefer, J. *Journal of Polymer Science Part B-Polymer Physics* **2007,** 45, (11), 1271-1282.

43. Harada, A. *Coordination Chemistry Reviews* **1996,** 148, 115-133.

44. Martinez, G.; Gomez, M. A.; Villar-Rodil, S.; Garrido, L.; Tonelli, A. E.; Balik, C. M. *Journal of Polymer Science Part a-Polymer Chemistry* **2007,** 45, (12), 2503-2513.

45. Shuai, X. T.; Porbeni, F. E.; Wei, M.; Bullions, T.; Tonelli, A. E. *Macromolecules* **2002,** 35, (6), 2401-2405.

46. Li, J.; Ni, X.; Zhou, Z.; Leong, K. W. *Journal of the American Chemical Society* **2003,** 125, 1788-1795.

47. Ceccato, M.; Lo-Nostro, P.; Baglioni, P. *Langmuir* **1997,** 13, 2436-2439.

48. Huang, L.; Allen, E.; Tonelli, A. E. *Polymer* **1998,** 39, (20), 4857-4865.

49. Rusa, C. C.; Tonelli, A. E. *Macromolecules* **2000,** 33, (5), 1813-1818.

50. Lo-Nostro, P.; Lopes, J. R.; Ninham, B. W.; Baglioni, P. *Journal of Physical Chemistry B* **2002,** 106, 2166-2174.

51. Okumura, H.; Okada, M.; Kawauchi, Y.; Harada, A. *Macromolecules* **2000,** 33, (12), 4297-4298.

52. Okumura, H.; Kawaguchi, Y.; Harada, A. *Macromolecules* **2001,** 34, 6338-6343.

53. Ikeda, T.; Lee, W. K.; Ooya, T.; Yui, N. *J. Phys. Chem. B* **2003,** 107, 14-19.

54. Yoshida, K.-i.; Shimomura, T.; Ito, K.; Hayakawa, R. *Langmuir* **1999,** 15, 910-913.

55. Shuai, X. T.; Porbeni, F. E.; Wei, M.; Bullions, T.; Tonelli, A. E. *Macromolecules* **2002,** 35, (8), 3126-3132.

56. Rusa, C. C.; Luca, C.; Tonelli, A. E. *Macromolecules* **2001,** 34, (5), 1318-1322.

57. Chen, W.; Wan, X.; Xu, N.; Xue, G. *Macromolecules* **2003,** 36, 276-278.

58. Rusa, C. C.; Wei, M.; Bullions, T. A.; Rusa, M.; Gomez, M. A.; Porbeni, F. E.; Wang, X. G.; Shin, I. D.; Balik, C. M.; White, J. L.; Tonelli, A. E. *Crystal Growth & Design* **2004,** 4, (6), 1431-1441.

59. Wei, M.; Davis, W.; Urban, B.; Song, Y. Q.; Porbeni, F. E.; Wang, X. W.; White, J. L.; Balik, C. M.; Rusa, C. C.; Fox, J.; Tonelli, A. E. *Macromolecules* **2002,** 35, (21), 8039-8044.

60. Lagrost, C.; Lacroix, J.-C.; Chane-Ching, K. I.; Jouini, M.; Aeiyach, S.; Lacaze, P.-C. *Adv. Mater.* **1999,** 11, (8), 664-667.

61. Takashima, Y.; Oizumi, Y.; Sakamoto, K.; Miyauchi, M.; Kamitori, S.; Harada, A. *Macromolecules* **2004,** 37, 3962-3964.

62. Uyar, T.; Rusa, C. C.; Wang, X. W.; Rusa, M.; Hacaloglu, J.; Tonelli, A. E. *Journal of Polymer Science Part B-Polymer Physics* **2005,** 43, (18), 2578-2593.

63. Wei, M.; Tonelli, A. E. *Macromolecules* **2001,** 34, (12), 4061-4065.

64. Porbeni, F. E.; Shin, I. D.; Shuai, X. T.; Wang, X. W.; White, J. L.; Jia, X.; Tonelli, A. E. *Journal of Polymer Science Part B-Polymer Physics* **2005,** 43, (15), 2086-2096.

65. Udachin, K. A.; Wilson, L. D.; Ripmeester, J. A. *Journal of the American Chemical Society* **2000,** 122, 12375-12376.

66. Lu, J.; Shin, I. D.; Nojima, S.; Tonelli, A. E. *Polymer* **2000,** 41, (15), 5871-5883.

67. Hernandez, R.; Rusa, M.; Rusa, C. C.; Lopez, D.; Mijangos, C.; Tonelli, A. E. *Macromolecules* **2004,** 37, (25), 9620-9625.

68. Bullions, T. A.; Edeki, E. M.; Porbeni, F. E.; Wei, M.; Shuai, X.; Rusa, C. C.; Tonelli, A. E. *Journal of Polymer Science Part B-Polymer Physics* **2003,** 41, (2), 139-148.

69. Gerardo Martínez, M. A. G., Silvia Villar-Rodil, Leoncio Garrido, Alan E. Tonelli, C. Maurice Balik,. *Journal of Polymer Science Part A: Polymer Chemistry* **2007,** 45, (12), 2503-2513.

70. Rusa, C. C.; Bridges, C.; Ha, S.-W.; Tonelli, A. E. *Macromolecules* **2005,** 38, (13), 5640-5646.

71. Hunt, M. A.; Jung, D. W.; Shamsheer, M.; Uyar, T.; Tonelli, A. E. *Polymer* **2004,** 45, (4), 1345-1347.

72. Uyar, T.; Gracz, H. S.; Rusa, M.; Shin, I. D.; El-Shafei, A.; Tonelli, A. E. *Polymer* **2006,** 47, (20), 6948-6955.

73. Hu, J.; Huang, R.; Cao, S.; Hua, Y. *e-Polymers* **2008,** 171, 1-15.

74. Dong, T.; He, Y.; Zhu, B.; Shin, K.-M.; Inoue, Y. *Macromolecules* **2005,** 38, (18), 7736-7744.

75. Dong, T.; Shin, K.-m.; Zhu, B.; Inoue, Y. *Macromolecules* **2006,** 39, (6), 2427-2428.

76. Zhang, S.; Yu, Z.; Govender, T.; Luo, H.; Li, B. *Polymer* **2008,** 49, (15), 3205-3210.

77. Vogel, R.; Tändler, B.; Häussler, L.; Jehnichen, D.; Harald Brünig. *Macromolecular Bioscience* **2006,** 6, (9), 730-736.

78. Tellini, V. H. S.; Jover, A.; Garcia, J. C.; Galantini, L.; Meijide, F.; Tato, J. V. *Journal of the American Chemical Society* **2006,** 128, (17), 5728-5734.

79. Crini, G.; Morcellet, M. *Journal of Separation Science* **2002,** 25, 789-813.

80. Lo Nostro, P.; Lopes, J. R.; Cardelli, C. *Langmuir* **2001,** 17, (15), 4610-4615.

81. Khan, A. R.; Forgo, P.; Stine, K. J.; D'Souza, V. T. *Chemical Reviews* **1998,** 98, 1977-1996.

82. Tian, W.; Fan, X.; Kong, J.; Liu, T.; Liu, Y.; Huang, Y.; Wang, S.; Zhang, G. *Macromolecules* **2009,** 42, (3), 640-651.

83. Cheng, J.; Khin, K. T.; Gregory S., J.; Liu, A.; Davis, M. E. *Bioconjugate Chemistry* **2003,** 14, 1007-1017.

84. Lee, M. H.; Yoon, K. J.; Ko, S.-W. *Journal of Applied Polymer Science* **2000,** 78, 1986-1991.

85. Gawish, S. M.; Ramadan, A. M.; Mosleh, S.; Morcellet, M.; Martel, B. *Journal of Applied Polymer Science* **2006,** 99, 2586-2593.

86. Lee, M. H.; Yoon, K. J.; Ko, S.-W. *Journal of Applied Polymer Science* **2001,** 80, 438-446.

87. Renard, E.; Volet, G.; Amiel, C. *Polymer International* **2005,** 54, 594-599.

88. Manakker, F. v. d.; Vermonden, T.; Morabit, N. e.; Hennink, C. F. v. N. W. E. *Langmuir* **2008,** 24, 12559-12567.

89. Ooya, T.; Akutsu, M.; Kumashiro, Y.; Yui, N. *Science and Technology of Advanced Materials* **2005,** 6, 447-451.

90. Gao, Z.; Zhao, X. *Polymer* **2003,** 44, 4519-4526.

91. Crini, G. *Bioresource Technology* **2003,** 90, 193-198.

92. Yu, J. C.; Jiang, Z.-T.; Liu, H.-Y.; Yu, J.; Zhang, L. *Analytica Chimica Acta* **2003,** 477, 93-101.

93. Busche, B. J.; Balik, C. M. *Abstracts of Papers of the American Chemical Society* **2006,** 231: 155-PMSE Mar 26.

94. Ogoshi, T.; Chujo, Y. *Macromolecules* **2003,** 36, 654-660.

95. Karaky, K.; Reynaud, S.; Billon, L.; François, J.; Chreim, Y. *Journal of Polymer Science Part A: Polymer Chemistry* **2005,** 43, (21), 5186-5194.

96. Yang, C.; Li, H.; Goh, S. H.; Li, J. *Biomaterials* **2007,** 28, (21), 3245-3254.

97. Adeli, M.; Zarnegar, Z.; Kabiri, R. *European Polymer Journal* **2008,** 44, (7), 1921-1930.

98. Li, J. S.; Xiao, H. N.; Kim, Y. S.; Lowe, T. L. *Journal of Polymer Science Part a-Polymer Chemistry* **2005,** 43, (24), 6345-6354.

99. Haddleton, D. M.; Kukulj, D.; Kelly, E. J.; Waterson, C. *Polymer Materials Science and Engineering* **1999,** 80, 145-146.

100. Ohno, K.; Wong, B.; Haddleton, D. M. *Journal of Polymer Science Part a-Polymer Chemistry* **2001,** 39, (13), 2206-2214.

101. Kakuchi, T.; Narumi, A.; Matsuda, T.; Miura, Y.; Sugimoto, N.; Satoh, T.; Kaga, H. *Macromolecules* **2003,** 36, (11), 3914-3920.

102. Miura, Y.; Narumi, A.; Matsuya, S.; Satoh, T.; Duan, Q.; Kaga, H.; Kakuchi, T. *Journal of Polymer Science Part a-Polymer Chemistry* **2005,** 43, (18), 4271-4279.

103. Stenzel, M. H.; Davis, T. P.; Fane, A. G. *Journal of Materials Chemistry* **2003,** 13, (9), 2090-2097.

104. Plamper, F. A.; Becker, H.; Lanzendorfer, M.; Patel, M.; Wittemann, A.; Ballauf, M.; Muller, A. H. E. *Macromolecular Chemistry and Physics* **2005,** 206, (18), 1813-1825.

105. Utracki, L. A. *Canadian Journal of Chemical Engineering* **2002,** 80, (6), 1008-1016.

106. Brown, S. B., Reactive compatibilization of polymer blends. In *Polymer Blends Handbook*, Utracki, L. A., Ed. Kluwer Academic Publishers: Dordrecht, The Netherlands, 2003; Vol. 1, pp 339-415.

107. Utracki, L. A., Role of polymers blends' technology in polymer recycling. In *Polymer Blends Handbook*, Utracki, L. A., Ed. Kluwer Academic Publishers: Dordrecht, The Netherlands, 2003; Vol. 2, pp 1117-1165.

108. Sperling, L. H.; Hu, R., Interpenetrating polymer networks. In *Polymer Blends Handbook*, Utracki, L. A., Ed. Kluwer Academic Publishers: Dordrecht, The Netherlands, 2003; Vol. 1, pp 417-447.

109. Akkapeddi, M. K., Commercial Polymer Blends. In *Polymer Blends Handbook*, Utracki, L. A., Ed. Kluwer Academic Publishers: Netherlands, 2003; Vol. 2, pp 1023-1115.

110. Paul, D. R., Interfacial Agents ("Compatibilizers") for Polymer Blends. In *Polymer Blends*, Paul, D. R.; Newman, S., Eds. Acadenic Press: New York, 1978; Vol. 2, pp 35-62.

111. Rusa, C. C.; Tonelli, A. E. *Macromolecules* **2000,** 33, (15), 5321-5324.

112. Uyar, T.; Oguz, G.; Tonelli, A. E.; Hacaloglu, J. *Polymer Degradation and Stability* **2006,** 91, (10), 2471-2481.

2. EXPERIMENTAL

2.1. Materials

ACS grade solvents and basic-alumina were purchased from Fisher Scientific or Sigma Aldrich Chemical Co. and used without further purification, unless otherwise noted. Reagents used in syntheses were purchased from Sigma Aldrich Chemical Co. and used without further purification, with the exception of the styrene monomer, which had the inhibitor removed by filtration through a basic-alumina column just before use. γ-Cyclodextrin was purchased from Cerestar, and randomly methylated γ-cyclodextrin (50% methylated) was purchased from Cyclodextrin Technologies Development Inc. of High Springs, Florida.

Low molecular weight PS standards used in glass transition temperature analysis in Chapter 3 were purchased from Pressure Chemical Company. PS was purchased from the Aldrich Chemical Company, and PDMS purchased from Gelest Incorporated. All polymers were used as received.

2.2. Physical and Chemical Structure Analysis

2.2.1. X-Ray Diffraction

Wide angle x-ray diffraction (WAXD) measurements were performed on a Siemens type-F x-ray diffractometer with a Ni-filtered Cu Kα radiation source (λ = 1.54 Å). The voltage and current were 30kV and 20mA, respectively. X-ray intensities were measured every 0.1° from 2θ = 5 to 30° at a scanning rate of (2θ = 3°) per minute.

2.2.2. Fourier Transform Infrared Spectroscopy

Fourier Transform Infrared Spectroscopy (FTIR) was performed on a Nicolet 510P Fourier Transform Infrared Spectrophotometer in transmittance mode. All samples were ground with potassium bromide and uniaxially pressed into pellets. The FTIR chamber was purged with

dry air to eliminate water vapor. The spectra were collected over a range of 4000 to 400 cm^{-1}, with a resolution of 2 cm^{-1} obtained after 64 scans.

2.2.3. Nuclear Magnetic Resonance Spectroscopy

^{1}H-NMR and ^{13}C-NMR were collected on a Varian Gemini 300 MHz Spectrometer equipped with a narrow bore magnet and 5 mm 4N (^{1}H, ^{13}C, ^{19}F, and ^{31}P) probe at room temperature. All samples examined by ^{1}H-NMR had 32 sampling repetitions whereas ^{13}C-NMR samples had 20,000 sampling repetitions. ^{1}H-NMR solutions were prepared at a concentration of 50mg/ml, whereas ^{13}C-NMR samples were prepared at 200mg/ml.

2.3. Solution Property Analysis

2.3.1. Capillary Viscometry

Capillary viscometery was conducted with a #25 Cannon Ubbelohde semi-micro dilution type viscometer. Viscosity measurements were conducted in a 25 gallon water bath which was equilibrated overnight at 25°C. The viscometer was allowed to equilibrate in the water bath before introducing the solution to be measured. All solutions were prepared just before introduction into the viscometer, and were filtered through a 1μm polytetrafluoroethylene (PTFE) syringe filter to remove any particulates. The amount of time for the meniscus to move between the two timing marks was recorded manually using a stop-watch that read to 0.01 seconds.

2.3.2. Dynamic Light Scattering

Dynamic light scattering experiments were performed with a Brookhaven 90-Plus Nanoparticle Size Analyzer. Sizing capabilities of this instrument are from <1nm to 6μm. All experiments were performed at 25°C at a wavelength of 660nm with a detector angle of 90°. All solutions were filtered through a 1μm PTFE syringe filter to remove any particulates before introduction into the sample cuvette. Each sample had at least 10 completed runs.

Solvents used were tetrahydrofuran (THF) with a viscosity of 0.480cP and a refractive index of 1.407, and chloroform ($CHCl_3$) with a viscosity of 0.542cP and a refractive index of 1.446.

2.3.3. Gel Permeation Chomatography

Gel permeation chromatography (GPC) was implemented to determine molecular weight distributions, M_w/M_n, of the star-molecule samples. These measurements were conducted using a Waters Breeze High Performance Liquid Chromatograph with wavelength absorbance and refractive index detectors. The GPC instrument was calibrated for quantitative measurement using linear polystyrene standards. The UV absorbance detector was calibrated for a wavelength of 254nm. The elutant used in all cases was tetrahydrofuran (HPLC grade). The solution concentration was 1mg/ml. All samples were examined at 25°C. All solutions were filtered through a 0.2μm PTFE syringe filter to remove any particulates before introduction into the sample cuvette.

2.4. Solid State Property Analysis

2.4.1. Thermal Property Analysis

2.4.1.1. Thermal Gravimetric Analysis

Sample degradation temperatures and thermal stability were examined with a TA Instruments Q5000 thermal gravimetric analyzer. The examined temperature range was from 25 °C to 600 °C at a ramp rate of 5 °C/min. Samples were heated under an atmosphere of nitrogen with sample masses of approximately 10mg. A platinum pan and hang-down wire were used when heating the samples.

2.4.1.2. Differential Scanning Calorimetry

Transition temperatures for the samples were found using a TA Instruments Q1000 differential scanning calorimeter with liquid nitrogen cooling capacity. Calibration of the cell constant was performed with circular sapphire disks from -140 °C to 300 °C. Temperature calibration was performed with indium metal having a melting point of

156.61 °C. The temperature accuracy after calibration is stated to be 0.1 °C per the manufacturer. Calibrations were done using standard aluminum sample pans with a heating rate of 10 °C/min under helium gas. Data was analyzed using the TA Universal Analysis software.

Thermal examination of the samples was performed while under a helium purge of 25ml/min. All heating and cooling rates were conducted at 10°C/min. The DSC traces reported within this dissertation are the second heating cycle. Sample masses for testing were on the order of 10mg and sealed in a standard aluminum sample pan.

2.4.2. Mechanical Property Analysis

2.4.2.1. Dynamic Mechanical Analysis

Dynamic mechanical analysis was conducted on a TA Instruments DMA-600 in tension using a frequency of 1Hz and a strain amplitude of 0.1%. Cryogenic temperatures and control was accomplished with a liquid nitrogen cooling system. The samples were tested in the temperature range of -130 °C to 130 °C with a ramp rate of 2 °C/min. Each sample was allowed to equilibrate at -130 °C before heating.

2.4.3. Surface Property Analysis

2.4.3.1. Water Contact Angle

Sessile drop experiments on the spun cast films were performed using a Rame-Hart contact angle goniometer (model 100-00, Rame-Hart, Mountain Lakes, NJ) equipped with a CCD camera. The liquid medium used in these measurements was deionized water. Each droplet on the surface had a constant volume of 8μl. Films were measured 3 times and the average water contact angle was obtained.

2.4.4. Microstructural Analysis

2.4.4.1. Optical Microscopy

Optical microscopy was performed with an Olympus BH-2 microscope. Both transmittance and reflectance images were collected and the images captured by a ProgRes C10-plus CCD camera with a J-clamp coupler fitted onto the microscope. TIF images were collected at 300dpi resolution

2.4.4.2. Scanning Electron Microscopy

Secondary electron images of the spun cast films were captured using a Hitachi S-3200N thermionic emission scanning electron microscope operating with an acceleration voltage of 5kV. Working distance was 11 mm. Specimen chamber vacuum level was in the regime of at least 10 E-5 Torr. The silicon wafer substrate was mounted to the aluminum sample stage with double-sided conductive carbon tape. Both the underside and edges of the sample were covered with this tape to promote conductivity. The spun cast films affixed to the sample stage were then coated with a thin layer of Au/Pd alloy in a Denton Desk II sputter coater to reduce sample charging.

2.4.4.3. Atomic Force Microscopy

Atomic force microscope images were collected with a Veeco Dimension 3000. These experiments were conducted in non-contact taping mode and scanned at 1 Hz with a resolution of 512 x 512 pixels. The scanning probes employed were Vista Probe T300R-25 noncontact mode silicon tips with a nominal resonance frequency of 300 kHz. The minimal digital z-step direction is 15 picometers.

3. SYNTHESES OF STAR POLYMERS CONTAINING γ-CYCLODEXTRIN CORES AND POLYSTYRENE ARMS

3.1. Background

It is well documented that cyclodextrin (CD) has the ability to entrap and retain various molecular guests into its hydrophobic cavity.[1, 2] If we were able to exploit the entrapping qualities of CD by blending it into films of polystyrene (PS) then these films could be modified and engineered to possibly give unique characteristics, depending on which guest resides in the CD core. A few examples of guests that have been shown to include into CD and that might be of interest for blending into polystyrene are polydimethylsiloxane,[3, 4] pharmaceuticals,[1, 5] dyes,[6, 7] flame retardants,[8] antibacterials,[9, 10] and pesticides.[11, 12]

Uniform blending of CD, a naturally occurring cyclic oligosaccharide,[1] into PS becomes challenging due to its hydrophilic exterior, making it insoluble in typical PS solvents. Additionally, this hydrophobic exterior causes an inability to homogeneously blend into the polymer matrix itself. Non-uniform mixing of CDs is partially caused by strong hydrogen bonds which can lead to crystallization and aggregation. Due to the occurrence of CD aggregation, this results in a roughened surface topology in PS films. By attaching compatibilizing arms of PS onto CD, CD can then be molecularly dispersed into a linear PS matrix providing consistency within the film. This method will allow for regular blending of molecular guests *via* the CD-core and resulting in uniform bulk properties.

Li and Xiao[13] report a convenient way to chemically attach bromine functionality to CDs by reacting 2-bromoisobutyryl bromide with the hydroxyls on the CD which provide sites for growing polymer arms from the CD. These polymerization initiation sites can then be used with atom transfer radical polymerization (ATRP) and be stoichiometrically varied to provide a statistical distribution of initiator attached to the CD. The CD initiator core can then be tailored to create a varying number of initiation sites, thereby giving a predictable

number of arms. This procedure can be implemented for synthesizing any number of CD-star species as long as the selected monomer can be polymerized by ATRP.

To date, most researchers have concentrated on synthesizing β-CD stars. Yang *et al.*[14] are the sole researchers working on α-CD stars, and nobody has synthesized γ-CD stars to the author's knowledge. β-CD stars have been reported with arms comprised of polystyrene,[15-17] poly(methyl methacrylate),[15, 17, 18] poly(t-butyl methacrylate),[18-20] and poly(lactide),[21] as well as other polymers.[22, 23] The number of PS arms grown on CD cores has ranged from one[24] to as high as twenty-one.[15, 22, 23] The core-first synthesis methods employed in making these stars have included 2,2,6,6-tetramethylpiperidine-1-oxyl (TEMPO)[16] initiation, reversible addition-fragmentation chain-transfer polymerization (RAFT),[25, 26] nitroxide mediated polymerization (NMP),[18] and ATRP,[17-20, 22, 23] all of which give good control over star architecture. Out of these methods, ATRP is an attractive method for CD-star synthesis due to very low coupling termination between polymer chains,[27] relative tolerance to hydroxyl groups being present,[28] and controlled polymerization resulting in uniform arm lengths on the stars.[29]

A few applications have been suggested for CD-stars which include increasing the nanoporosity of PS films,[30] enhancing flocculation of clay particulates,[23] or using them as small molecule nanocarriers.[14, 21] Most of these applications use CD-star in the pure state without blending with other polymers/materials. However, the flocculated clay particle work was conducted in a blended solution that examined the effect of a dual-polymer system (cationic-CD-stars and anionic polymer) on flocculation. Nonetheless the primary role cyclodextrin plays in most other CD-star syntheses works has been to provide a core for growing uniform stars to which many arms can be attached.

The work outlined in this chapter has a specific purpose for CD, other than just being the core to which arms are grown. The primary objective is to use the CD-core as a

compatibilizer for blending guests into a PS matrix. Core dimensions of commonly available CDs were carefully evaluated for their ability to thread polymer guests where the three core sizes surveyed had dimensions of 5.7Å, 7.8Å, and 9.5Å, for α-cyclcodextrin, β-cyclodextrin, and γ-cyclodextrin, respectively.[31] In the present work, the specific core that was chosen is γ-cyclodexrin (γ-CD), due to its proven capacity for threading several polymer guests into its large core.[32]

Three principle goals are to be accomplished for the γ-CD-star syntheses in this work. First, the γ-CD-star must be synthesized with a moderate number of arms so interference of the arms with the cavity is minimized and solubility in an organic solvent can be accomplished. Second, control over arm length is needed so that arms of oligomeric length can be produced, resulting in a high CD molar ratio for the star. Third, the polymer arm species selected must have a large enough cross-section to prevent self-threading of its arms within the CD core leaving the cavity open for molecular guests, polymeric and otherwise.

PS has been chosen for the arm species because of it having a larger cross-sectional area which is unlikely to fit into the γ-CD cavity, although this has been found to be somewhat dependent on tacticity.[33] This is in contrast to the proven ability of γ-CD to thread many types of homopolymers into the interior cavity due to its larger inner core dimension of 9.5Å. Isotactic sequences of PS have been modeled to show that threading is possible with a cross-sectional dimension of 8.5Å. However, the syndiotactic cross-sectional diameter of 10.5Å has been shown to be too large for threading into the γ-CD cavity (illustrated in Figure 3.1.).[33] Thus an atactic PS with isotactic sequences on the end of the polymer chain will have some tendency for inclusion, but full threading of the chain is unlikely thereby preserving the core for other guests. Any partial threading of an arm end (due to isotactic sequences) will tend to be displaced by a guest which has a higher propensity for threading. In this chapter we report the syntheses of twelve armed PS γ-CD-stars with arm lengths of five to fifty-one styrene repeat units.

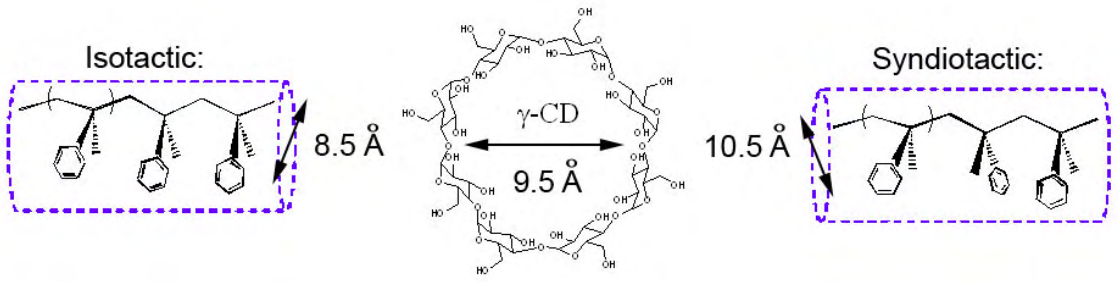

FIGURE 3.1. Illustration of PS chains with different tacticities and their cross-sectional dimensions compared with the γ-CD core diameter.

3.2. Synthesis of α-bromo Cyclodextrin ATRP Initiator

Synthesis of brominated cyclodextrin ATRP initiator is previously described by Li and Xiao, where they use β-CD.[13] However in our work we will use γ-CD. The quantities of the reagents used in this synthesis were 10.00g (7.713 mmol) of γ-CD that was dried overnight in a vacuum oven at 80°C, and 15.2ml (123.41 mmol) of 2-bromoisobutyryl bromide (98%). The reagent, 2-bromoisobutyryl bromide, contains a bromine functional group similar to the initiator used by Matyjaszewski *et al.*[34-36] in ATRP reactions. The amount of 2-bromoisobutyryl bromide employed targets sixteen of the twenty-four hydroxyls (or 66.7%) on γ-CD for bromine modification. Figure 3.2.(i) illustrates the bromination route of the γ-CD, and shows the final synthesized brominated cyclodextrin ATRP initiator (Br-γ-CD).

Following the synthesis, ^{1}H-NMR in d_6-DMSO was performed where it was found that twelve of the twenty-four hydroxyls were modified (or 50% substituted) with bromine (which will be discussed further in Section 3.4.2) giving an overall reaction yield of 75%. The physical appearance of the powdered product was off-white/light-brown in color and it had a recovered mass of 17.68g.

3.3. Synthesis of PS Stars with a γ-Cyclodextrin Core

Atom transfer radial polymerization[29, 36] was carried out with initial molar ratios of $[M]_0/[I]_0/[Cu_IBr]_0/[bpy]_0/[Cu_{II}Br_2]_0$ = 120 / 1 / 1 / 3 / 0.05, where [M] is the styrene monomer, [I] is the number of bromine groups on the Br-γ-CD ATRP initiator, $[Cu_IBr]$ is copper(I) bromide, [bpy] is 2,2'-bipyridine, and $[Cu_{II}Br_2]$ is copper(II) bromide. An illustration of the synthesis route is shown in Figure 3.2(ii), and demonstrates an example polymerization reaction for one arm, where in fact twenty-four arms are potentially possible. The previously synthesized Br-γ-CD initiator powder was added to a round bottom flask equipped with a Teflon coated magnetic stir bar. A vacuum of 500mtorr was pulled on the round bottom flask three times with subsequent nitrogen back-filling. After nitrogen washing was completed, 1/3 of the styrene monomer was introduced *via* syringe into the flask. The initiator was allowed to fully dissolve in the styrene monomer while stirring under nitrogen.

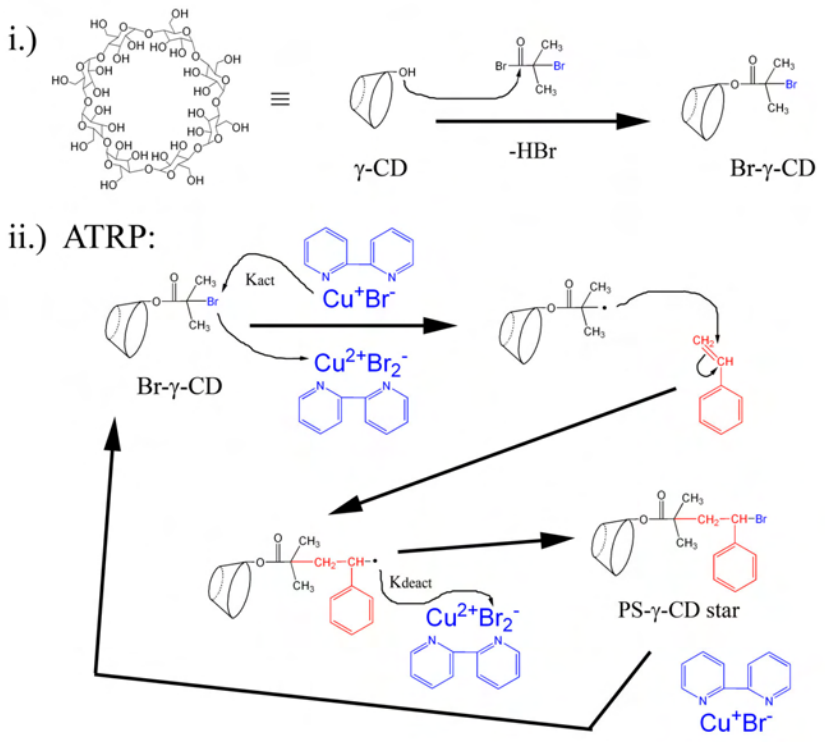

FIGURE 3.2. General synthesis route of CD-stars where (i.) is the Br-γ-CD ATRP initiator route, and (ii.) is the ATRP route for the PS-γ-CD stars. For ATRP, $K_{deact} > K_{act}$.

A second reaction vessel was prepared in parallel using an oven dried round bottom flask equipped with a Teflon coated magnetic stir bar. To this flask copper(I) bromide, copper(II) bromide, and bipyridine were added, followed by administering a vacuum of 500mtorr three times with subsequent back filling of nitrogen. The remaining 2/3 of the styrene monomer was added *via* syringe to the second flask which instantly turned the mixture black in color and was heterogeneous. This mixture was placed into an oil bath preheated to 90°C and allowed to equilibrate over the next 10 minutes while stirring.

The initial homogeneous styrene/Br-γCD solution was added rapidly to the second heterogeneous copper/styrene solution *via* a syringe while continuously stirring under a nitrogen environment. After ATRP was allowed to proceed for a given amount of time (arm length is a function of time), the reaction vessel was removed from the oil bath and the reaction solution precipitated into a beaker containing a 60/40 mixture of methanol/water (10 times the reaction volume). The solid was allowed to settle and then was collected.

Shorter reaction times (between 45 to 75 mins) produced very short armed-stars, which were soluble in methanol/water, therefore purification had to be by selective solvation. Chloroform was used to selectively solvate the star which was separated from the methanol/water by pipetting off the bottom solvent layer from the beaker. The collected layer of chloroform could then be evaporated to recover the solid.

Any recovered solid was dissolved in chloroform and twice filtered through basic alumina in order to remove residual copper. The collected elutant was then stirred with acid ion-exchange resin (Dowex Marathon, Dow Chemical Co.) for two hours and again filtered through basic alumina and directly precipitated into stirred methanol. The recovered off-white solid was air-dried overnight and then vacuum dried for 24 hours at 80°C and

500mtorr. All of the synthesized star molecules readily dissolved in chloroform giving homogeneous solutions.

An attempt was also made to synthesize a six-arm CD-star. However problems occurred due to the brominated intiatior not dissolving in the styrene monomer and sticking to the round-bottom flask or remaining suspended in the styrene. When ATRP synthesis was carried out on the suspension, the final product yield was very low rendering it impractical.

3.3.1. Kinetic Analysis of ATRP Polymerization

Living polymerizations, such as ATRP, are well controlled reactions having a linear relationship between the reaction time and the chain length.[29, 34] Figure 3.3 shows a first order kinetic plot for the CD-star polymerization, where M_o is defined as the initial monomer concentration and M is the remaining concentration of unpolymerized monomer. The remaining monomer M was found by subtracting the initial amount of monomer M_o from the quanity of styrene repeats found on the CD-stars by ^{1}H-NMR. This plot illustrates that the CD-star synthesis follows first order kinetic trends that are typical of ATRP.

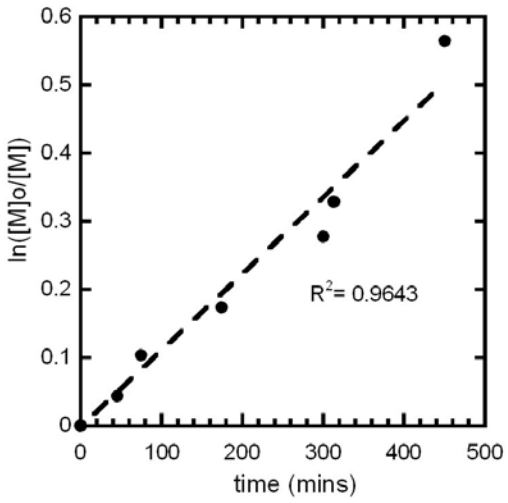

FIGURE 3.3. ATRP first-order kinetic plot for the synthesized CD-stars.

3.4. Molecular Structure Analysis

3.4.1. X-Ray Diffraction

It is well known that γ-CDs are able to arrange themselves into two types of crystal structures.[37] The first is a columnar structure where the CDs stack on top of each other aligning the cores to form a molecular tube. The second structure is a cage structure (the as-received structure) forming a herring-bone type morphology where the cores alternate and are perpendicular to one another. Since these structures are observed for γ-CD, then investigation into whether CD-stars have some type of structural order would be of interest in their characterization. This type of characterization might also be helpful to investigate whether some residual CD remains in the synthesized material and if either of these characteristic signature peaks for the crystals is observed for the stars.

To probe if a crystalline structure was formed in the synthesis of the CD-stars, powder x-ray diffraction (XRD) was conducted.[38] XRD patterns of as-received γ-CD and precipitated columnar γ-CD having the characteristic peaks of $2\theta = 7.5$ or $2\theta = 22$, respectively, were collected. These patterns were then compared to the XRD patterns of Br-γ-CD initiator and the shortest armed CD-star, PS_5-γ-CD, which has five styrene repeat units per arm (data not shown). No characteristic peaks from either the columnar or cage structures were discovered to align with the initiator or CD-star materials. In fact, the patterns for the XRD traces for these materials were very noisy and of low intensity, therefore concluding that the material was amorphous and does not contain any residual neat CD crystals.

3.4.2. Determination of Star-arm Number and DP *via* ^{1}H-NMR

ATRP initiator characterization was achieved with ^{1}H-NMR. The NMR spectra of our molecules were compared with the results of Schneider *et al,*[39] who completed a detailed analysis of cyclodextrins using NMR. Figure 3.4(A) presents a ^{1}H-NMR spectrum for γ-CD where the peaks were assigned from Schneider's work in d_6-DMSO. Likewise, in Figure 3.4(B), the ^{1}H-NMR spectrum is shown for the Br-γ-CD initiator in d_6-DMSO. Direct

comparison of γ-CD and Br-γ-CD peaks can now be made. Assessment of the NMR peaks was made and their assignments are also shown in (A) and (B), which includes insets of the relevant chemical structure. For the Br-γ-CD initiator in (B), if the area of the methyl proton peak associated with the bromine group, H-9, is compared to that of a CD core proton peak, H-1, then it is found and established that an average of twelve bromine groups modify each cyclodextrin. Therefore this gives twelve initiation sites that are available for star arm polymerization.

Area integration was also conducted on the remaining protons associated with the secondary hydroxyls on the Br-γ-CD initiator. A total of twenty-four hydroxyls are found on γ-CD where eight of these are primary hydroxyls and sixteen of these are secondary hydroxyls. Comparison of the secondary hydroxyls (OH-2, OH-3) to the H-1 proton in Figure 3.6(B) shows eight of the secondary hydroxyls remain unmodified. Based on a total of twelve bromine atoms modifying the CD, these results suggest that half of the secondary hydroxyls (or eight) are modified with bromine, and half of the primary hydroxyls (or four) are modified with bromine. Consequently, when polymerization is carried out, this will result in one side of the CD torus having eight arms and the other side having four arms. Thus, if a prediction is to be made on which side threading of a guest might take place, then it is reasonable that the primary hydroxyl side could be the prominent threading side due to only four arms being present.

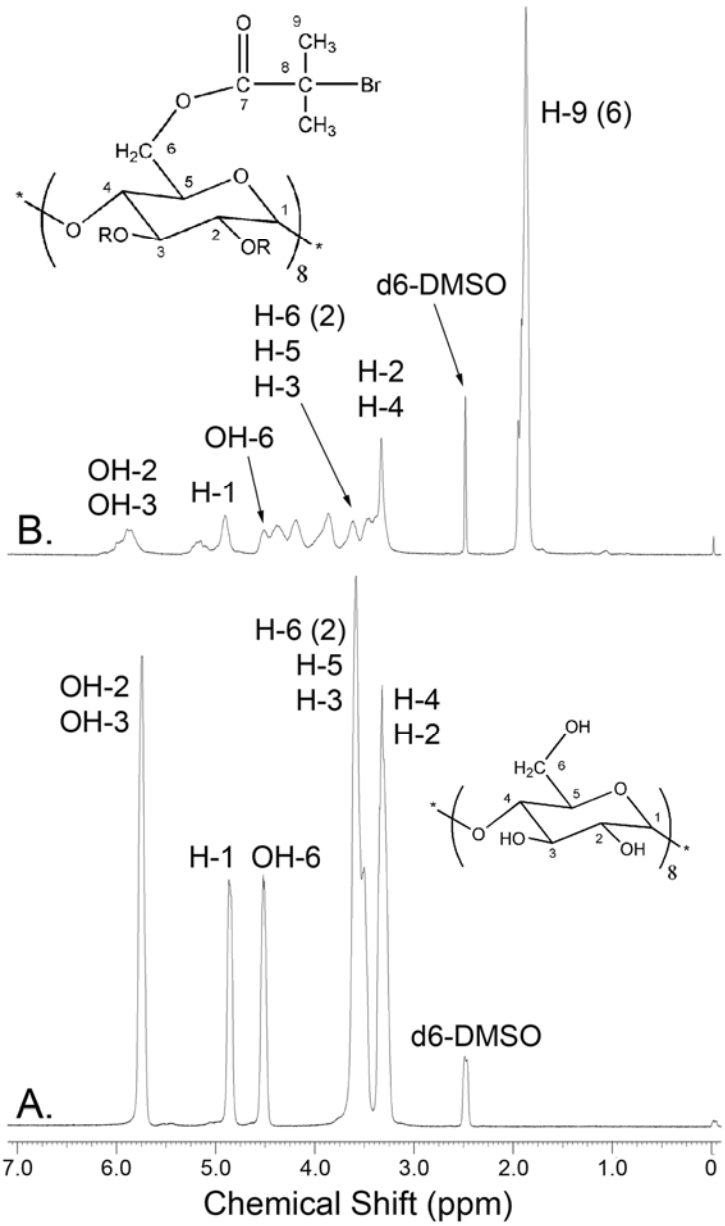

FIGURE 3.4. ^{1}H-NMR of A.) γ-CD, and B.) Br-γ-CD initiator.

Star arm lengths (or degrees of polymerization (DP)) were determined also using ^{1}H-NMR but in deuterated methylene chloride (CD_2Cl_2). Since it was established that bromine modifies an average of twelve hydroxyls on γ-CD, then it is known how many hydrogens (12arms X 6H's = 72H's) are responsible for the peak seen at ~0.9 ppm in Figure 3.5. This

peak can then be ratioed with the peaks at ~7.1ppm and ~6.8ppm, which are attributed to the number of protons on the styrene phenyl ring, to find the number of repeat units per arm.

Table 3.1 below shows the CD-star arm stoichiometry resulting from the ^{1}H-NMR analysis and the resulting molecular weights (M_n) of the CD-stars. The M_n of the CD-star takes into consideration the initial mass of the Br-γ-CD initiator, the number of arms attached, and the DP per arm. Furthermore, it should be noted that the sample nomenclature of the form "PS_x-γ-CD" designates a PS twelve armed γ-CD-star where the subscript "x" denotes the degree of polymerization of styrene per arm.

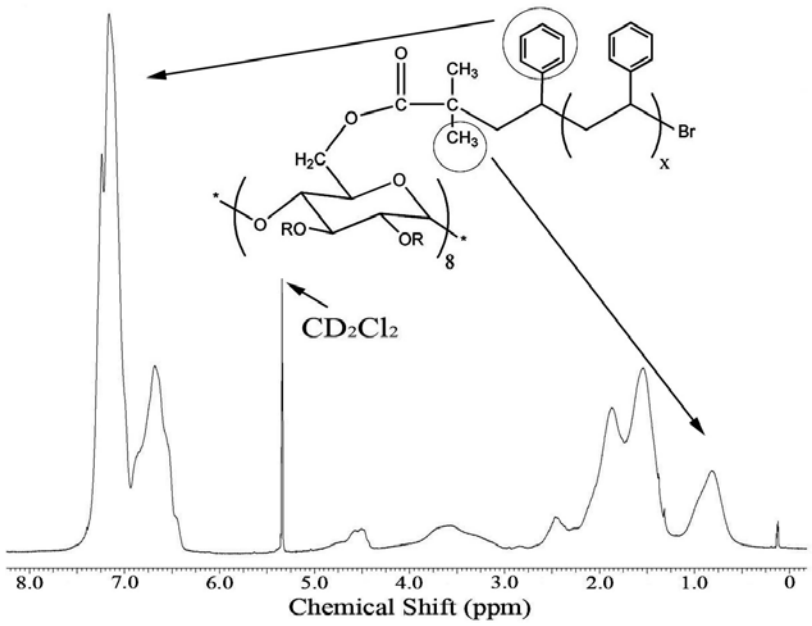

FIGURE 3.5. ^{1}H-NMR of PS_5-γ-CD star showing the peaks ratioed to determine arm length.

Other significant peaks seen in Figure 3.5 are mainly due to the PS, such as ~4.5ppm being from the hydrogen that is attached to the same carbon as the bromine,[36, 40] and 1.9ppm and 1.5ppm being due to the PS backbone hydrogens (-CH-) and (-CH_2-), respectively. The other

peaks observed between ~2.4ppm and 4.0ppm are attributed to the hydrogens attached to the cyclodextrin core.

TABLE 3.1. Molecular weights of the CD-stars found by ^{1}H-NMR.

Sample:	Br-γ-CD	PS_5-γ-CD	PS_{11}-γ-CD	PS_{19}-γ-CD	PS_{29}-γ-CD	PS_{51}-γ-CD
ATRP reaction time (mins)	n/a	45	75	174	300	450
DP/arm[a]	n/a	5.1	11.8	19.1	29.1	51.8
γ-CD core[b] (wt%)	41.69	13.60	7.21	4.77	3.26	1.90
γ-CD core[b] (mol%)	7.69	1.61	0.70	0.43	0.29	0.16
M_n (g/mol)	3085	9460	17800	27000	39500	67800

a. Degree of polymerization (DP) per arm calculated from ^{1}H-NMR data using solution samples having a concentration of ~55mg/ml in CD_2Cl_2.
b. Calculations of wt% and mol% are as follows: mole % γ-CD = [mols γ-CD / (mols styrene repeats + mols γ-CD)]*100; wt% γCD = [M_n γ-CD / (M_n star,^{1}H-NMR)]* 100. The M_n of γ-CD is *[1298 g/mol – 12 (hydrogen atoms)] = 1286 g/mol*, accounting for the attachment of 12 initiator/arm sites.

3.4.3. Chemical Structure Analysis Using FTIR and ^{13}C-NMR

Presented in Figure 3.6 are comparison FTIR spectra of (a) γ-CD and (b) PS, the major components making up the star, compared to (c) Br-γ-CD initiator and (d) PS_5-γ-CD star. The peak residing at 1278.8cm^{-1} in (c) (shown by the arrow) is considered to be the ester group interacting with the tertiary bromine two bonds away (–**O(C=O)**-C(CH_3)$_2$-**Br**). When ATRP polymerization occurs, this peak disappears in (d.) and is thought to shift and overlap with other PS and CD absorption peaks. Liu *et al.* also observed the disappearance of the 1278cm^{-1} band proceeding ATRP.[41] Another key shift that verifies a change in chemical environment is the carbonyl peak shown in (d) by the arrow. A shift in the carbonyl peak from 1739.6cm^{-1} to 1733.1cm^{-1} was noticed post-polymerization, as seen in (c) to (d) respectively. Additionally, the IR spectrum of PS_5-γ-CD in (d) shows that the individual

components making up the CD-star are present as evidenced by comparing it to the pure components of γ-CD, PS, and Br-γ-CD, shown in (a), (b), and (c), respectively.

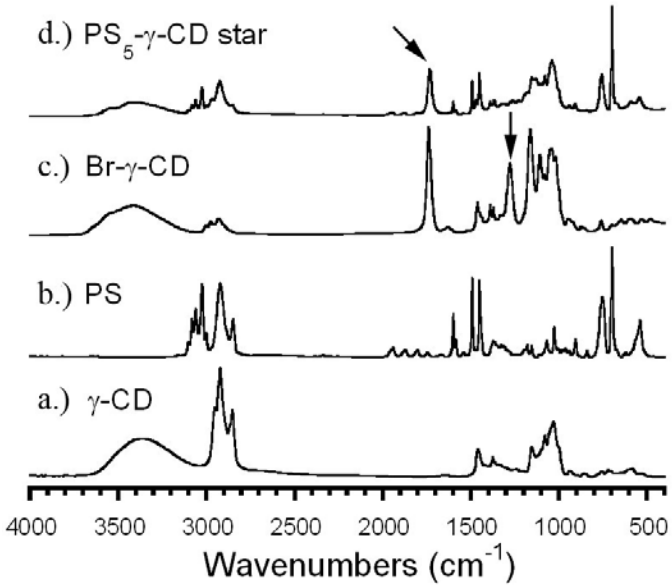

FIGURE 3.6. FTIR of a.) γ-CD, b.) PS, c.) Br-γ-CD initiator, and d.) PS_5-γ-CD star.

Verification of the observed carbonyl peak shifts can be accomplished by comparing model compounds of 2-bromoisobutyrylbromide (**Br-C(=O)-**$C(CH_3)_2$-Br), 2-bromo-2-methylpropionic acid (**HO-C(=O)-**$C(CH_3)_2$-Br), and 2,2-dimethylvaleric acid (**HO-C(=O)-**$C(CH_3)_2$-**CH_2-CH_2-CH_3**), having peaks of 1766.6cm^{-1}, 1713.1 cm^{-1}, and 1700.3 cm^{-1}, respectively. These compounds show a carbonyl shift to lower wavenumbers once the acid bromide (1766.6cm^{-1}) is converted to an acid (1713.1cm^{-1}) which is analogous to the synthesis of the Br-γ-CD initiator. From the acid (1713.1cm^{-1}), the tertiary bromine is removed and an aliphatic group is attached (1700.3cm^{-1}), which is analogous to polymerization of styrene *via* ATRP onto the Br-γ-CD. Therefore the identical peak shift trends are observed for the CD-stars confirming the expected chemical architecture.

Haddleton *et al*.[17] have reported FTIR spectra of brominated initiators made with β-CD and glucose which show very similar spectra to the Br-γ-CD spectrum that we collected. However, they did not report actual peak assignments of the synthesized CD-stars. Li and Xiao[13] do not show a FTIR spectrum for the bromine β-CD initiator they synthesized; however they do list wavenumbers of the major peaks which seem to be in good agreement with the peaks we observe.

^{13}C-NMR was used to investigate the chemical structure of the CD-star and the tacticity[42] of the star arms. Figure 3.7 shows the ^{13}C-NMR spectra for (A.) Br-γ-CD initiator, (B.) PS_5-γ-CD star, and (C.) PS_{29}-γ-CD star. The smallest armed star, PS_5-γ-CD, was primarily analyzed due to the higher concentration of CD being present within this star. The longer armed star, PS_{29}-γ-CD, is presented to emphasize the dilution effect of the longer PS arms on the CD-core.

In Figure 3.7(A) and (B), it can be seen that the C-9 methyl groups associated with Br-γ-CD, shifted up field from 30.9ppm to 24.9ppm, respectively, following ATRP attachment of the polystyrene arms on PS_5-g-CD. The peak associated with C-9 methyl groups at 30.9ppm in (A.) is not present in (B.) or (C.) for either of the CD-star spectra. This leads to the conclusion that all of the bromine initiator on the Br-γ-CD was involved with PS polymerization. If this was not the case, two peaks would be seen at 30.9ppm and 24.9ppm in (B.) or (C.) indicating incomplete substitution of the PS arms, but only one peak at 24.9ppm is observed. Additionally a down field shift is seen in (A.) and (B.) for the initiator carbonyl peak, C-7, from 170.8ppm to 176.3ppm, respectively. Again only one peak is observed for C-7 in (B.) and (C.) which is further evidence that all initiator sites reacted during growth of the PS arms.

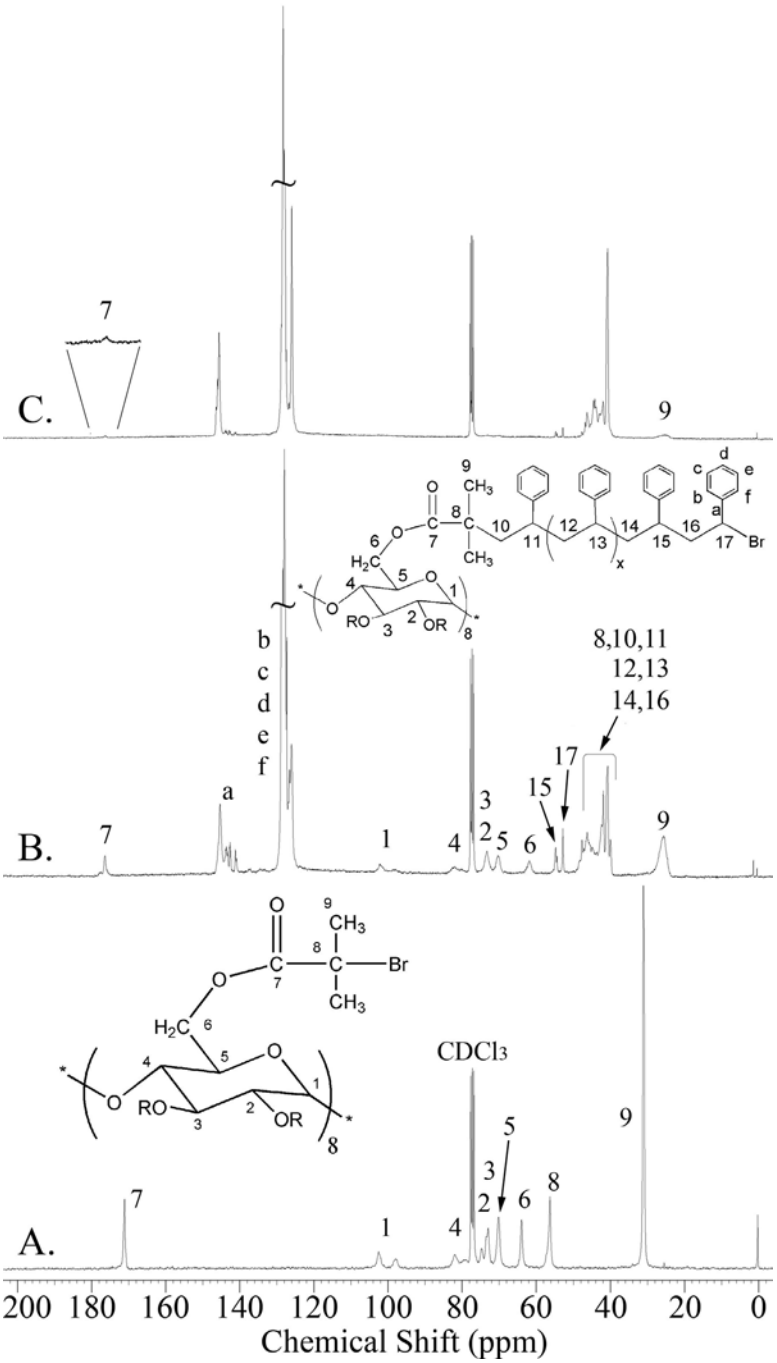

FIGURE 3.7. ^{13}C-NMR of (A.) Br-γ-CD, (B.) PS_5-γ-CD star, and (C.) PS_{29}-γ-CD.

Figure 3.7(C) shows some signs of the underlying γ-CD core structure for C-7 and C-9, but lacks the spectral details necessary to identify all the carbon peaks present. Therefore it

appears that when the star arm DP is greater than twenty-nine, the concentration of γ-CD is too dilute to successfully determine the chemical architecture using ^{13}C-NMR, as evidenced by the weak spectral peaks for the CD-core. While larger armed stars with low concentrations of γ-CD made it difficult to analyze the chemical structure by NMR, the shorter arm star did show the correct chemical structure. Thus, since all stars were synthesized in the same manner, a reasonable assumption is that all of the stars will contain the same underlying chemical architecture. These analyses indicate that the CD-stars were successfully synthesized and had the expected chemical structure.

Further information can be found for the CD-star arms in Figure 3.7(B) and (C). By analyzing the PS peaks grouped between ~41-45ppm in these figures, it can be determined that the PS arms are atactic. This was confirmed by comparing the stereosequence studies done by Sato and Tanaka,[43] and Kawamura *et al.*[44] in d-chloroform to our CD-star spectra in (B) and (C). The larger peak at 41ppm is due to the (-CH_2-) group in the PS backbone, whereas the peaks from 41-45ppm are due to the (-CH-) group of the PS backbone. If a sharp peak is observed ~44.5ppm then this signifies a syndiotactic morphology, whereas a peak observed at ~42.8ppm indicates an isotactic morphology. However, since we observe multiplets between 41-45ppm this establishes that the PS arms on the CD-stars are atactic.

3.4.4. Polydispersity Analysis of Stars

Gel permeation chromatography (GPC) was conducted on the CD-stars to measure the distribution of star sizes. These stars were compared to linear PS calibration standards. This method does not give exact molecular weights due to star structures being of a different architecture than linear chains, therefore, producing different hydrodynamic volumes compared to linear PS used in GPC calibration. On the other hand, it does give a relative comparison of the molecular weights and molecular size distribution between CD-stars. Figure 3.8 presents the GPC elution time traces for the stars as well as their relative

polydispersity indices (PDI). It can be seen that all of the stars have a narrow size distribution (PDI = $M_w/M_n \approx 1.1$) which is characteristic of ATRP reactions.[27]

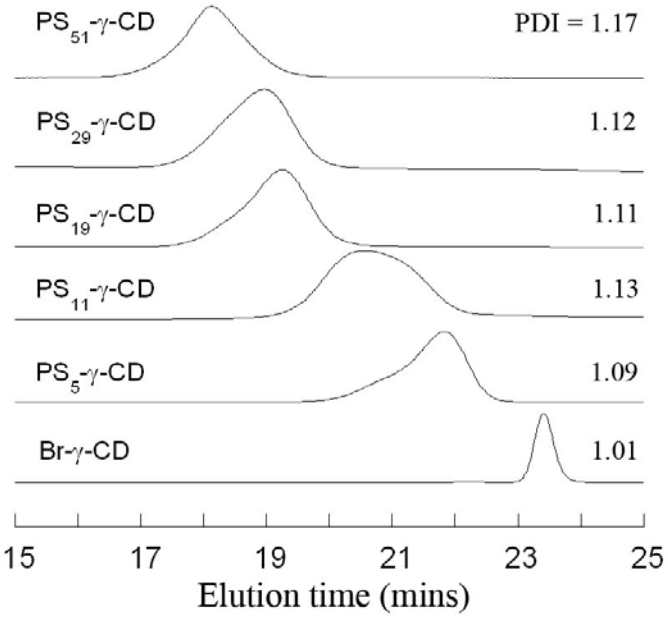

FIGURE 3.8. GPC elution time traces and polydispersity indexes (PDI) of stars.

In Table 3.2, the molecular weights (M_n) for the CD-stars from the GPC analysis are presented and compared to the calculated CD-star M_n from H^1-NMR analysis. It is noticed that GPC consistently gave a lower M_n than ^{1}H-NMR for all samples. As mentioned above, the star structure is compared to linear analogs in GPC analysis; therefore this comparison can give an insight to the reduction in the hydrodynamic volume for the stars with respect to linear PS. The disparity in M_n values confirms that the stars have an overall lower hydrodynamic volume (or higher core packing density) due to the convergence of arms connected to the CD core.

TABLE 3.2. Comparison of GPC and ^{1}H-NMR molecular weights for CD-stars.

Sample:	Br-γ-CD	PS_5-γ-CD	PS_{11}-γ-CD	PS_{19}-γ-CD	PS_{29}-γ-CD	PS_{51}-γ-CD
M_n, g/mol (^{1}H-NMR)	3085	9460	17800	27000	39500	67800
M_n, g/mol (GPC)	2050	5020	9100	21400	25200	36100
PDI (GPC)	1.01	1.09	1.13	1.11	1.12	1.17

3.5. Solution Property Analyses

3.5.1. Radius of Gyration Studies of Stars

To evaluate the radius of gyration (R_g) of the stars, a ratio of the star R_g to the linear R_g can be constructed which gives insight into the relative size disparities of the star polymer with respect to equivalent linear analogs. Equation 3.1, which defines the radius of gyration ratio, *g*, was derived by Zimm and Stockmayer.[45] The summation expression in equation 3.1 is based on a random walk calculation and finds a theoretical value of $g = 0.236$ for any 12 armed stars. It utilizes the actual arm length ($DP_{arm} = N_v$), the number of star arms (in this case $v = 12$), and the total number of polymer repeat units (N) for an equivalent linear M_n. However, this equation assumes that all star arms diverge from a single point that can be neglected in volume.

In our work, there are three ways in which the radius of gyration ratio, *g*, was found for the CD-stars: (1) dynamic light scattering (DLS), (2) gel permeation chromatography (GPC), and (3) *via* equation 3.1.

$$g = \frac{R_{g,star}}{R_{g,linear}} = \frac{< s^2 >_{star}^{1/2}}{< s^2 >_{linear}^{1/2}} = \sum_v \left[\frac{3N_v^2}{N^2} - \frac{2N_v^3}{N^3} \right] \text{---------- (3.1)}$$

In DLS studies, HPLC grade THF was used to solubilize the stars at the same temperature and concentration (25 °C at 1g/dl) that were used for the GPC analysis. The DLS data was found to reflect the apparent solubility of the stars in the solution. All solutions appeared clear and fully solubilized to the eye, however, the DLS data showed that the smaller armed stars tended to agglomerate in the solution whereas the larger armed stars illustrated better solubility. This is made clear in Table 3.3 where the standard error for each measured effective diameter (d_{eff}) is shown. For the smaller-armed stars the error observed is quite large indicating that these values are unreliable and agglomeration is taking place. For the larger armed stars, the d_{eff} values and their standard errors are within a reasonable range and are thereby thought to be fairly accurate (shown in bold in Table 3.3). Thus, the larger armed stars can be used for calculating and comparing R_g values of the stars to the linear analogs.

The relationship seen in equation 3.2, can be used to calculate the radius of gyration, $<s^2>_{lin}^{1/2}$, where M is the molecular weight of the polymer, M_b is average molecular weight per backbone bond of the polymer repeat unit, C_n is the characteristic ratio, and l is the bond length. For atactic PS, the characteristic ratio C_n is 9.85[46, 47], the bond length l is taken to be 1.54Å for a C-C bond, and M_b is 52.1g/mol (104.15g/mol ÷ 2 = 52.1g/mol).

$$R_g = (< s^2 >_{lin})^{1/2} = \left(\frac{Ml^2 C_n}{M_b 6} \right)^{1/2} \text{ ---------- (3.2)}$$

Table 3.3 lists the calculated g ratios using $R_{g,star}$ (= $d_{eff}/2$) from the DLS data in Table 3.3. The trend observed is a decreasing g ratio with increasing star arm length. This is thought to be due to the CD core contributing more to the overall size of the CD-star when the arms are shorter than its overall contribution when the arms are larger.

TABLE 3.3. Dynamic light scattering (DLS) data for CD-stars and the corresponding calculated *g* ratios.

Sample	d_{eff} (nm)	Std. Error	$\langle s^2 \rangle^{1/2}_{star,DLS}$ * (nm)	$M_{n\ star}$,H-NMR (g/mol)	$\langle s^2 \rangle^{1/2}_{lin}$ † (nm)	$g_{,DLS}$ ‡
PS_5-γ-CD star	8074	3031.9	--	9460	2.66	--
PS_{11}-γ-CD star	52.3	42.8	--	17800	3.65	--
PS_{19}-γ-CD star	**8.6**	0.2	4.3	27000	4.49	0.958
PS_{29}-γ-CD star	**8.8**	0.7	4.4	39500	5.43	0.810
PS_{51}-γ-CD star	**10.2**	0.1	5.1	67800	7.12	0.716

* $\langle s^2 \rangle^{1/2}_{star,DLS} = (d_{eff}/2)$

† Used equation 3.2 with $M_{n,star}$ (^{1}H-NMR) as linear equivalent.

‡ Used the following relationship for $g_{,DLS} = (\langle s^2 \rangle^{1/2}_{star,DLS})/ (\langle s^2 \rangle^{1/2}_{lin})$.

Since the GPC data provides M_n values based on linear PS standards, we can use this measured M_n value to estimate the R_g equivalent for the stars using equation 3.2 for linear polymers. In Table 3.4 below, the *g* ratios resulting from these calculations are shown. Conceptually, when *g* approaches 1, then the coil size of the star becomes equivalent to a similarly sized linear chain. However the CD-core dimension will be more prominent when the star arms are short causing a skewed *g* ratio to be calculated. Two inaccuracies arise when calculating the *g* values for the shorter armed stars: (1) when the star arms are short, the calculations to find the linear R_g using the M_n of the CD-star become artificially skewed to larger values due to a large weight fraction being made up of the CD-core (recall values in Table 3.1), and (2) equation 3.2 that finds R_g is not valid for the CD-core but was derived for linear polymers, thereby inducing false values of *g*. On the other hand, when the star arms become sufficiently long then the CD-core is diluted to a point where the added diameter from the CD-core becomes increasingly negligible.

TABLE 3.4. GPC data for CD-stars and the corresponding radius of gyration ratio (g) calculations comparing star and linear polymers.

Sample	$M_{n\ star,\ H\text{-}NMR}$ (g/mol)	$\langle s^2\rangle^{1/2}_{lin}$ * (nm)	$M_{n\ star,\ GPC}$ (g/mol)	$\langle s^2\rangle^{1/2}_{star,\ GPC}$ † (nm)	$g_{,GPC}$ ‡
PS_5-γ-CD	9460	2.66	5020	1.94	0.728
PS_{11}-γ-CD	17800	3.65	9100	2.61	0.715
PS_{19}-γ-CD	27000	4.49	21400	4.00	0.890
PS_{29}-γ-CD	39500	5.43	25200	4.34	0.799
PS_{51}-γ-CD	67800	7.12	36100	5.20	0.730

* Solved for using equation 3.2 with M_n,star (^{1}H-NMR) as linear equivalent.
† Solved for using equation 3.2 with M_n,star (GPC).
‡ The relationship used to solve $g_{,GPC} = (\langle s^2\rangle^{1/2}_{star,\ GPC})/(\langle s^2\rangle^{1/2}_{lin})$.

Interestingly, the *g* values for CD-stars with DP>19 from the DLS data in Table 3.3 correspond reasonably well with values calculated from the GPC data in Table 3.4, therefore lending more confidence to these calculated *g* ratios. However, the GPC data for the shorter armed stars do not fit the data set well and are subject to miscalculation due to the reasons stated earlier. In addition, the decrease in the *g* ratio observed for the larger armed stars (DP>19) is thought to be due to a decrease in the core packing effect giving rise to more of the PS component influencing the overall R_g.

Table 3.5 shows the *g* ratios that were calculated using Zimm-Stockmayer (ZS) equation 3.1. Both the arm length and M_n values are taken from the ^{1}H-NMR analysis of the CD-stars. This data set shows an increasing *g* with increasing arm length, which is opposite to what is experienced with the DLS and GPC data. However, this data does seem to be trending toward the theoretical value of 0.236 with increasing arm length which was predicted by Zimm and Stockmeyer. Furthermore, this method assumes that all of the arms converge to a single point, therefore not taking into account the CD core volume. This explains the

discrepancy of the smaller *g* values for the shorter armed stars and why the data seems to trend to 0.236 as the CD-core becomes more diluted and less significant.

TABLE 3.5. Zimm-Stockmayer radius of gyration ratios, g, for stars.

Sample	$N\nu$ (DP/arm)	M_n, ^{1}H-NMR (g/mol)	N (total repeat units)	$g_{,ZS}$ *
PS_5-γ-CD	5.1	9460	90.83	0.109
PS_{11}-γ-CD	11.8	17,800	170.91	0.164
PS_{19}-γ-CD	19.1	27,000	259.24	0.186
PS_{29}-γ-CD	29.1	39,500	379.26	0.201
PS_{51}-γ-CD	51.8	67,800	650.98	0.216

* Last part of equation 3.1 was used to solve for $g_{,ZS}$.

Figure 3.9 compares and illustrates the *g* ratios calculated from each method. Therefore it would be expected that if very large arms were to be attached to the CD-stars, then both methods (DLS and GPC) would exhibit decreasing *g* ratios until reaching the theoretical value of 0.236 which was predicted by Zimm and Stockmayer using equation 3.1.[45] Roovers *et al*.[48] found for a regular twelve-armed PS star the experimental value of *g* was 0.243 in toluene at 35°C ($M_n = 5.6 \times 10^6$ g/mol), which is very close to the 0.236 value predicted.

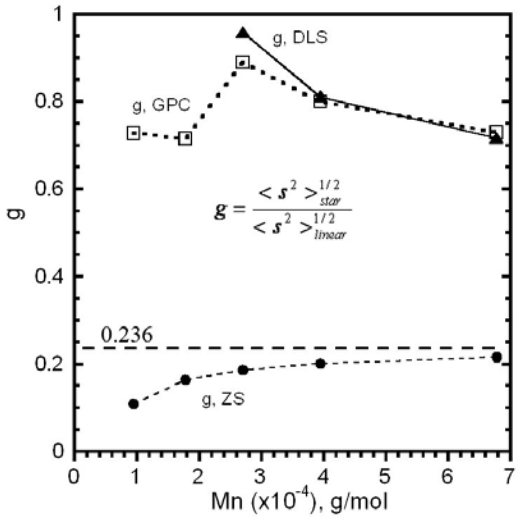

FIGURE 3.9. Plot comparing (g) for equal M_n of star and linear polymers using DLS data, GPC data, and calculated by ZS (equation 3.1).

3.5.2. Dilute Solution Viscosity Studies of Stars

Dilute solution viscosities of the CD-stars were measured in THF with a Cannon Ubbelohde viscometer (#25) designed specifically for low viscosity solutions. Additionally, all solutions were prepared just before introduction into the viscometer, and were filtered through a 1μm polytetrafluoroethylene (PTFE) syringe filter to remove any particulates. Once introduced into the viscometer, the solutions were maintained at 25° C in a large water bath. Intrinsic viscosities, [η], for the stars were found using the Huggins and Kraemer relationships[49] described in equations 3.3 and 3.4, respectively.

$$\frac{\eta_{sp}}{c} = [\eta] + k_H[\eta]^2 c \text{ ----------(3.3)}$$

$$\frac{\ln(\eta_r)}{c} = [\eta] + k_k[\eta]^2 c \text{ ----------(3.4)}$$

The variables within these equations are the specific viscosity η_{sp}, the relative viscosity η_r, the Huggins constant k_H, the Kraemer constant k_k, and the polymer concentration c. Figure 3.10

presents a representative plot used to find the intrinsic viscosity for CD-star DP = 51. The intrinsic viscosity is obtained as the average of the intercept values for the two fitted lines. All other samples were evaluated in a similar manner.

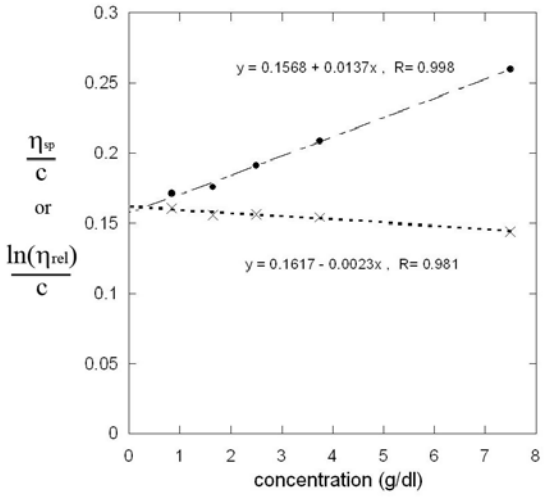

FIGURE 3.10. Representative viscosity measurement showing CD-star DP = 51. Data set (- • —) is fitted to equation 3.3, and (- × -) is fitted to equation 3.4 to find the intrinsic viscosity.

Intrinsic viscosity measurements were conducted on the stars to compare with their linear counterparts and to find the viscosity ratio, *g'*, shown in equation 3.5. To compare the viscosity of the stars to their linear analogs, the Mark-Houwink equation 3.6 was used to find the viscosity of the linear molecules, where κ and a are the Mark-Houwink parameters, and M_v is the viscosity average molecular weight. The molecular weight (M_v) chosen for the linear intrinsic viscosity calculations was from the star M_n ^{1}H-NMR data in Table 3.1 and is presented again in Table 3.6. Substitution of $M_v = M_n$ is reasonable due to the PDI of the stars being ~1.1 thereby $M_n \approx M_v \approx M_w$. The Mark-Houwink parameters for atactic PS (anionic polymerization) were referenced to be $\kappa = 13.63 \times 10^{-3}$ (ml/g), a = 0.714 in THF at 25° C.[46]

$$g' = \frac{[\eta]_{star}}{[\eta]_{linear}} \quad \text{---------- (3.5)}$$

$$[\eta] = \kappa M_v^{\ a} \quad \text{---------- (3.6)}$$

TABLE 3.6. Summary of CD-star intrinsic viscosities measured in THF at 25° C and some related values.

sample	$[\eta]_{star}$ (ml/g)	K_h	K_k	M_n,star (^{1}H-NMR)	$[\eta]_{linear}$* (ml/g)	g'
Br-γ-CD	2.19	1.251	0.209	3085	5.21	0.420
PS_{11}-γ-CD	5.94	0.312	-0.170	17800	19.05	0.312
PS_{19}-γ-CD	10.86	0.331	-0.144	27000	25.92	0.419
PS_{29}-γ-CD	12.54	0.534	-0.083	39500	34.35	0.365
PS_{51}-γ-CD	15.98	0.529	-0.090	67800	51.24	0.312

* Calculated using equation 3.6 with M_v being equivalent to M_n, star (^{1}H-NMR).

Table 3.6 shows that as the arm length of the CD-star increases, [η] increases. The g' values are also shown in this table and are between 0.312 and 0.420. This indicates that the hydrodynamic volume of the star is about 30 to 40% the volume of a linear chain of the same molar mass. The g' values we obtain are lower than the theoretical random-walk value for a twelve arm star that Graessley gives which is *g'* = 0.508.[50] Other researchers have measured symmetric twelve arm stars to show g' values between 0.335 to 0.370,[50] which is in good agreement with the values in Table 3.6.

The relationship between hydrodynamic volume and intrinsic viscosity is shown in equation 3.7 below where the variables are defined as $[\eta]$ is the intrinsic viscosity, N_A is Avagodro's number, V_h is the hydrodynamic volume, and M is the molar mass of the polymer.[49]

$$[\eta] = \left(\frac{5}{2}\right)\frac{N_A V_h}{M} \text{ ---------- (3.7)}$$

The observed Huggins (K_h) and Kraemer (K_k) constants from the viscosity measurements are also provided in Table 3.6. It has been said that as K_h gets larger, a trend toward being denser (or becoming more particle like) occurs for a dissolved polymer chain.[50] It was found by Roovers that as the number of arms increases, K_h becomes higher, reaching ~0.9 when the number of arms is ~55 (note: no molar masses were provided for this data).[50] For a twelve-arm star, K_h was found to have an approximate value of 0.68.[50] The K_h data for the CD-stars in Table 3.6 appear to be trending to the value of 0.68 as the arm length increases.

The viscosity data for the CD-stars can be combined with the elution volumes from the GPC measurements and the M_n values found from either the ^{1}H-NMR or GPC, to plot a universal calibration curve.[51] Figure 3.11 shows this plot with both CD-star and linear polymers. The plotted linear PS data set was used from the earlier GPC calibration where the linear chain [η] values were calculated via equation 3.6. This plot illustrates that the CD-star data sets follow the universal-calibration trend and do not behave differently than data from other star-polymers and polymers with other architectures.[51] In addition, the data points obtained from both ^{1}H-NMR and GPC M_n values appear to be in relatively good agreement with respect to the linear PS standards, indicating that both methods produce reasonable values.

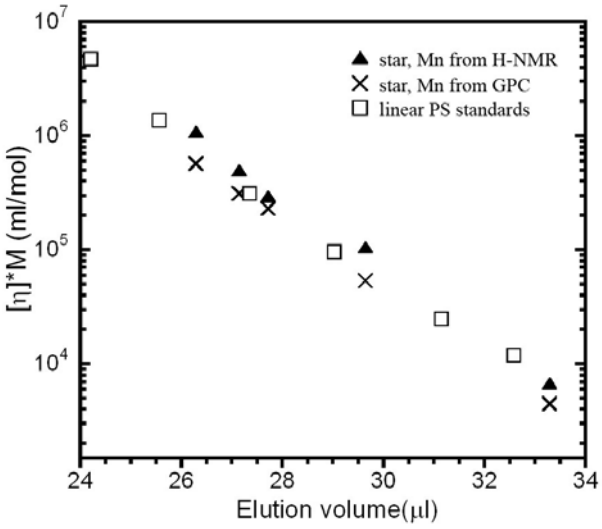

FIGURE 3.11. Universal calibration plot comparing PS-γ-CD stars with linear PS polymer standards.

3.6. Thermal Analysis of Stars

3.6.1. Glass Transition Temperature of Stars

The CD-star glass transition temperatures were compared to those of linear PS chains in order to inquire about any unique thermal properties. The Br-γ-CD initiator was examined by DSC (data not shown) and, as expected, did not exhibit a glass transition temperature (T_g) or a melting point (T_m). Furthermore it was discovered that all of the CD-stars exhibited glass transition temperatures, and surprisingly, even the shortest armed star with DP = 5 exhibited a T_g of 87° C. Increasing the arm length of the star tended to increase its T_g, as shown in Figure 3.12(A). Once the star-arms reached a DP of nineteen the arms behaved more like polystyrene having a T_g of around 100° C.

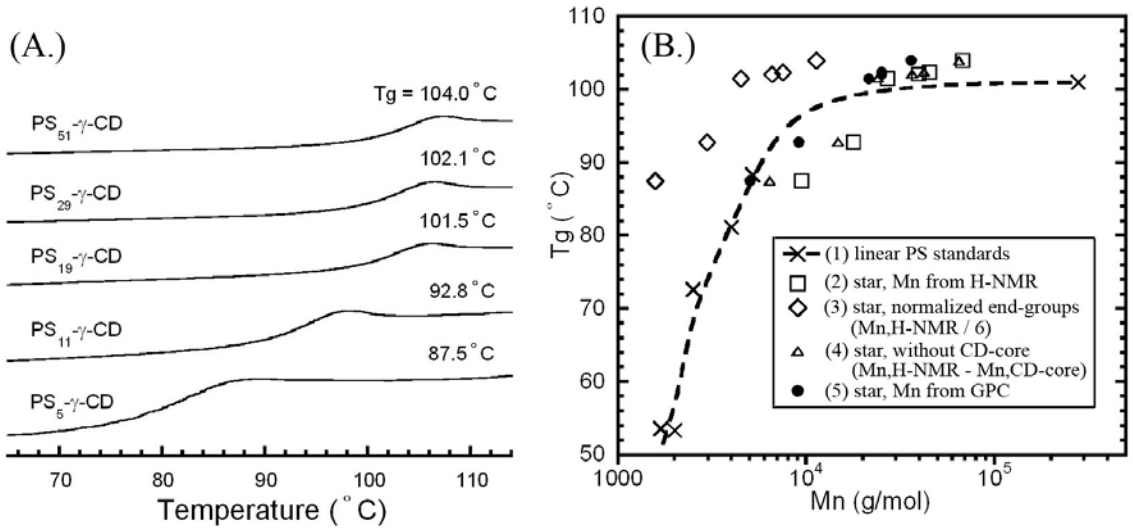

FIGURE 3.12. (A.) DSC traces showing T_g dependance with respect to CD-star arm length, and (B.) comparison of T_g data with linear PS standards, where the M_n of the star is found various ways (see text for details).

For comparision to the T_gs of the stars, PS standards with molecular weights similar to that of the star arms were analyzed. Figure 3.12(B) explores five data sets: (1) is linear PS standards, (2) uses the M_n from the ^{1}H-NMR analysis, (3) normalizes the twelve end groups on the CD-stars to linear chains by dividing the star M_n (^{1}H-NMR) by six, (4) subtracts the M_n of the CD-core from the M_n (H-^{1}NMR) of the star, and (5) uses the M_n from the GPC analysis. The linear PS standards were observed to follow a relationship found by Fox and Flory (dashed line Figure 3.12(B)) and shown in equation 3.8.[52]

$$T_g = T_{g_\infty} - \frac{Kn_e}{M_n} \quad \text{---------- (3.8)}$$

The variables in equation 3.8 are defined as the glass transition temperature T_g, the number average molar mass M_n, the glass transition temperature at infinite M_n $T_{g\infty}$, the number of polymer chain end-groups n_e (for linear polymers, n_e = 2), and K is defined by equation 3.9.[49] When viewing the data sets (2), (4), and (5), the slightly higher T_gs observed for the CD-stars

(DP>19) are probably a function of the arms being coupled to the CD, which prohibit certain thermal motions. This is in contrast to the slightly lower T_gs observed for CD-stars (DP<19), which are influenced more by the free volume contribution of the end groups which increases molecular mobility and lowers Tg.

However, for the most part, all data sets in Figure 3.12(B) have the same level of agreement with equation 3.8 except for set (3). Set (3) presents the star M_n divided by six in order to normalize the end-groups to directly compare to linear PS chains.[53] In this case, the data shifts to the left giving T_g values that are much higher with respect to linear M_n. To examine the end-group effect further, this data can be evaluated by looking at the T_g verses M_n relationship in equation 3.8.[49]

One limitation in using Equation 3.8 is that it is known to be valid only for low numbers of branches (or low n_e).[49] This is because the higher the branching, the higher the density at the cental branch point, therefore decreasing chain mobility and increasing T_g. The constant K is shown in equation 3.9 where the variables are defined as ρ, the density of the polymer, N_A, Avogadro's number, θ, the contribution of one chain end to the free volume, and α_f, the thermal expansion coefficient of the free volume.

$$K = \left(\frac{2}{M_n}\right)\left(\frac{N_A \rho \theta}{\alpha_f}\right) \text{---------- (3.9)}$$

By plotting T_g *vs* $(1/M_n)$ the constant K in equation 3.8 can then be found by fitting the data to a linear relationship. Figure 3.13 shows linear-fitted equations for the data sets examining (1) linear PS standards, (2) CD-stars with M_n from ^{1}H-NMR, (3) CD-stars with M_n from ^{1}H-NMR without the M_n of the CD-core ($M_n = M_{n,\,star} - M_{n,\,CD\text{-}core}$), and (4) CD-stars with M_n from GPC.

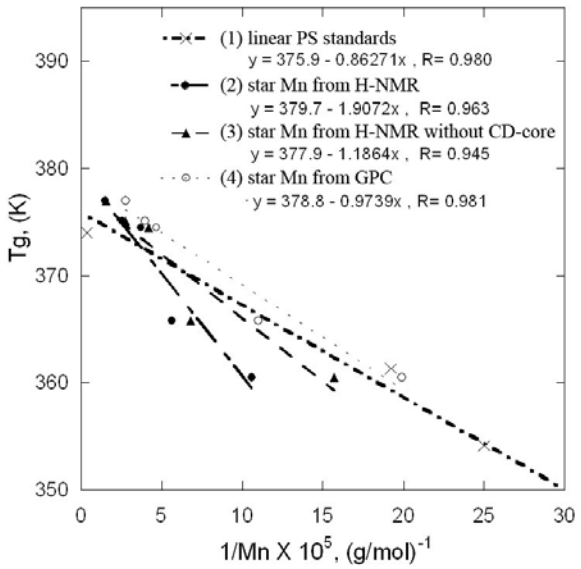

FIGURE 3.13. Plot of ($1/M_n$) vs. T_g for various sample sets. The various sample sets (1) to (4) are described in the legend, where each set shows the fitted linear equation.

For linear analogs of PS, Fox and Flory[52] give the empirical relationship $T_g = 373 - 100{,}000/M$, which corresponds to $K \bullet n_e = 100{,}000$. The value $K \bullet n_e$ that is found from the measured linear PS standards from our work, seen in Figure 3.13, has a value of 86,271 which is in approximate agreement with the Fox and Flory value of 100,000. All of the fitting parameters from these data sets are tallied in Table 3.7. It can be seen that the *K* values for the stars are 3 to 5 times less than the linear K values. In addition, $T_{g\infty}$ values for the stars are slightly higher than linear values.

TABLE 3.7. Linear-fitting values found from Figure 3.13 for equation 3.8.

	Fox-Flory*	Linear PS standards	CD-star (^{1}H-NMR)	CD-stars w/o core	CD-stars (GPC)
$T_{g,\infty}$	373	376	380	378	379
n_e	2	2	12	12	12
K	50,000	43,100	15,900	9800	8100

* From reference [52] for linear PS standards.

Typically, as the concentration of chain end-groups increases (M_n decreasing) the T_g decreases for the polymer. On the other hand, if the concentration of end-groups is very low (M_n high) T_g trends to a constant value noted as $T_{g\infty}$ in equation 3.8. This trend was observed by Roovers and Toporowski[53] who synthesized four and six armed PS stars and showed that the T_g of the stars decreased with increased branching. While their conclusion confirmed the dependence of T_g on the end-groups, they credited Meares with realizing that if a star with short enough chains were synthesized, then an effect opposite to the end-group effect might be found.

3.6.2. Thermal Stability

The thermal stability of the star is of interest due to the fact that thermal processing (either solution or melt) might be needed to introduce the CD-star compatibilizer into a polymer blend. Therefore it is important to know the temperature stability of the CD-star molecules. Thermal gravimetric analysis (TGA) was conducted to measure the degradation temperatures of the stars and to compare these temperatures to the individual components making up the stars. All measurements were conducted under a stream of nitrogen. Figure 3.14(A) presents derivative weight loss thermograms for all of the samples over the entire temperature range tested. Figure 3.14(B) and (C) show important expanded areas within this set of curves for easier analysis of the interesting regions that are attributed to the degradation of the CD-core and the degradation of the PS arms, respectively.

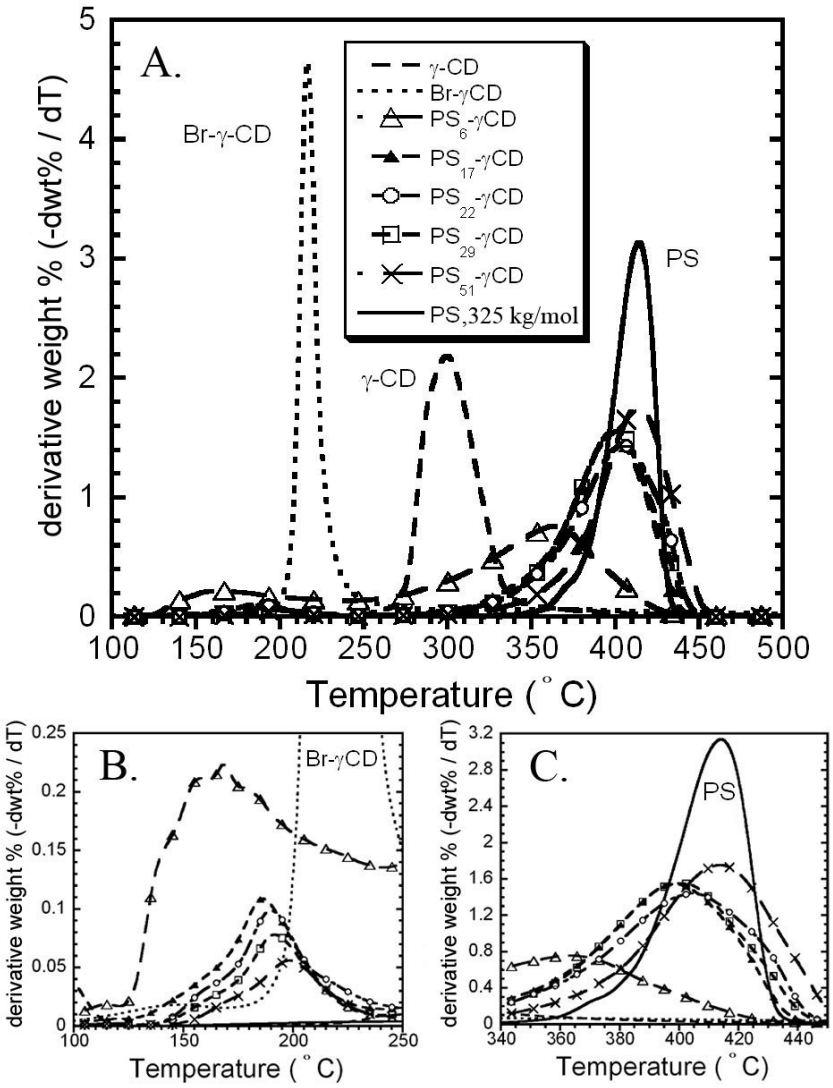

FIGURE 3.14. Comparative TGA derivative plots for various arm lengths of CD-stars where (A.) presents all of the data collected, (B.) shows an expanded low temperature regime focused on the CD-core fraction of the stars, and (C.) gives an expanded high temperature regime around the PS-arm/PS decomposion temperature.

Initial analysis of Figure 3.14(B) shows that the degradation temperature of the stars (starting at ~120° C) are much lower than that of the Br-γ-CD initiator (starting at ~180° C) and significantly less than the pristine γ-CD (starting at ~260° C). Additionally, a trend can be

seen that as the arm length of the CD-star increases, the magnitude of this degradation peak decreases. This trend was expected due to the longer arms diluting the quantity of CD within the overall star mass. For the temperature range of 260 to 340 °C, which is the degradation range for pristine γ-CD, no degradation peaks are observed for the CD-stars (expanded area not shown).

Figure 3.14(C) shows the expanded degradation region of PS. The trend observed within this region is, as the arm length of the CD-star increases, the peak area increases. This trend was also expected since the longer armed stars will contain a higher PS fraction in their total mass than smaller armed stars. Therefore, CD-stars show the expected trends with respect to CD-core and PS arm degradation fractions.

3.7. Conclusions

PS-γ-CD stars have been successfully synthesized containing atactic arms (therefore limiting self-threading) as evidenced by the FTIR, ^{1}H-NMR, and ^{13}C-NMR analyses. Control over CD-star arm length and number of arms was also accomplished. A monodisperse size distribution was observed for the CD-stars having a PDI of ~1.1. The radii of gyration of the synthesized stars are on average ~80% of the R_g for linear PS having similar M_n values, but the *g* ratio tends to decrease with increasing arm length as dilution of the CD-core becomes more substantial. Furthermore, as expected, the CD-stars were found to have viscosities that increase with increasing arm length. Universal-calibration analysis shows that the stars follow relationships typical of linear and star polymers very well.

For smaller armed stars, the end-group free volume affect is pronounced causing star T_gs to be less than that of linear equivalents. In addition, larger armed stars tend to have T_gs slightly greater than similar linear analogs, which can be attributed to the arms being tied on one end to the CD requiring more thermal energy to produce motions within the chain.

Additionally, thermal degradation of the stars starts at approximately 120° C, thereby limiting the thermal processing temperature of PS-γ-CD stars.

3.8. References

1. Singh, M.; Sharma, R.; Banerjee, U. C. *Biotechnology Advances* **2002,** 20, (5-6), 341-359.

2. Martin Del Valle, E. M. *Process Biochemistry* **2004,** 39, (9), 1033-1046.

3. Okumura, H.; Okada, M.; Kawauchi, Y.; Harada, A. *Macromolecules* **2000,** 33, (12), 4297-4298.

4. Porbeni, F. E.; Edeki, E. M.; Shin, I. D.; Tonelli, A. E. *Polymer* **2001,** 42, (16), 6907-6912.

5. Chen, W.; Chang, C.-E.; Gilson, M. K. *Biophys. J.* **2004,** 87, (5), 3035-3049.

6. Buschmann, H. J.; Denter, U.; Knittel, D.; Schollmeyer, E. *Journal of the Textile Institute* **1998,** 89, (3), 554-561.

7. Szejtli, J. *Starch-Starke* **2003,** 55, 191-196.

8. Huang, L.; Gerber, M.; Lu, J.; Tonelli, A. E. *Polymer Degradation and Stability* **2001,** 71, (2), 279-284.

9. Huang, L.; Taylor, H.; Gerber, M.; Orndorff, P. E.; Horton, J. R.; Tonelli, A. *Journal of Applied Polymer Science* **1999,** 74, (4), 937-947.

10. Lu, J.; Hill, M. A.; Hood, M.; Jr., D. F. G.; Horton, J. R.; Orndorff, P. E.; Herndon, A. S.; Tonelli, A. E. *Journal of Applied Polymer Science* **2001,** 82, (2), 300-309.

11. Kamiya, M.; Kameyama, K.; Ishiwata, S. *Chemosphere* **2001,** 42, (3), 251-255.

12. Sawunyama, P.; Bailey, G. W. *Journal of Molecular Structure (Theochem)* **2001,** 541, (1-3), 119-129.

13. Li, J.; Xiao, H. *Tetrahedron Letters* **2005,** 46, (13), 2227-2229.

14. Yang, C.; Li, H.; Goh, S. H.; Li, J. *Biomaterials* **2007,** 28, (21), 3245-3254.

15. Ohno, K.; Wong, B.; Haddleton, D. M. *Journal of Polymer Science Part A: Polymer Chemistry* **2001,** 39, (13), 2206-2214.

16. Kakuchi, T.; Narumi, A.; Matsuda, T.; Miura, Y.; Sugimoto, N.; Satoh, T.; Kaga, H. *Macromolecules* **2003,** 36, (11), 3914-3920.

17. Haddleton, D. M.; Kukulj, D.; Kelly, E. J.; Waterson, C. *Polymer Materials Science and Engineering* **1999,** 80, 145-146.

18. Miura, Y.; Narumi, A.; Matsuya, S.; Satoh, T.; Duan, Q.; Kaga, H.; Kakuchi, T. *Journal of Polymer Science Part A: Polymer Chemistry* **2005,** 43, (18), 4271-4279.

19. Karaky, K.; Reynaud, S.; Billon, L.; François, J.; Chreim, Y. *Journal of Polymer Science Part A: Polymer Chemistry* **2005,** 43, (21), 5186-5194.

20. Plamper, F. A.; Becker, H.; Lanzendörfer, M.; Patel, M.; Wittemann, A.; Ballauff, M.; Müller, A. H. E. *Macromolecular Chemistry and Physics* **2005,** 206, (18), 1813-1825.

21. Adeli, M.; Zarnegar, Z.; Kabiri, R. *European Polymer Journal* **2008,** 44, (7), 1921-1930.

22. Li, J.; Xiao, H.; Kim, Y. S.; Lowe, T. L. *Journal of Polymer Science Part A: Polymer Chemistry* **2005,** 43, (24), 6345-6354.

23. Li, J.; Modak, P. R.; Xiao, H. *Colloids and Surfaces A: Physicochemical and Engineering Aspects* **2006,** 289, (1-3), 172-178.

24. Miura, Y.; Narumi, A.; Matsuya, S.; Satoh, T.; Duan, Q.; Kaga, H.; Kakuchi, T. *Journal of Polymer Science Part a-Polymer Chemistry* **2005,** 43, (18), 4271-4279.

25. Stenzel, M. H.; Davis, T. P. *Journal of Polymer Science Part A: Polymer Chemistry* **2002,** 40, (24), 4498-4512.

26. Stenzel, M. H.; Davis, T. P.; Fane, A. G. *Journal of Materials Chemistry* **2003,** 13, 2090-2097.

27. Patten, T. E.; Xia, J.; Abernathy, T.; Krzysztof, M. *Science* **1996,** 272, (5263), 866-868.

28. Coessens, V.; Matyjaszewski, K. *Macromolecular Rapid Communications* **1999,** 20, (3), 127-134.

29. Matyjaszewski, K.; Xia, J. *Chemical Reviews* **2001,** 101, (9), 2921-2990.

30. Stenzel, M. H.; Davis, T. P.; Fane, A. G. *Journal of Materials Chemistry* **2003,** 13, (9), 2090-2097.

31. Larsen, K. L. *Journal of Inclusion Phenomena and Macrocyclic Chemistry* **2002,** 43, 1-13.

32. Tonelli, A. E. *Polymer* **2008,** 49, (7), 1725-1736.

33. Hunt, M. A.; Jung, D. W.; Shamsheer, M.; Uyar, T.; Tonelli, A. E. *Polymer* **2004,** 45, (4), 1345-1347.

34. Matyjaszewski, K.; Shipp, D. A.; Wang, J.-L.; Grimaud, T.; Patten, T. E. *Macromolecules* **1998,** 31, (20), 6836-6840.

35. Matyjaszewski, K.; Miller, P. J.; Pyun, J.; Kickelbick, G.; Diamanti, S. *Macromolecules* **1999,** 32, (20), 6526-6535.

36. Coessens, V.; Pintauer, T.; Matyjaszewski, K. *Progress in Polymer Science* **2001,** 26, (3), 337-377.

37. Harata, K. *Chemical Reviews* **1998,** 98, (5), 1803-1828.

38. Rusa, C. C.; Bullions, T. A.; Fox, J.; Porbeni, F. E.; Wang, X. W.; Tonelli, A. E. *Langmuir* **2002,** 18, (25), 10016-10023.

39. Schneider, H.-J.; Hacket, F.; Rudiger, V.; Ikeda, H. *Chemical Reviews* **1998,** 98, (5), 1755-1786.

40. Zhu, S.; Yan, D.; Zhang, G. *Polymer Bulletin* **2001,** 45, (6), 457-464.

41. Liu, C.; Wang, G.; Zhang, Y.; Huang, J. *Journal of Applied Polymer Science* **2008,** 108, 777-784.

42. Tonelli, A. E. *Macromolecules* **1979,** 12, (2), 252-255.

43. Sato, H.; Tanaka, Y.; Hatada, K. *Journal of Polymer Science: Polymer Physics Edition* **1983,** 21, (9), 1667-1674.

44. Kawamura, T.; Toshima, N.; Matsuzaki, K. *Macromolecular Rapid Communications* **1994,** 15, (6), 479-486.

45. Zimm, B. H.; Stockmayer, W. H. *The Journal of Chemical Physics* **1949,** 17, (12), 1301-1314.

46. Brandrup, J.; Immergut, E. H.; Grulke, A., *Polymer Handbook*. 4th ed.; A Wiley-Interscience Publication: Toronto, Canada, 1999.

47. Yoon, D. Y.; Sundararajan, P. R.; Flory, P. J. *Macromolecules* **1975,** 8, (6), 776-783.

48. Roovers, J.; Hadjichristidis, N.; Fetters, L. J. *Macromolecules* **1983,** 16, (2), 214-220.

49. Young, R. J.; Lovell, P. A., *Introduction to Polymers*. 2nd ed.; CRC Press: Boca Raton, FL, 1991; p 1-443.

50. Graessley, W. W., *Polymeric Liquids & Networks: Structure and Properties*. Garland Science: New York, 2004; Vol. 1, p 1-559.

51. Grubisic, Z.; Rempp, P.; Benoit, H. *Journal of Polymer Science Part B: Polymer Letters* **1967,** 5, (9), 753-759.

52. Fox, T. G.; Flory, P. J. *Journal of Polymer Science* **1954,** 14, (75), 315-319.

53. Roovers, J. E. L.; Toporowski, P. M. *Journal of Applied Polymer Science* **1974,** 18, 1685-1691.

4. SOLUTION COMPATIBILIZATION EFFECTS BETWEEN INCOMPATIBLE POLYMERS PS/PDMS AND PS ARMED γ-CYCLODEXTRIN STARS

4.1. Background

Solutions of incompatible polymers, such as polystyrene (PS) and polydimethylsiloxane (PDMS), commonly exhibit bilayer phase segregation,[1] or if rapidly mixed at high concentrations, an unstable turbid emulsion. However, incompatible blends can be encouraged to mix by the addition of a compatibilizing component that is designed to help bridge the interfacial energy variances between phases to stabilize the mixture.[2] PS and PDMS blended systems are no exception. Block copolymers made up of PS and PDMS (PS-*b*-PDMS) have been used in this fashion to physically bridge phases within PS and PDMS blends.[3, 4] Typically if block copolymers are added to a solution for compatibilization they take on a "surfactant-like" quality where one of the blocks is soluble and the other is not, forming a corona and core respectively. Abbas *et al*.[5] observed that block copolymers of PS-*b*-PDMS, in selective solvents, will self organize into micelles where they take the shape of vesicles, cylinders, or spheres, depending on solvent quality.

In our research, star polymers containing a γ-cyclodextrin (γ-CD) core with polystyrene arms will be blended as a compatibilizer into a solution of PS, PDMS, and chloroform. The core of γ-CD has the largest diameter of the three naturally occurring cyclodextrins with a cavity measuring 9.5Å.[6] This specific CD has been established to thread several polymers[7] into its core, including PDMS,[8, 9] which has a cross sectional diameter of 8Å.[10] The threading of the PDMS into the CD-core is the interaction which compatibilizes PDMS into the solution, while the PS arms on the CD-star enhances solubility. Figure 4.1 shows the structure and dimensions of PS,[11] PDMS, and PS armed γ-CD star (CD-star).

Previous work by Baulin *et al.* theoretically explored sliding ring CD-graft-copolymers, where they modeled surface interactions and micelle formation.[12, 13] Their work examined a CD graft-copolymer that is comprised of a polymer tail attached to one CD that is threaded onto one guest-polymer chain. The threaded polymer guest was then end-capped to prevent the CD-polymer from dethreading. Depending on solvent conditions, the CD-graft-copolymer unimers will aggregate to form small or large micelles. For example, if solvent conditions are such that the guest chain is preferentially solvated, and since the CD-polymers are trapped on the guest chain, then the CD-polymer will slide to one side of the guest allowing the guest to highly extend into the solvent. Agglomeration of the CD-polymers will form the micelle core and cause the highly extended unimers to produce a large micelle because of the longer backbone of the included polymer extending into the solvent. While micelle formation has been successfully modeled by Baulin *et al.* with a slip-ring CD-polymer, the model has not been experimentally verified. However, one caveat within this model is the threading of a single CD-polymer onto one guest-chain which is statistically very difficult. In practice, it is more likely that many CD-polymers will be threaded onto a single guest polymer.

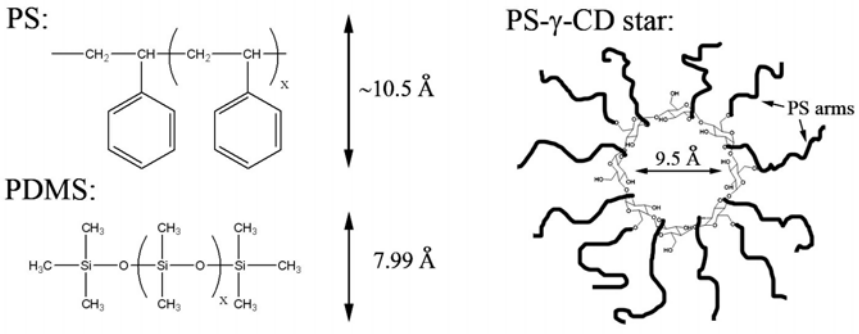

FIGURE 4.1. Structure of polystyrene (PS), polydimethylsiloxane (PDMS), and star polymer with a γ-cyclodextrin core and PS arms (CD-star).

Graft copolymers have shown micelle behavior in solution depending on the solvent quality established for either the backbone or grafts. The hydrodynamic diameters of these micelles have been demonstrated to be a function of the number of grafts, where the more grafts found,

the smaller the diameter.[14] If many grafts are introduced on the backbone, then unimolecular micelles are often formed.[15] Furthermore, lower chain aggregation numbers have been established for graft copolymer micelles, whereas block copolymers of the same molecular weight and composition will form micelles with higher aggregation numbers.[15]

Conceptually, in our work, many CD-stars will thread onto the PDMS creating an *in situ* slip-ring graft copolymer. The number of CD-stars (or slip-ring grafts) threaded onto the backbone will be dictated by the equilibrium conditions concerning the CD-star concentration, the PDMS concentration, and the interfacial energy between the PS/PDMS phases. This hybrid copolymer will essentially be made up of a backbone of PDMS with slip-ring grafts provided by the PS arms on the CD-star (PDMS-*graft*-(PS-CD-star)). The solvent selected in this study will be one which is preferential for PS, but poor for PDMS, thereby creating a rich environment for micelle formation. Figure 4.2 illustrates our working model, where the slip-ring graft-copolymer formation is thought to involve the following stages: (1) PDMS is introduced into the PS/CD-star solution and a PS/PDMS interface is formed to which oligomeric CD-stars will migrate, (2) concentration of the CD-star at the interface helps to initiate threading of PDMS, (3) threading of the CD-stars onto the PDMS takes place which breaks up the PDMS phase domain through CD-star arm compatibilization, (4) micelle formation occurs stabilizing the PDMS in the PS solution.

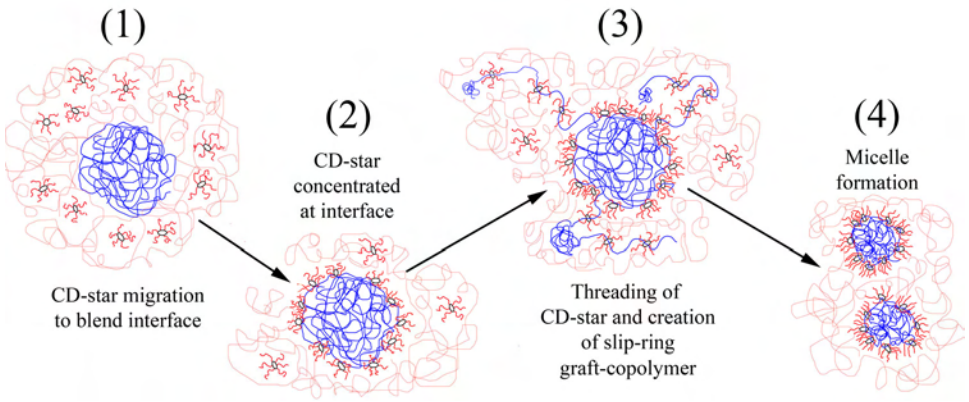

FIGURE 4.2. Stages of solution compatibilization and micelle formation with CD-stars.

Support for the conceptual formation of the PDMS-*graft*-(PS-CD-star) comes from a few important findings in polymer research. First, it has been established that for a compatibilizer to be successful it is important that it be capable of migrating to the phase interface and dissolve in both phases, which creates a thermodynamic environment that is more likely to form micelles.[2] Helfand and Tagami[16, 17] employed a self-consistent-field theory to demonstrate that oligomeric concentration at an interface will build up in order to lower the interfacial energy. This increase in oligomeric concentration at the interface has been found to apply to both polymer melts and concentrated polymer solutions.[18, 19] Furthermore, Helfand and Tagami, and Kajiyama *et al.*[20] showed that end-groups are more likely to be found at the phase interface,[21] which will result in an increased opportunity for the CD-stars to thread onto the PDMS. Finally, as pointed out previously, it is well established that graft copolymers will form micelles in a selective solvent. With the combined effects of CD-stars migrating to the interface, as well as a higher concentration of PDMS end-groups found at the interface, an environment conducive to PDMS threading into CD-stars is established. The incompatible polymers PS and PDMS will be effectively compatibilized by the physical tying of these two species together *via* the PS arms on the CD-star. These arms can then interact with the PS solution to stabilize the PDMS chain by the extension of the CD-star arms into the solution, thereby possibly forming a micellar structure.

Terminology that describes the final compatibilized structure as a micelle in Figure 4.2, stage (4), stems from the nomenclature for a copolymer micelle in a selective solvent.[22] The difference between a polymer micelle and a surfactant micelle is the thermodynamic nature of their formation. Development of a polymer micelle is an enthalpy driven process, whereas surfactant micelle formation is an entropy driven process.[22] Initially the blended solution in stage (1) is an unstable emulsion. However, after the addition of the CD-star, PDMS threads into the CD-core forming a slip-ring copolymer structure that can create a polymer micelle in select solvents. An argument could be made for the “micelle” to be instead termed a

microemulsion. Chevalier and Zemb report that there is no difference in nature between a micelle, reverse micelle, or a microemulsion.[23] Therefore, the aggregates formed in stage (4) of Figure 4.2 will be referred to as a micelle and this terminology will be used throughout this dissertation.

In this chapter we report our observations of turbid immiscible solutions of PS and PDMS becoming clear (compatibilized) when CD-star is added. Evaluation of the interaction parameters for the immiscible polymer system is conducted in an attempt to try to understand this clearing effect and the conditions under which clearing is observed. In addition, these cleared solutions are characterized by nuclear magnetic resonance (NMR) spectroscopy, viscometry, dynamic light scattering (DLS), and gel permeation chromatography (GPC) to validate the model in Figure 4.2.

4.2. Preparation of Solutions

4.2.1. Room Temperature Processing

Immiscible solutions of PS/PDMS *with and without* CD-star were prepared at concentrations of 10g/dl in chloroform. Rapid stirring was employed using a PTFE coated magnetic stirbar in an appropriately sized vial (typically 2 dram) and was heavily sealed with PTFE tape around the vial threads to minimize solvent evaporation. An ink mark was placed on the vial directly on the solvent line to determine if more solvent needed to be added due to evaporation. The prepared solutions were placed on a stirplate on the laboratory bench at room temperature and stirred constantly for up to 2 months.

4.2.2. Heat Processing

Identical sample preparation was implemented as stated in section 4.2.1 with the exception that the vials were additionally sealed with electrical tape around the cap edge and placed into a 250ml beaker that was partially submersed in an oil bath at 60° C. Again the solutions were rapidly and continuously stirred between 2 to 4 days. After heating the vials, the samples were removed from the beaker and cooled to room temperature.

4.3. Effect of CD-Stars on Compatibilization of PDMS and PS

Compatibilization of PS and PDMS solutions was accomplished by the addition of a star polymer containing twelve polystyrene arms with a γ-cyclodextrin core. Table 4.1 lists the mass compositions for the blended samples. It should be noted that whenever the sample composition changes (eg. more PDMS is added) then PS is removed to keep the total solids mass constant at 500mg. Also it should be noted that the term "1 wt% CD-core" refers to 5mg of γ-CD within a total sample mass of 500mg. This disregards the arm mass of the CD-star and only takes into consideration the CD-core. Samples containing PDMS were prepared with molecular weights of 62kg/mol (PDMS-62) or 308kg/mol (PDMS-308) in order to learn if molecular weight changed the compatibilization outcome.

TABLE 4.1. Mass compositions for sample blends containing 1 wt% CD-core with varying PDMS content.

sample	CD-star* (mg)	PDMS† (mg)	PS‡ (mg)	Total mass (mg)
0 wt% PDMS	40.3	0	459.7	500.0
1 wt%	40.3	5	454.7	500.0
5 wt%	40.3	25	434.7	500.0
10 wt%	40.3	50	409.7	500.0
20 wt%	40.3	100	359.7	500.0

* CD-star, in this case, refers to PS_6-γ-CD which has 12 PS arms of DP = 6 with a γ-CD core. The molecular weight of the star is 10,460 g/mol with a GPC found PDI = 1.12. Each sample containing 1wt% CD-core has 3.85 X 10^{-6} moles of star (for a 500 mg sample) which is a molar equivalent of 5mg of pristine γ-CD.

† Two molecular weights (M_w) of PDMS are used in this work, 62.7 or 308 kg/mol. The manufacturer claims a typical PDI ≈ 2 to 3, for both samples.

‡ The PS molecular weight (M_w) is 325 kg/mol with a PDI = 2.95, as found by GPC.

All chloroform solutions containing PS and PDMS (with and without CD-star) were initially observed to be incompatible and cloudy at a concentration of 10g/dl. Solution clearing for the CD-star samples was seen to take place *via* two processing methods: (1) heating the solution for ~2-4 days at 60° C, or (2) letting the solution stir at room temperature for ~1-3 weeks. Non-star containing solutions did not clear under either of these processing methods. All visual observations of clearing or turbidity were mutually observed for both molecular weights of PDMS. The CD-star containing solutions were observed to clear after processing, suggesting that either intimate blending has occurred or the PDMS domain size decreased to less than 500nm thereby not scattering visible light. Due to the extreme chemical incompatibility of PS and PDMS,[24] the latter explanation is more likely.

The initial method of sample processing involved heating the prepared solutions to 60° C, with varying amounts of PDMS (1 to 20wt%), in chloroform while leaving the star amount constant (1wt% CD-core). Images in Figure 4.3 compare solutions *with and without* CD-star before and after heat processing. It was observed that after heating for two days, the samples containing 1-10wt% PDMS cleared but the 20wt% sample remained slightly turbid. After four days of heating, the 20wt% PDMS sample cleared as well. Once the samples were finished heating, the cleared solutions were allowed to cool to room temperature. The solutions containing CD-star were observed to be stable and to remain so for several months, whereas the samples without star molecules remained turbid and segregated into bilayers shortly after cooling to room temperature. These results suggest that compatibilization has occurred with the addition of CD-star due to the long-term stability of the solution (no bilayer formed over time) and the final dispersed PDMS droplets being smaller than 500nm, as evidenced by the lack of light being scattered.

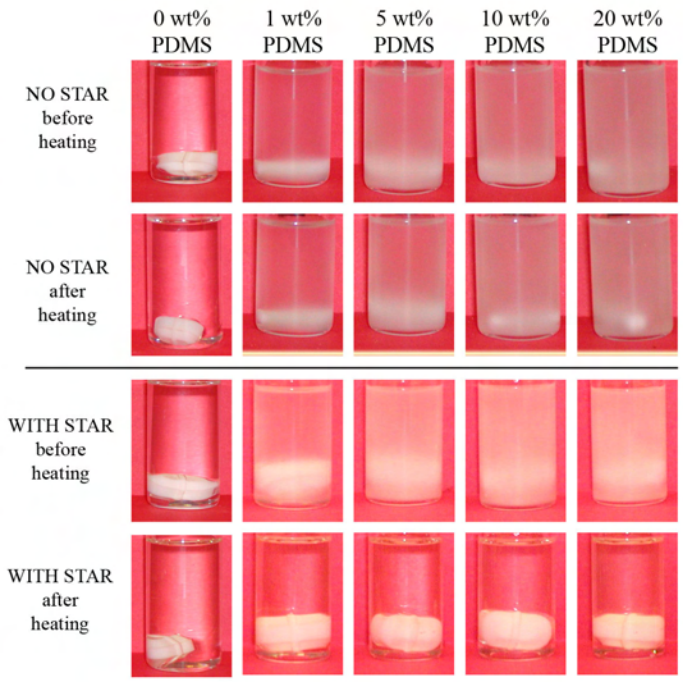

FIGURE 4.3. Blended solutions of PS and PDMS in chloroform containing no star and with CD-star before and after heating to 60° C. The white Teflon coated magnetic stir bar on the bottom of the vials can be used to gauge solution clarity.

This clearing effect was again seen for the CD-star containing solutions stirred at room temperature, as can be viewed in Figure 4.4. For room temperature processing, the clearing of the solutions required more time (6 to 16 days) depending on the amount of PDMS added. This is in contrast to the 2-4 days it took to observe clearing for the heat processing method at 60° C. However the clearing of these solutions at room temperature indicates there is a sufficient enthalpic driving force for threading of the CD-core[25, 26] onto the PDMS guest. Like the heat-processed samples, the room temperature processed samples were stable at room temperature and did not show bilayer phase segregation.

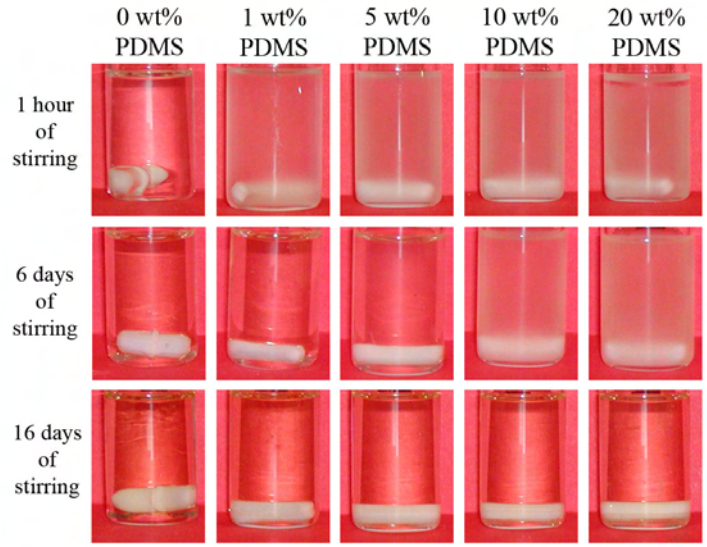

FIGURE 4.4. All solutions above were stirred at room temperature and contained a constant CD-star amount (1wt% CD-core) with varying amounts of PDMS (308 kg/mol). The white Teflon coated magnetic stirbar on the bottom of the vials can be used to gauge solution clarity.

The disparity between the clearing times of the two processing methods might be due to the increased mobility that chains experience at elevated temperatures thus affecting their threading kinetics. Also the expansion of the CD cavity at high temperatures may cause more room for easier and earlier PDMS threading. It has been shown by Cameron and Cooper[27] that β-CD has a higher thermal expansion coefficient for an empty cavity than for a guest-filled cavity, where these results almost certainly translate to γ-CD as well. Together these effects offer a plausible explanation for the increased rate at which the clearing takes place at higher temperatures.

Since this clearing effect was seen for the three component blend of PS/PDMS/CD-star, an experiment was performed that removed the PS homopolymer from the blend. Again the CD-core was held constant at 1wt% (compositional mass remains the same for CD-star and PDMS, as seen in Table 4.1, but without PS) and the concentration of the solutions remained at 10g/dl in chloroform. Figure 4.5 shows images of the 2-component blend solutions. After two days of heating at 60° C, no solution clearing for the 2-component system was observed

for any of the samples. In light of these results, the appropriate amounts of PS and $CHCl_3$ were added to the 2-component solutions, now making them a 3-component system, to inquire if clearing would still take place. Initially upon adding the PS and $CHCl_3$ (to achieve 10g/dl) all of the solutions remained turbid. These samples were again heated for two days at 60° C where it was observed that the clearing of the solutions did in fact take place once more, as can be seen in Figure 4.5.

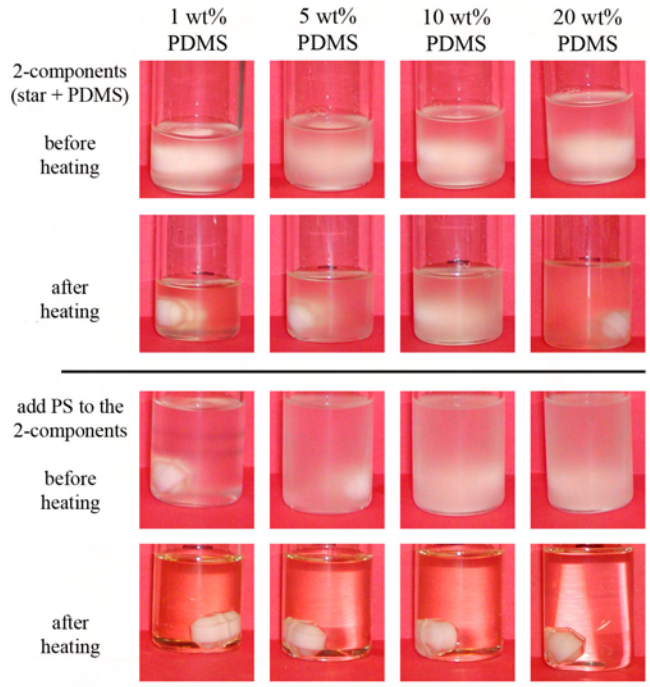

FIGURE 4.5. The images above probe whether a 2-component blend (CD-star and PDMS only) will clear in solution. It is observed that no clearing of solutions is accomplished for a 2-component blend. If PS is added to the 2-component mixture, and again heated, clearing of the solution results. All solutions above maintain a concentration of 10g/dl in chloroform. The white Teflon coated magnetic stir bar on the bottom of the vials can be used to gauge solution clarity.

The observed clearing of the CD-star solutions is particularly significant when considering the molar ratios of CD-star to PDMS shown in Table 4.2. For example, if all CD-stars threaded onto PDMS for a 20wt% PDMS-308 sample, then this would provide only 12 CD-

star “grafts” per PDMS chain, which is only 1% of the total PDMS repeats being covered by CD-star. Considering that only a small amount of CD-star needs to be added to accomplish compatibilization, then this may speak to the practicality of using this method for compatibilizing immiscible blends such as PS and PDMS.

TABLE 4.2. Relative molar ratios of CD-stars to PDMS.

	Amount of PDMS			
	1 wt%	5 wt%	10 wt%	20 wt%
CD-stars : PDMS chains using PDMS-308, (mol/mol)	237 : 1	47 : 1	24 : 1	12 : 1
CD-stars : PDMS chains using PDMS-62, (mol/mol)	48 : 1	10 : 1	5 : 1	2.5 : 1
CD-stars : PDMS repeats (mol/mol)	1 : 18	1 : 88	1 : 175	1 : 350
PDMS repeats not covered by CD-star† (mol%)	82.9	96.6	98.3	99.1

† calculated by [1 – ((moles CD-stars x 3) ÷ (moles PDMS repeats))] x 100.

4.3.1. Confirmation of PDMS Threading in Compatibilized Solutions

^{1}H-NMR experiments were conducted in order to probe if any localized interactions could be identified that confirm PDMS threading. A set of solutions were prepared in deuterated chloroform ($CDCl_3$) in which the amount of CD-star (PS_6-γ-CD) was varied within the blend while leaving the PDMS-308 amount constant at 1wt%. These sample compositions are shown in Table 4.3. Blends with 1wt% PDMS were used to maximize interactions between CD-star and PDMS (more CD-star per PDMS chain). These blends were heat processed at 60° C for two days and all solutions were observed to clear.

TABLE 4.3. Compositions of solutions prepared in $CDCl_3$ for ^{1}H-NMR analysis.

Sample: CD-core (wt%)	CD-star (mg)	PDMS-308 (mg)	PS (mg)
0.2	8.2	5.0	486.8
0.6	24.7	5.0	470.5
1	40.3	5.0	454.7

Figure 4.6 shows the ^{1}H-NMR spectra for these compatibilized blends. Since the amount of CD-star in the blends was low, it was difficult to recognize the CD-star signals due to the majority of the signal strength belonging to the PS homopolymer. Other researchers who have investigated PDMS and γ-CD inclusion compounds used ^{13}C-NMR to characterize the inclusion of PDMS into γ-CD,[8, 28] but due to the very low mass of CD-core incorporated within the blends, this technique was not possible. For the samples examined by ^{1}H-NMR, shown in Figure 4.6, a small peak due to the PDMS is seen at ~0.2 ppm, whereas no CD-star peaks can be seen from 2.5ppm to 4.5ppm. An expanded PDMS region for each sample is also shown within this figure. Peaks at ~7.1ppm and ~6.8ppm are attributed to the styrene phenyl ring and peaks at 1.9ppm and 1.5ppm are due to the PS backbone hydrogens (-CH-) and (-CH_2-), respectively.

It can be seen in Figure 4.6 that the PDMS peak at ~0.2ppm decreases and broadens with increasing CD-core amount. This might be an indication that threading of the PDMS into the CD-star is occurring. As more threading interactions between PDMS and the CD-core take place, the PDMS segments in the CD cavity are found in a different environment than the PDMS/PDMS interactions, which is indicated by the broadening of the PDMS peak.

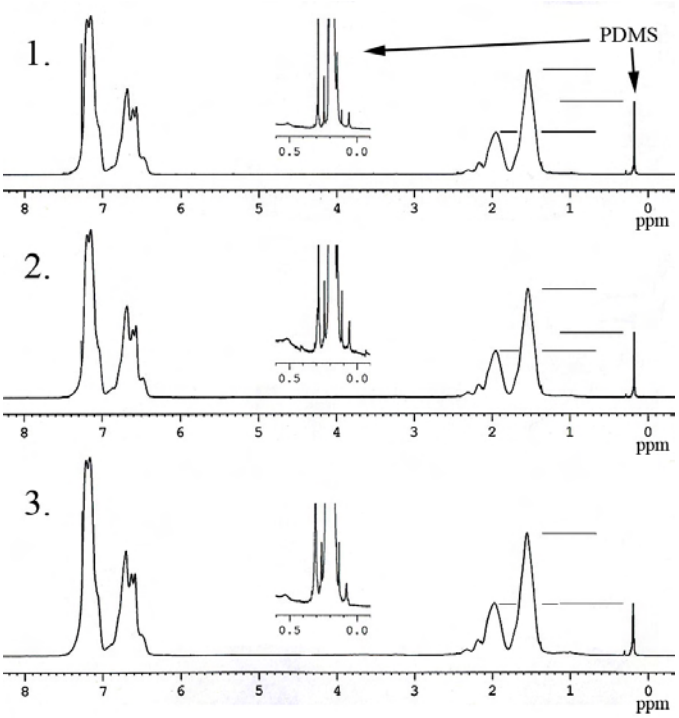

FIGURE 4.6. ^{1}H-NMR spectra for PS and PDMS blends containing 1wt% PDMS-308 with (1) 0.2wt% CD-core, (2) 0.6wt% CD-core, and (3) 1wt% CD-core.

If the CD-star spectral area between 2.5ppm and 4.5ppm is magnified for the samples seen in Figure 4.6, then peaks emerge that belong to the CD-core, as can be seen in Figure 4.7(B-D). Figure 4.7(A) shows the full spectrum for the sample with 1wt% CD-core and shows the expanded area in which CD-core resonances occur. For these compatibilized blends, it was observed that as the CD-core amount increases, an increasing baseline curvature occurs as observed in Figure 4.7(B-D). This baseline curvature effect is probably an indication of a more prohibitive and confined environment for the CD hydrogens, however, this observation is not fully understood.

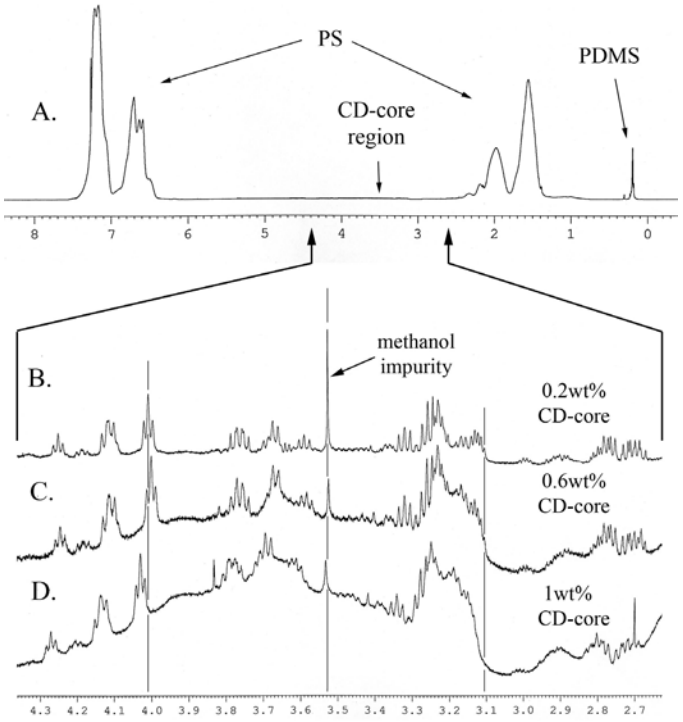

FIGURE 4.7. (A.) Typical ^{1}H-NMR spectra of compatibilized CD-star blends. For (B.-D.) these spectra show an expanded CD-core region for samples containing 0.2wt%, 0.6wt%, and 1wt% CD-core, respectively. Vertical lines were drawn to emphasize peak shift occurance.

In addition, several down-field peak shifts in Figure 4.7(D) were observed with increasing CD-core amounts. It was observed by Ma and coworkers that when pluronics form micelles they induce up-field peak shifts and broadening for the propylene oxide (PO) peaks due to the confinement of the retracted core which is an indication of an increasingly shielded environment.[29] However, in a separate study by Ma *et al.* they observed that when urea was added to a pluronic solution then down-field shifts occur indicating deshielding for ethylene oxide (EO) and PO groups.[30] They attributed these down-field shifts to an increased hydration of the EO and PO groups. Based on these findings, two scenarios might be the cause for the down-field shifts observed for our sample in Figure 4.7(D). First, the oxygen groups in the PDMS backbone may interact with the hydrogens on the CD-core (possibly the free hydroxyl groups unmodified with PS arms) causing a deshielding effect, or second,

water that is complexed within the CD cavity is released by the threading of the PDMS. Either water or PDMS can interact with the remaining (unmodified) hydroxyl groups on the CD-core. Because of these reasons, the down-field shifts that we observe might be due to the PDMS guest interacting with the CD cavity.

Rotating frame Overhauser effect spectroscopy (ROESY)[31] 2D-NMR was performed to confirm whether the PDMS guest was threaded in the CD cavity. Several researchers have used this technique to see localized guest interactions in CDs. Tellini and coworkers saw proton-proton interactions between the β-CD H-3 and H-5 core protons and the di-adamantyl acetic acid (Ad_2) guest in D_2O confirming the inclusion of the guest in the β-CD cavity.[32] Whang *et al.* saw cross peaks from H-3, H-4, H-5, and H6 protons on the β-CD with that of the guest cloprostenol indicating inclusion into the cavity.[33] Furthermore a novel β-CD-(PEG)-β-CD was complexed with a guest of bisadamantane-PEG-dimer (Ad-PEG), and ROESY was used to determine that the H-3 and H-5 protons for the β-CD coordinated with Ad-PEG within the cavity.[34] ROESY has also been successfully used with γ-CD to correlate the guest to the cavity, where again, H-3 and H-5 protons were seen to interact with flavonol kaempferol.[35] These findings are just a few examples illustrating the use of ROESY NMR to correlate interactions with CD inclusion complexes, where it is apparent that a common guest interaction with the CD cavity is with the H-3 and H-5 protons.

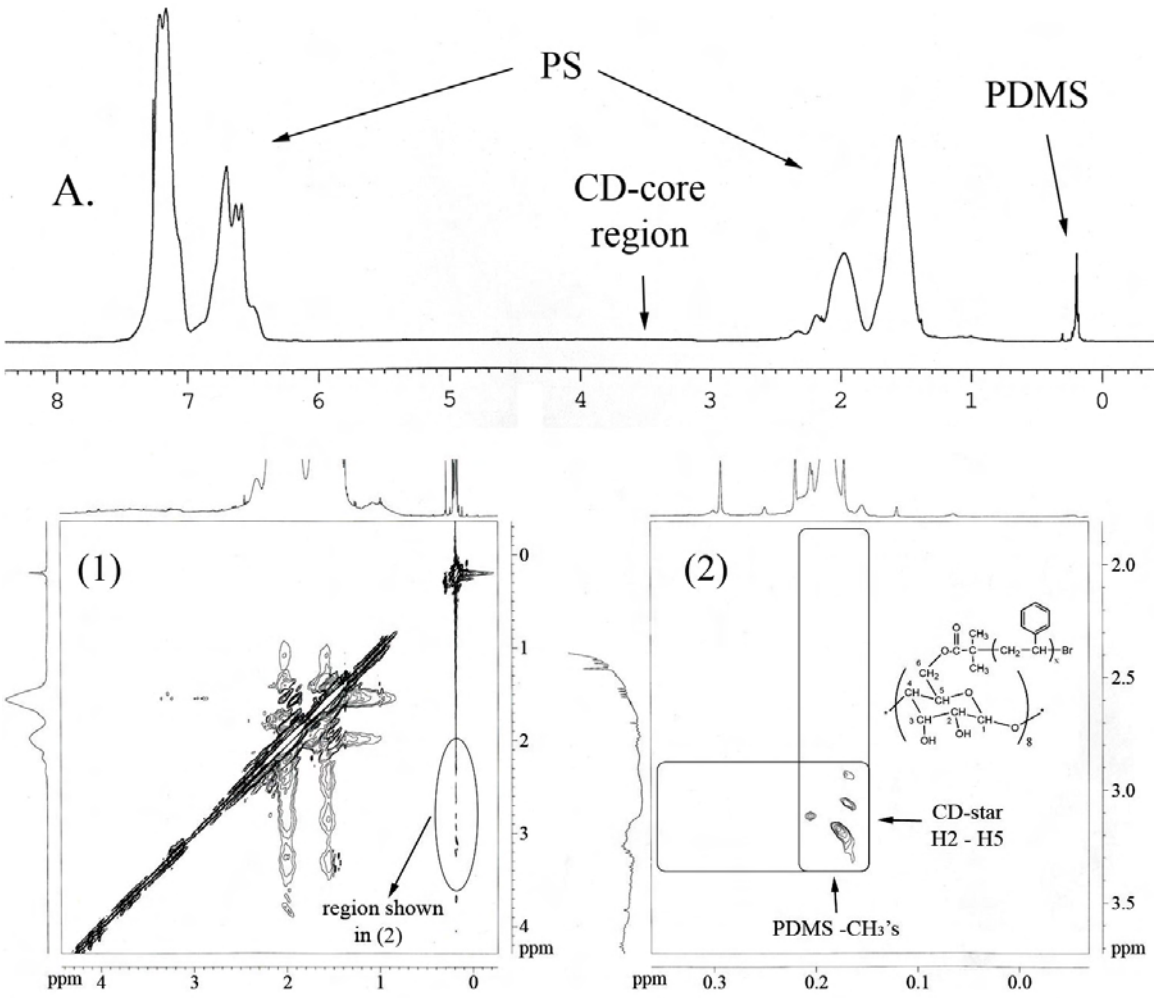

FIGURE 4.8. (A.) ^{1}H-NMR of the compatibilized CD-star solution whereas (1) and (2) show a partial correlated 2D-ROESY from this solution.

The sample solution used in the ROESY experiment contained 1wt% CD-core with 1wt% PDMS-308, which is the same sample used previously for the ^{1}H-NMR experiments in Figures 4.6 and 4.7. As a reference, Figure 4.8(A) presents the ^{1}H-NMR spectrum for the compatibilized CD-star blend examined, and (1) and (2) show partial correlated 2D ROESY NMR spectra. Due to the low concentrations of PDMS and CD-star in the blend, this guest/host interaction appears to be almost "drowned" within the experimental "noise" seen within the circled region in image (1). However, if the circled region in (1) is magnified, as can be seen in image (2), protons H-2, H-3, H-4, and H-5 on the CD-star are detectable just

above the noise and appear to be showing cross-peaks with the methyl groups on the PDMS. Because of the statistical distribution of the arms attached to the γ-CD core, there are many environmental effects that can play into the CD core hydrogen responses, which is evidenced as a broad peak between 3.1ppm and 3.3ppm in Figure 4.6(2). This leaves the exact identification of the CD cavity hydrogens responsible for the PDMS guest cross-peaks difficult to determine with certainty. However, threading of PDMS into the γ-CD cavity is confirmed.

4.3.2. Effect of Star Components on Compatibilization

An experiment was conducted to test the possible reasons behind the clearing of the solutions, and the following questions were posed:

1. Are the PS arms on the CD-star even necessary? Can either γ-CD or a chloroform-soluble CD like methyl-γ-CD be used to clear the solutions?
2. Is the bromine group on the CD-star responsible for the clearing? Can Br-γ-CD initiator be added instead of the CD-star and clearing still be observed?
3. Is the clearing effect due to favorable entropic mixing from the short arms on the stars? Can oligomeric PS be added instead of the CD-star and clearing be observed?

The evaluation of compatibilizer additives to test the above questions involved γ-cyclodextrin (γ-CD), 50%-methylated-γ-cyclodextrin (methyl-γ-CD), brominated-γ-cyclodextrin (Br-γ-CD), and 2500g/mol polystyrene oligomer (PS-oligomer), all of which were compared to CD-star (PS_6-γ-CD). All of the modified cyclodextrin materials had on average 12 of their 24 hydroxyls chemically substituted. The PS-oligomer was added to the solution to reflect the mass of the entire CD-star weight fraction within a typical sample (40.3mg within a 500mg sample). All of the solutions contain 5wt% PDMS-308, whereas solutions with CD had the same molar quantity of cyclodextrin core in each case. Sample

solutions were all prepared with concentrations of 10g/dl. These solutions were heated to 60°C in chloroform for two days to observe whether clearing took place.

Figure 4.9 compares the samples of possible compatibilization additives before and after heat processing. It was observed that the only solution to show clearing was the sample containing CD-star. This indicates that the PS arms are important for compatibilization to occur. Furthermore, clearing was not observed for the PS-oligomer therefore pointing to the CD-core being an important component for clearing as well.

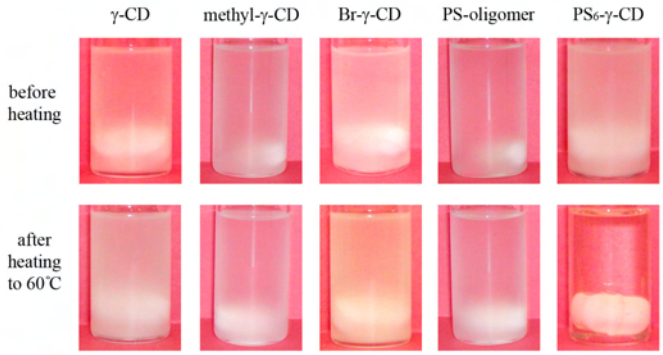

FIGURE 4.9. Control solutions comparing various additives testing compatibilization. All solutions were prepared in chloroform with 5wt% PDMS (308 kg/mol) and, where applicable, contained 1 wt% γ-CD core. The white Teflon stirbar on the bottom of vials can be used to gauge solution clarity.

4.3.3. Solvent Effects on Compatibilization

In order to test different solvent conditions for blend compatibilization, various solvents were selected that were increasingly good for PDMS. The examined blend had components of CD-star/PDMS/PS with 1wt% CD-core and 5wt% PDMS-308 and was heat processed for three days with a concentration of 10g/dl. Methyl ethyl ketone (MEK) was used to confirm if clearing would take place in a solvent environment similar to $CHCl_3$ (comparable χ values).

Equation 4.1 describes the relationship between blend solubility parameters (δ) and their resultant interaction parameter (χ), where the other variables within this relationship are

described as the average molar volume V_i ($=\sqrt{v_1^* \times v_2^*}$), the gas constant *R (=1.987cal/mol-K)*, the temperature *T (=298K)*, and the solubility parameter values for the two components δ_1 and δ_2. Table 4.4 lists the variables used to calculate χ between the homopolymers and solvents of interest.

$$\chi = \frac{V_i}{RT}(\delta_1 - \delta_2)^2 \text{ ---------- (4.1)}$$

TABLE 4.4. Variables used to calculate χ between homopolymers and solvents.

	solubility parameter, δ $(cal/cm^3)^{1/2}$	Mw (g/mol)	density, ρ (g/cm^3)	molar volume, v* (cm^3/mol)
PS	9.095	104.15	1.05	99.19
PDMS	7.423	74.2	0.97	76.49
$CHCl_3$	9.3	119.38	1.492	80.01
MEK	9.3	72.11	0.805	89.58
toluene	8.9	92.14	0.865	106.52
cyclohexane	8.2	84.16	0.779	108.04

Tabulated values of χ between the homopolymers and solvents are given in Table 4.5 as well as providing observations of whether the solution cleared or remained turbid. Based on the χ values in this table, these results show that the blending solvent needs to be selective for PS and poor for PDMS in order for clearing to be observed. Furthermore, this points to the conclusion that if the solvent offers a lower energetic environment for PDMS than the CD-core, then the PDMS will prefer the lower energy state in the solvent, thereby removing the driving force for threading PDMS into the CD-core (such as evidenced for toluene and cyclohexane). Further evidence pointing to a failed compatibilization for toluene and

cyclohexane blended solutions is, after heating, phase segregation into bilayers occurred demonstrating that compatibilization stability was not achieved.

TABLE 4.5. Calculated χ for PS and PDMS in various solvents and the observation of whether the solution blend achieved clearing or remained turbid. For reference, the χ value for PS/PDMS is 0.411.

Solvent, s	$\chi_{PS,s}$	$\chi_{PDMS,s}$	observation
$CHCl_3$	0.0063	0.4655	clear
MEK	0.0067	0.4925	clear
toluene	0.0066	0.3326	turbid
cyclohexane	0.1400	0.0927	turbid

4.3.4 Effect of Star Arm Length on Compatibilization

Thus far we have seen compatibilization effects for the shortest armed CD-star (PS_6-γ-CD), which successfully demonstrated its ability to clear and stabilize PS and PDMS blended solutions. However, what would happen if we systematically increased the arm length of the CD-stars? Would threading still take place with longer arms that can increase the steric interference to the cavity? Would the processing conditions still affect the clearing? To answer these questions a set of solutions were prepared with various amounts of CD-star (0.2wt% to 1wt% CD-core) and various star arm lengths, but leaving the PDMS concentration constant at 10 wt%. Compositional fractions for the prepared samples are represented in a bar graph in Figure 4.10. When the longer armed stars are blended, a larger amount of CD-star needs to be added to obtain the desired CD-core wt%. Moreover, it is important to keep in mind that as the CD-star mass increases, an equivalent amount of PS is removed in order to maintain a total solids mass of 500mg. All of the CD-stars used in this experiment have 12 arms with DP lengths of 6, 17, 29, and 51, corresponding to the sample nomenclature of PS_6-γ-CD, PS_{17}-γ-CD, PS_{29}-γ-CD, and PS_{51}-γ-CD, respectively.

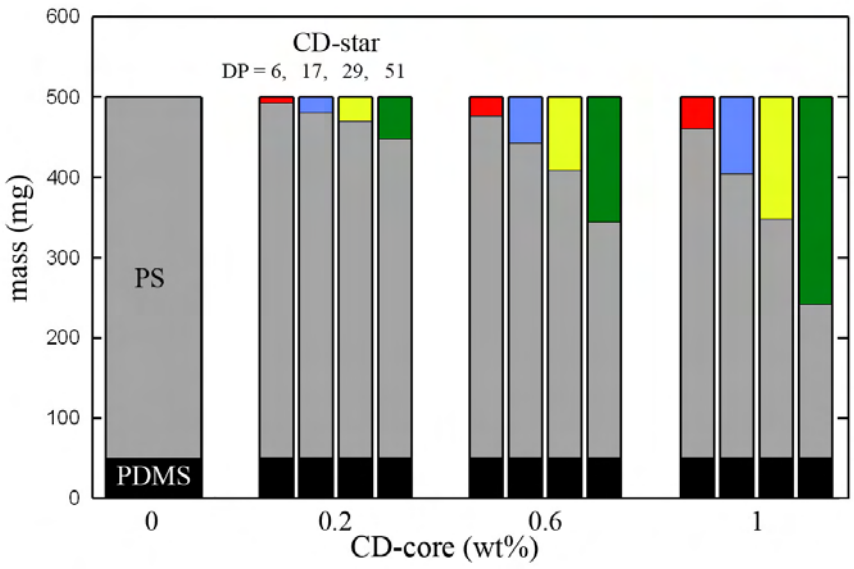

FIGURE 4.10. Mass compositions for samples containing different CD-star arm lengths. 1wt% CD-core is equivalent to 3.85 X 10^{-6} moles where the CD-star molecular weights (Mn) of DP = 6, 17, 29, and 51 are 10460g/mol, 24950g/mol, 39500g/mol, and 67800g/mol, respectively.

It was discovered that the processing conditions *did* affect solution clearing with respect to increasing arm length of the CD-star. Processing the solutions by stirring at room temperature for up to two months produced clear solutions for only the shortest armed star, PS_6-γ-CD, while all of the larger armed CD-star solutions remained cloudy. However, if these solutions were heat processed at 60° C in $CHCl_3$, clearing took place for most of the solutions, but not in an expected fashion. Figure 4.11 shows the heat processed samples as a function of days heated at 60° C for most of the CD-star arm lengths studied. All sample solutions blended with PS_6-γ-CD star (not shown) successfully cleared after 2 days of heating. The two smallest armed CD-stars (DP = 6, 17) showed sequential clearing in the order of 1wt%, 0.6wt%, and 0.2wt% CD-core as time progressed. However, the two largest armed CD-stars (DP = 29, 51) showed a sequential clearing in the opposite direction, where clearing initially occurred for 0.2wt%, then 0.6wt%, and 1wt% CD-core as time progressed.

Only three solutions failed to clear in this experimental set, those containing CD-stars of DP=17 (0.2 wt% CD-core), and DP=51 (0.6 wt% and 1 wt% CD-core). The images of these turbid solutions are outlined in black in Figure 4.11. To seek an understanding of these unsystematic compatibilization results, solubility parameters (δ) were calculated for each of the CD-stars in order to evaluate blend interactions.

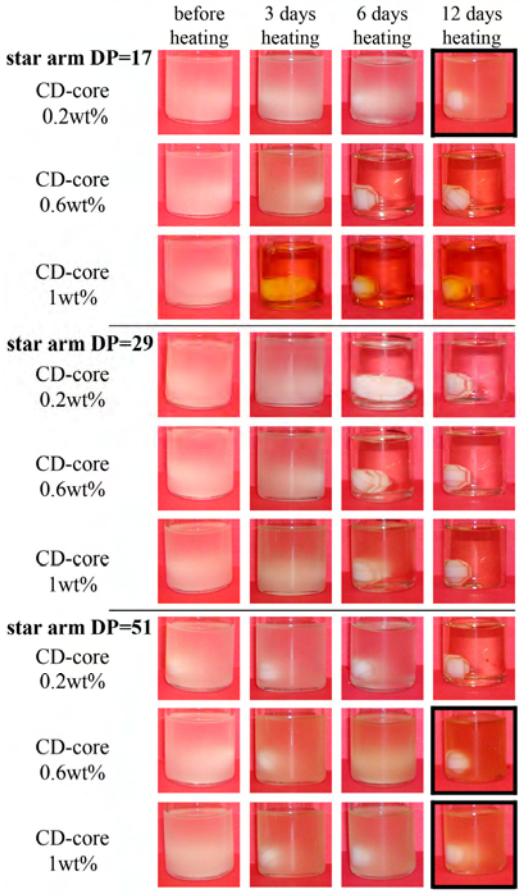

FIGURE 4.11. Heat processed solutions of PS/PDMS blends containing varying arm length DPs for CD-stars and the observed effects on solution clarity. All solutions above contain 10wt% PDMS-308 with concentrations of 10g/dl. The white Teflon stirbar on the bottom of vials can be used to gauge solution clarity.

Calculations of δ were conducted using the molar attraction constants tabulated by Small, then refined by Hoy.[36] Table 4.6 lists the molar attraction constants (F_i) for the functional groups found (n_i) in the CD-star molecule. These molar attraction constants were used with the general equation for δ shown in equation 4.2. Other pertinent variables in equation 4.2 are given in Table 4.7.

$$\delta = \frac{\rho \sum n_i F_i}{M_w} \text{ ---------- (4.2)}$$

TABLE 4.6. Summary of functional groups and their corresponding molar attraction constants for a twelve armed γ-CD-star.

Star Structure:		functional group	quantity found (n_i)	molar attraction constant, F_i (cal-cm^3)$^{1/2}$
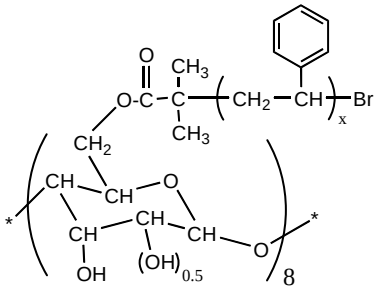	*CD core:*	CH	40	89.99
		CH_2	8	131.5
		O	16	114.98
		OH	12	225.84
	Arms:	COO	12	326.58
		C	12	32.03
		CH_3	24	147.3
		phenyl	12(x)*	738.5
		CH_2	12(x)*	131.5
		CH	12(x)*	85.99
		Br	12	257.8

* x = DP of star arms. See chemical structure in Table.

Table 4.7 presents the calculated δ values for the CD-stars. The difference in solubility parameters ($(\delta_1 - \delta_2)^2 = \Delta\delta^2$) between the stars and the blended components were calculated and are graphically shown in Figure 4.12(A). Calculations for $\Delta\delta^2$ rather than χ were performed due to the difficulty of estimating V_i between the star molecule and the other components making up the blend. Differences in V_i for various pairs of blended components are expected to be small. Often for homopolymers, V_i = 100cm^3/mol can be used as the average molar volume without significantly affecting the results.[36] Equation 4.1 describes the relationship between $\Delta\delta^2$ and χ. Trends in $\Delta\delta^2$ should reflect trends in χ and still provide a good relative assessment of the interactions between components. For reference, the calculated $\Delta\delta^2$ values for PDMS/PS, PDMS/$CHCl_3$, and PS/$CHCl_3$, are 2.80, 3.52, and 0.042, respectively.

TABLE 4.7. Calculated solubility parameters for the CD-stars.

star arm:	DP=6	DP=17	DP=29	DP=51
M_w (g/mol)	10,460	24,950	39,500	67,800
CD-core (wt%)	12.29	5.15	3.26	1.90
$\rho_{\text{law of mix}}$ (g/cm^3)†	0.989	1.024	1.034	1.041
Solubility parameter, δ (cal/cm^3)$^{1/2}$ §	8.397	8.824	9.231	9.290

† Using law of mixtures: $\rho = (y/100)*(\rho_{CD}) + (1-(y/100))*(\rho_{PS})$ where y = CD-core (wt%), ρ_{CD} = 0.55g/cm^3, ρ_{PS} = 1.05 g/cm^3

§ Calculated using Equation 4.2 and $\rho_{\text{law of mix}}$.

Distinct trends are noticed in Figure 4.12(A), where $\Delta\delta^2$ for CD-star/PS and CD-star/$CHCl_3$ decrease as arm DP increases which gives insight to the increasingly favorable interactions between these components. On the other hand, $\Delta\delta^2$ increases dramatically for CD-star/PDMS as the arm DP increases showing unfavorable interactions as arm DP increases. These trends present opposing interactions between CD-star with PDMS, and CD-star with

the other blend components, which may aid in explaining the clearing characteristics we observe as DP of the star arm increases.

An interpretive illustration for the changing solution environment as arm length increases is shown in Figure 4.12(B). These diagrams were drawn to aid in the understanding of the interactions between the CD-star and the other blend components. For the shorter armed stars, it is thought that the CD-star may be partially soluble in PDMS, as evidenced by their lower $\Delta\delta^2$ values with PDMS. It can be seen that as the DP of the CD-star arm increases, interactions with both PS and $CHCl_3$ get increasing favorable and more CD-star is found intermixed in these components. This is in contrast to the interactions between the CD-star and PDMS which become increasingly repulsive for the larger armed stars, resulting in a decreasing solubility in PDMS.

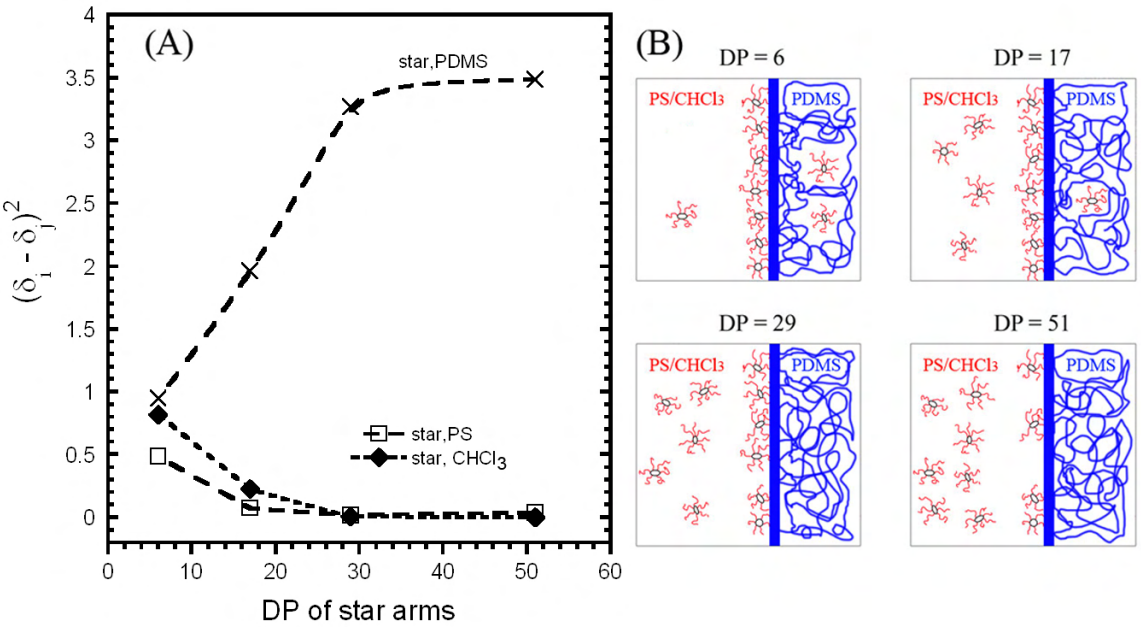

FIGURE 4.12. (A) Interaction parameters between CD-stars and other blended components with respect to star arm length and (B) an interpretive illustration based on the relative $\Delta\delta^2$ values for each CD-star arm DP at the PDMS interface.

For the shortest armed stars of DP = 6 and 17, interactions with PDMS are slightly more favorable than the longer armed stars as evidenced by lower $\Delta\delta^2$ values. This may result in a small amount of CD-star being dissolved within the PDMS. Furthermore, the oligomer nature of these stars in the PS/chloroform solution may aid their migration to the interface. This set of stars show sequential clearing in the order of 1 wt% to 0.2 wt% CD-core. This indicates that the compatibilization mechanism for the shorter armed stars is concentration dependent, or in other words, when more CD-core is present, the faster the solution clearing occurs. However, for the solution of DP = 17 (0.2 wt% CD-core) that did not show clearing in Figure 4.10, two possible reasons for non-clearing are evident: (1) in Figure 4.12(A) the decrease in $\Delta\delta^2$ shows an increased favorability for the star interaction with PS or $CHCl_3$, which probably leads to more star in the solution and less at the interface, and (2) the partial solubility of the star in PDMS may enhance the decrease in concentration at the interface. These reasons may explain why this sample solution did not clear, but this observation is not fully understood.

It was seen earlier in Figure 4.5 that when 2-component blends of star and PDMS were heat processed in $CHCl_3$, clearing did not occur. However when PS was added to this blend, then clearing of the solution was observed again. Therefore, this illustrates the important role PS plays in the compatibilization processes. With this in mind, two simultaneous causes may be occurring for the blend samples of DP = 51 (0.6 wt% and 1 wt% CD-core) that did not show clearing in Figure 4.11. First, since this star has the longest arms, more PS is removed to compensate for the dilution of the CD-core within the CD-star (recall Figure 4.10). This results in a reduced driving force for CD-star migration to the interface due to decreased interactions with PS. Second, in Figure 4.12(A), it is observed that the most favorable interactions between CD-star and $CHCl_3$ occur at star-arm DP = 51 which increasingly places more CD-star in the solution. These reasons may explain why the two samples with DP = 51 did not clear.

4.4 Evidence of Micelle Formation

4.4.1. Intrinsic Viscosity Measurments of Compatibilized Solutions

Dilute solution viscosity measurements were performed to probe whether any change in viscosity for the compatibilized solutions could be observed due to micelle formation. In order to perform viscosity measurements, the dilute regime boundary for the blend needs to be found in order to stay within a concentration where coil overlap does not occur. Calculations were performed to find the concentration at which coil overlap occurs (c^*) for PS and PDMS. The intimacy quotient (IQ) is described[37] in equation 4.4 and was used to find c^*. Equation 4.5 describes the relationship of IQ to c^*.

$$IQ = \frac{V_j}{V_o} = \frac{4\pi}{3}\left[\frac{C_n M l^2}{6M_b}\right]^{3/2} \frac{\rho N_A}{M} \text{ ---------- (4.4)}$$

$$c^*(\%) \sim \frac{1}{IQ} \times 100 \text{ ---------- (4.5)}$$

The variables within equation 4.4 are described as the volume pervaded or influenced by a randomly coiling polymer V_j, the volume physically occupied by the polymer V_o, the characteristic ratio C_n, the molecular weight of the polymer M, the backbone bond length l, the average molecular weight per backbone bond of the polymer M_b, the density of the polymer ρ, and Avagadro's number N_A. Table 4.8 lists these variables as well as the calculated values for c^* using equations 4.4 and 4.5.

TABLE 4.8. Calculated polymer overlap concentration (c^*) for the blended polymers.

	M(g/mol)	M_b(g/mol)	C_n	l(Å)	ρ(g/cm^3)	IQ	c*(%)
PS	325,000	52.1	9.8	1.54	1.05	30.5	3.3
PDMS	308,000	37.1	6.2	1.64	0.97	27.7	3.6
PDMS	62,700	37.1	6.2	1.64	0.97	12.5	8.0

Values found for c* show that the lowest overlap concentration for the homopolymers examined was 3.3% v/v (for PS), and is the maximum concentration that can be employed in the viscosity measurements before coil overlap occurs. Therefore a concentration of 1% (1g/dl or ~1ml/dl) was used in order to be confident that the viscosity measurements were measured in the dilute regime.

Dilute solution viscosities were measured with a Cannon Ubbelohde viscometer (#25). All sample solutions were diluted with $CHCl_3$ from an initial 10g/dl (as-compatibilized) concentration to 1g/dl. Additionally, all 1g/dl solutions were prepared just before introduction into the viscometer and were filtered through a 1μm polytetrafluoroethylene (PTFE) syringe filter to remove any particulates. Once introduced into the viscometer, the solutions were equilibrated and maintained at 25° C in a large water bath. Intrinsic viscosities, [η], for the blends were found using the Huggins and Kraemer relationships[38] as described previously in section 3.5.2. Viscosity flow times were recorded for concentrations of 1, 0.833, 0.625, 0.428, and 0.231g/dl.

In this series of experiments, two viscosity studies were conducted for blends of PS/PDMS/CD-star in which (a) the amount of PDMS was held constant and (b) the amount of CD-core was held constant. Both of these studies showed the same relative trends for the compatibilized solutions containing CD-star.

Figure 4.13(A) shows the [η] results with constant PDMS and varying CD-core amounts, and (B) shows the compositions of the blends examined. In this Figure, three sample sets are compared having (1) no PDMS, (2) constant 5wt% PDMS, and (3) constant 10wt% PDMS. Intrinsic viscosity values for the compatibilized solutions with CD-star were found to be significantly lower than solutions without CD-star. It was expected that if the CD-star had no effect on the solution then a rule-of-mixtures outcome would be observed for data sets (2)

and (3) in which each would run parallel to the "no PDMS" data set (1). However this is not the case. It can be seen in Figure 4.13(A) that all of the compatibilized solutions had an initial drop in viscosity once the CD-star was added. Furthermore, subsequent increases of CD-star within each sample composition set did not produce lower viscosities, instead [η] remained relatively constant. In general, it is observed that the 5wt% PDMS samples gave slightly higher viscosity values than the 10wt% PDMS samples. This observation might be due to the fact that 5 wt% solutions have a higher CD-star amount per PDMS chain than for the 10 wt% solutions. This higher CD-star ratio then increases the bulkiness of the micelle and therefore gives a greater [η]. It is also noted that PDMS-62 solutions gave slightly higher viscosities in data sets (2) and (3) compared to PDMS-308.

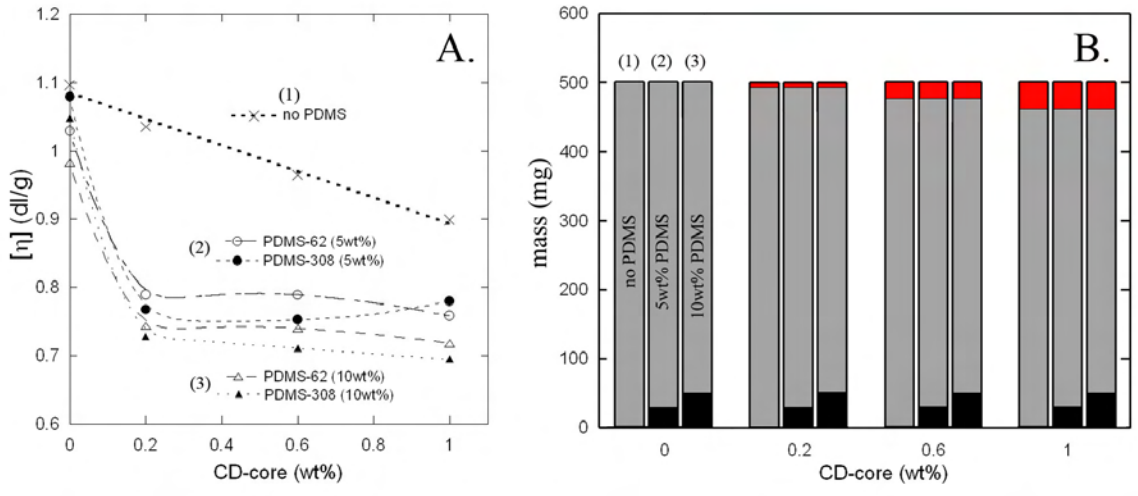

FIGURE 4.13. (A) Intrinsic viscosities of the blended solutions containing constant amounts of PDMS while the amount of CD-star (or CD-core) is varied. (B) mass compositions of the sample solutions in which data set (1) has no-PDMS, (2) has 5wt% PDMS, and (3) has 10wt% PDMS. Within (B) the black bar represents the PDMS, the gray bar is the PS, and the red bar is the CD-star mass component.

In the second viscosity experiment, the amount of CD-star was held constant at 1wt% CD-core as the amount of PDMS was varied. Figure 4.14(A) shows intrinsic viscosities of compatibilized and non-compatibilized solutions and (B) presents the compositions for the

sample sets examined. These two samples sets have a fixed CD-core amount and variable PDMS content, without (1) and with (2) CD-star. Sample sets of (1) are shown in Figure 4.14(A) to present representative viscosity trends for each PDMS examined without any CD-star added.

It is seen in Figure 4.14(A) that when the CD-star is added to PS solutions (0wt% PDMS), a decrease in the intrinsic viscosity occurs, illustrating the dilution of the PS by the CD-star. As the PDMS content increases, it would be expected that if the compatibilized solutions of (2) do not show any interactions with PDMS, then the rule-of-mixtures would be observed and the sample sets of (2) would run parallel to the sample sets of (1).

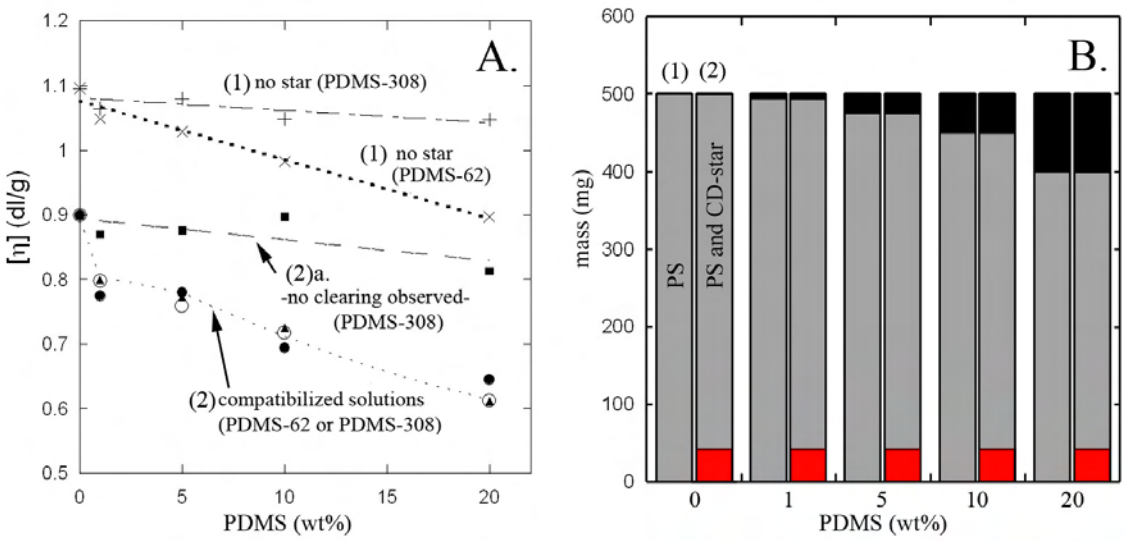

FIGURE 4.14. (A) Intrinsic viscosities of cleared solutions containing a constant amount of CD-star (1wt% CD-core) with various amounts of PDMS. Compatibilized solutions with PDMS-62(-○-) and PDMS-308(-●-) room temperature processed, and with PDMS-308(-▲-) heat processed. (B) Mass compositions of the sample solutions. Data set (1) has no CD-star, (2) has CD-star. The composition represented by black bar is the PDMS, the gray bar is the PS, and the red bar is the CD-star mass component.

In order to examine the solution properties before clearing is observed, sample set ((2)a) in Figure 4.14(A) was prepared which contained all three blended components (CD-star/PS/PDMS-308). All these solutions were stirred at room temperature for one hour and none exhibited clearing. As predicted, the sample set (2(a)) shows a slope that is parallel to sample set (1) containing just PS and PDMS (no star). However the sample solution sets of (2) that were compatibilized showed a more significant decrease in viscosity compared to (2)a. It is interesting to note that all of the compatibilized solutions of (2) made with either PDMS-62 or PDMS-308 gave nearly the same intrinisic viscosities which suggest similar hydrodynamic volumes in the blend.

Several researchers have seen this same trend of reduced intrinsic viscosities[39] for block[40] and graft-copolymers[41] in selected solvents after micelle formation. For example, it was found that graft copolymers of PS-graft-(4-vinyl-N-ethylpridium bromide) in an aqueous solution formed unimers regardless of concentration and displayed a reduction in intrinsic viscosity.[42] Reverse micelle behavior was seen for PMMA-g-PEO[43] or PS-g-PEO[44] in toluene and these samples exhibited a decrease in viscosity once micelles were formed. Graft copolymers of PS-g-PMMA in THF, a selective solvent for PS, had intrinsic viscosities that were lower than single chains in a good solvent for both blocks.[45] It is apparent that graft copolymers in selected solvents show the same type of decreased viscosity trends that we see in our blends, suggesting micelle formation is occurring which leads to compatibilized solutions.

4.4.2. Dynamic Light Scattering of Compatibilized Solutions

Another commonly used technique to confirm whether micelles are being formed is dynamic light scattering (DLS) which can be used to observe changes in the radius of gyration of the dissolved species.[15, 39] Therefore DLS was performed in order to inquire whether or not a change in average micelle size could be observed for the compatibilized CD-star blends. Equation 3.2 from section 3.5.1 was used to estimate the radius of gyration for each

homopolymer in order to compare with the DLS data. The molecular weights (M) used in these calculations for PS (PDI = 2.95), PDMS-308 (PDI = 2.5), and PDMS-62 (PDI = 2.5) are the number-average values which are established to be 110.2kg/mol, 123.2kg/mol, and 25.1kg/mol, respectively.

Radii of gyration values from equation 3.2 for PS, PDMS-308, and PDMS-62 were multiplied by two to give diameter values of 18.1nm, 17.7nm, and 8.0nm, respectively. The DLS measurements for pure PS in $CHCl_3$ gave a mean effective diameter of 19.1nm, which is in good agreement to the calculated diameter of 18.1nm. Lastly, DLS measurements for the CD-star alone were unreliable and suggested formation of agglomerates. Thus, for reference, the CD-star can be assigned the reasonable mean effective diameter (d_{eff}) value of 5nm, which was found by calculating the diameter of the CD-star with fully extended arms.

DLS produced anomalous results for the PDMS homopolymers. Their extreme insolubility in $CHCl_3$ gave d_{eff} values on the order of micrometers with large standard errors pointing to agglomeration within the solution. Turbidity was not visually observed for these solutions due to the similar indices of refraction for PDMS and $CHCl_3$. In addition, sample solutions containing only blends of PS and PDMS showed large swings in the d_{eff} data from tens of nanometers to micrometers with no consistent pattern observed with PDMS content. For these reasons, the DLS data from these solutions are not presented.

Two sample sets were successfully measured by DLS: (1) compatibilized blends containing CD-star 2 hours after diluting to 1g/dl from 10g/dl, and (2) same solutions as in (1) but re-examined 2 days after diluting to 1g/dl. Aggressive stirring was implemented for the "2-day" blends just before DLS measurements in an attempt to make the solutions more homogeneous and to keep the PDMS from agglomerating. The 2-hour sample solutions remained homogenous; therefore, aggressive stirring was not warranted. Turbidity was not visually observed for either of these solutions at 1g/dl.

Figure 4.15 shows d_{eff} for the blends with respect to PDMS weight fraction, where (A) shows the d_{eff} of the solutions 2 hours after diluting to 1g/dl, and (B) shows the d_{eff} of the solutions 2 days after diluting to 1g/dl. It can be seen in Figure 4.15(A) that the CD-star solutions measured 2 hours after diluting to 1g/dl show a slight increase in d_{eff} with increasing PDMS amount. Also, data set (A) has low standard deviations suggesting homogeneity within the solutions. The d_{eff} values that were measured have sizes that are on the order of the PS and PDMS polymer coils calculated above. Furthermore, this sample set shows fairly constant diameters for both PDMS molecular weights examined, indicating that if micelles are present, they are of a similar size. This trend correlates well with the intrinsic viscosity measurements seen previously for data set (2) in Figure 4.14 where similar intrinsic viscosities for both PDMS samples indicate similar hydrodynamic volumes.

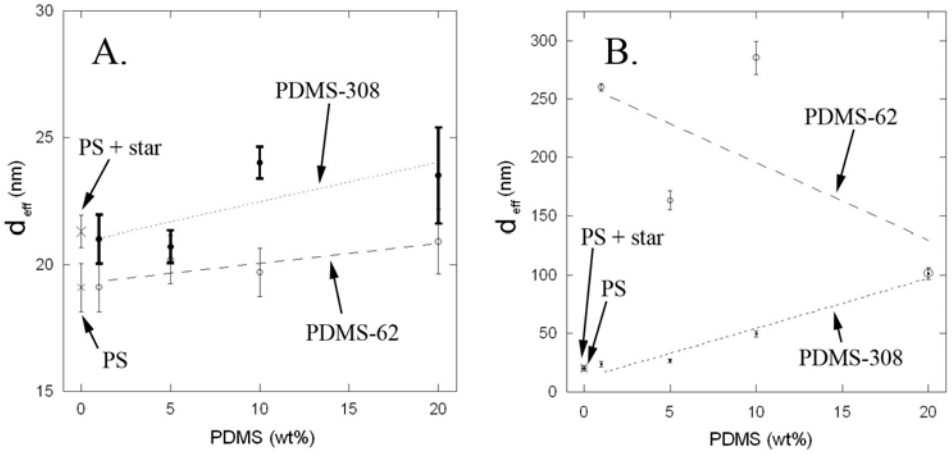

FIGURE 4.15. DLS of cleared solutions with CD-star where A.) shows d_{eff} after 2 hours in 1g/dl solution, and B.) shows d_{eff} after 2 days in 1g/dl solution.

However, after 2 days at 1g/dl solution concentration, the d_{eff} values dramatically increase, as seen in Figure 4.15(B). This indicates at a concentration of 1g/dl these blends are not stable and start to behave more like solutions containing no star. This is in contrast to the observed stability for the initial concentrations of 10g/dl seen in Figures 4.3 to 4.5, where these clear solutions have been noticed to be stable for several months. Dethreading of the CD-stars at

lower solution concentrations might be the cause of this trend. When more of the PDMS chains are exposed, this may give rise to increased chain agglomeration and larger mean d_{eff} values. These results may also indicate that the critical micelle concentration occurs between 1-10 g/dl. However, experiments that cap the PDMS end-groups to prevent the CD-star from sliding off prior to DLS measurements would need to be conducted to confirm this.

In the literature it has been primarily seen that graft copolymers decrease in size when micelle formation occurs. Large decreases in the radius of gyration (R_g) have been seen for graft copolymers, such as PS-graft-polyisoprene, that form micelles in selective solvents, correlating well with decreasing intrinsic viscosity measurements.[46] Likewise polystyrene-b-poly(4-vinylpyridine) micelles have been successfully examined by DLS where they give a R_g size range between 20 and 100nm.[47] Even bottle-brush graft copolymers have been shown to have a reduction in R_g when they are in a selective solvent.[48] So again, we see experimental results that point to possible micelle formation in selective solvents.

4.4.3. GPC of Compatibilized Solutions

Gel permeation chromatography (GPC) has been implemented to find out whether micelles can be detected and their distributions observed separately from individual chains.[15] Unfortunately the GPC technique can give mixed results for micelle characterization. A few possible complications that can occur are (1) micelles at a given concentration are in equilibrium with unimers, and may become destabilized due to unimers or micelles being eluted at different times, therefore changing their equilibrium size distribution,[15, 39] (2) micelles are of a different structure than polymer coils (usually more dense and possibly consisting of spheres, cylinders, or vesicles) thereby not interacting with the elution column in the same way that a polymer coil would,[15, 39] and (3) the shear flow of the solvent may disrupt micelle structures. However, with that said, several researchers have used this technique successfully to characterize micelles.[15, 41, 42, 49, 50]

All solutions examined by GPC originally had concentrations of 10g/dl in $CHCl_3$ that were diluted to 0.1g/dl using HPLC grade THF. The solubility parameters for $CHCl_3$ and THF are relatively similar, with values of $9.3(cal/cm^3)^{1/2}$ and $9.4(cal/cm^3)^{1/2}$, respectively, which preserves the selective solvation of PS. Solutions were prepared just before injection into the GPC column. The GPC UV photodetector was calibrated at a wavelength of 254nm, which is the absorbance wavelength for PS, but not for PDMS. Therefore PDMS will be transparent to this wavelength causing only PS to be detected as it is eluted through the column. Sample solutions with only PDMS-308 were examined (none with PDMS-62). In addition, if solutions contain CD-star, they were prepared with 1wt% CD-core.

Two GPC data sets are presented in Figure 4.16 where (A) presents the GPC traces for the control samples and (B) presents the compatibilized CD-star containing solutions. Expanded subset regions in (A) and (B) contain magnified PS and CD-star peak areas, noted as (1) and (2) respectively. Within the sample legends of Figure 4.16, parentheses indicate the wt% of that blend component. All data traces in (A) were normalized to the PS peak to see if the PDMS within a sample blend of PS/PDMS had any effect on the PS distribution as the blends were eluted through the column. This normalization only matched the intensities of the peaks, and the horizontal position of the curves were not changed. Additionally, it can be seen that the PS and CD-star elution regions are well separated and are easily identified as evidenced in (A). Lastly, control samples in (A) with only PS and PDMS show that the PDMS has no effect on the elution of the PS through the column as evidenced by the perfectly overlapping PS traces in A(1).

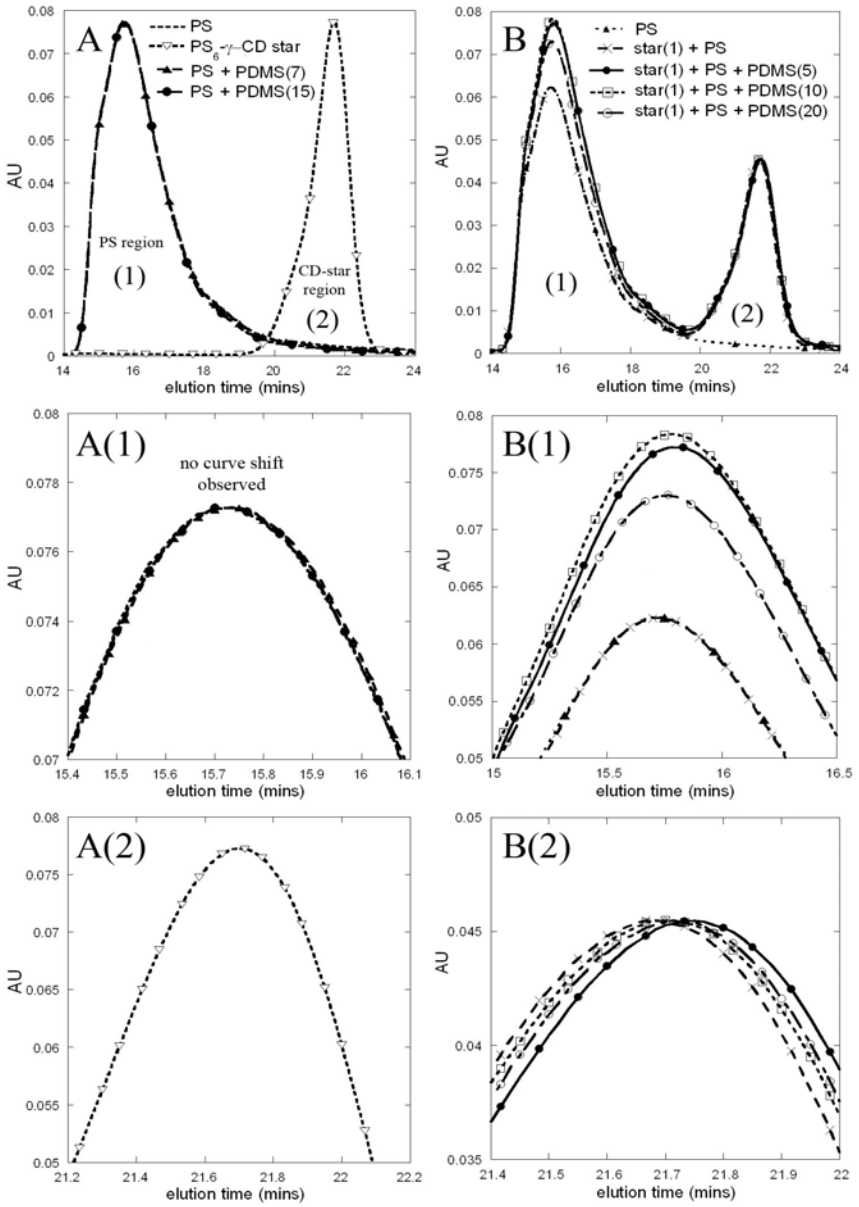

FIGURE 4.16. GPC traces of blends and the individual components making up the blends. (A) GPC traces for control blends/samples (B) shows traces for the compatibilized solutions. Within (A) and (B) there are two numbered regions (1) and (2) that correspond to the PS and CD-star distributions, respectively. These regions are expanded and are shown as A(1) and B(1) for the PS region, and A(2) and B(2) for the CD-star region. All star blends contain 1wt% CD-core (where applicable), and all PDMS containing samples were made with PDMS-308.

Since all sample solutions in Figure 4.16(B) have 1wt% CD-core (except for the pure PS trace), peak heights in this set were normalized to the CD-star peak. Again, normalization only matched the intensities of the peaks, not the horizontal position of the curves. It can be seen in B(1) that the presence of the star has no effect on the PS peak due to the CD-star/PS blend overlaying directly onto the PS peak (triangles and crosses in B(1)). However it is observed in B(1) and B(2) that changes in peak intensity and position do occur for the compatibilized blends of PS/PDMS/CD-star.

Integration of the area under the PS and CD-star peaks can be conducted and their areas ratioed to investigate micelle formation. Hypothetically, if micelles are eluting within the PS region, then the GPC PS/CD-star area ratio should be larger than expected. A ratio increase stems from the CD-star threading onto the PDMS which then forms the threaded complex to be eluted through the column as a micelle. When this threaded complex is detected by the UV photodetector (due to the PS arms on the CD-star), it would be expected that the elution time would be similar to the PS (due to its similarity in size to pure PS, as evidenced in the DLS measurements). This will increase the PS elution peak area. The PS/CD-star ratio would simultaneously increase in the numerator and decrease in the denominator due to the addition of more material (micelles) under the PS peak *and* a reduction of CD-star (due to threading) from the CD-star peak. Since the areas of the peaks are proportional to the amount of material in the solution,[51] we can estimate the expected ratios if no micelle formation occurs from the molar composition of the solutions. Thus the molar ratio of styrene repeats to CD-star should correspond well with the GPC area ratio.

Figure 4.17(A) shows the calculated PS/CD-star styrene molar ratios and the ratioed PS/CD-star GPC areas from the compatibilized solutions for CD-star/PS/PDMS, and (B) shows the compositions of the CD-star containing solutions. In principle, the largest ratio in the sample series should come from the CD-star and PS sample (0wt% PDMS), as can be seen in Figure

4.17(B). However this ratio is observed to be the least intense for the GPC area ratios in Figure 4.17(A).

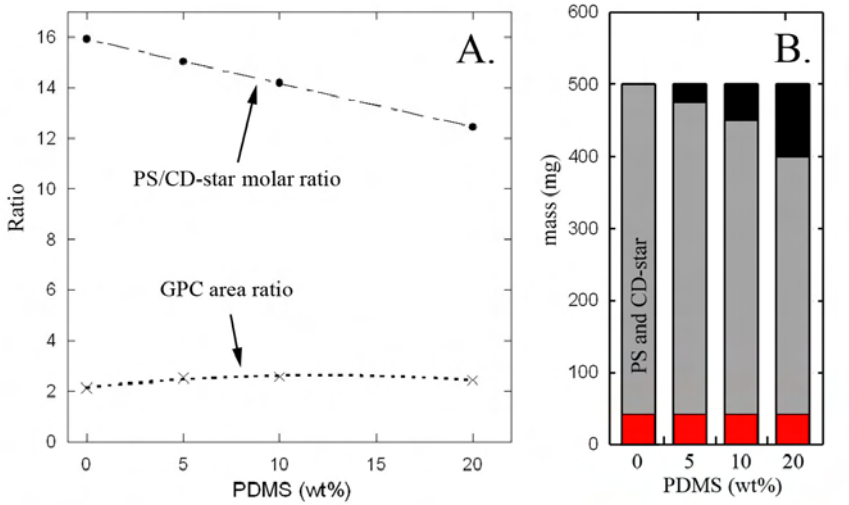

FIGURE 4.17. (A) Comparison plot of the GPC trace area ratios for PS/CD-star from Figure 4.13(B), and molar ratios of PS/CD-star from the compatibilized solutions. (B) shows the mass compositions for the compatibilized sample solutions examined, which CD-star is shown in red, and PDMS in black.

It is not clear why the ratio values in Figure 4.17(A) are so different. This may be caused by some of the material being trapped in the column and therefore not being detected. Nevertheless, it is noticed in Figure 4.17(A) that a slight increase for the GPC area ratios does occur whereas a monatomic decrease is observed for the calculated ratios. While it is unclear as to why these GPC ratioed areas for the PS/CD-star are so low, the fact that the GPC ratios increase slightly with PDMS content may still be an indication of micelle formation.

It has been observed by a few researchers that due to micelles being of a different compaction than polymer coils, they will have a different interaction with the elution column which occasionally results in longer elution times than expected.[41] The peak shifts observed in Figure 4.16.B(1) and B(2) might be a result of this unusual interaction with the column

which may indicate a longer elution time is occurring for the micelles. The elution times for the peaks in region B(1) slightly shift in the order PS/CD-star < PDMS(20) < PDMS(10) < PDMS(5), and in region B(2), in the order PS/CD-star < PDMS(10) < PDMS(20) < PDMS(5). It can be ruled out that these peak shifts are due to the presence of PDMS since it is shown in Figure 4.16.A(1) that the PS and PDMS blends do not show any abnormal shifting. Therefore, the observed peak shifts might be due to micelles; however, these shifts are not fully understood.

4.5. Conclusions

It has been shown that incompatible solutions of PS/PDMS can be compatibilized by addition of a star polymer containing a γ-CD core with PS arms. Visual evidence of compatibilization occurs when turbid concentrated solutions become clear. The resultant compatibilized solutions have been observed to remain clear for months thereby displaying temporal stablility. In addition compatibilization has been found to be dependent on processing conditions, solvent, and the star arm length.

Cross peaks between the CD cavity protons and the PDMS methyl protons, as found by 2D ROESY NMR, confirm that interactions are occurring which point to successful threading of the PDMS into the CD core. Characterization of the compatibilized solutions by dilute solution viscosity, DLS, and GPC, point to characteristics similar to graft-copolymers in selective solvents which have been shown to form micelles. Attributes of the compatibilized solutions similar to graft copolymers include lower viscosities, temporal and size stabilities, as well as possible redistribution of mass allocations under GPC curves suggesting micelle formation.

4.6. References

1. Kuleznev, V. N.; Krokhina, L. S. *Russian Chemical Reviews* **1973,** 42, (7), 570-586.

2. Utracki, L. A. *Canadian Journal of Chemical Engineering* **2002,** 80, (6), 1008-1016.

3. Maric, M.; Macosko, C. W. *Journal of Polymer Science Part B-Polymer Physics* **2002,** 40, (4), 346-357.

4. Hu, W.; Koberstein, J. T.; Lingelser, J. P.; Gallot, Y. *Macromolecules* **1995,** 28, (15), 5209-5214.

5. Abbas, S.; Li, Z. B.; Hassan, H.; Lodge, T. P. *Macromolecules* **2007,** 40, (11), 4048-4052.

6. Larsen, K. L. *Journal of Inclusion Phenomena and Macrocyclic Chemistry* **2002,** 43, 1-13.

7. Tonelli, A. E. *Polymer* **2008,** 49, (7), 1725-1736.

8. Porbeni, F. E.; Edeki, E. M.; Shin, I. D.; Tonelli, A. E. *Polymer* **2001,** 42, (16), 6907-6912.

9. Okumura, H.; Okada, M.; Kawauchi, Y.; Harada, A. *Macromolecules* **2000,** 33, (12), 4297-4298.

10. DeBolt, L. C.; Mark, J. E. *Macromolecules* **1987,** 20, (10), 2369-2374.

11. Hunt, M. A.; Jung, D. W.; Shamsheer, M.; Uyar, T.; Tonelli, A. E. *Polymer* **2004,** 45, (4), 1345-1347.

12. Baulin, V. A.; Johner, A.; Marques, C. M. *Macromolecules* **2005,** 38, (4), 1434-1441.

13. Baulin, V. A.; Lee, N. K.; Johner, A.; Marques, C. M. *Macromolecules* **2006,** 39, (2), 871-876.

14. Eckert, A. R.; Webber, S. E. *Macromolecules* **1996,** 29, (2), 560-567.

15. Hadjichristidis, N.; Pispas, S.; Floudas, G. A., *Block Copolymers*. John Wiley & Sons, Inc.: Hoboken, New Jersey, 2003; p 1-419.

16. Helfand, E.; Tagami, Y. *Journal of Polymer Science Part B: Polymer Letters* **1971,** 9, (10), 741-746.

17. Helfand, E.; Tagami, Y. *The Journal of Chemical Physics* **1972,** 56, (7), 3592-3601.

18. Baeurle, S. A.; Efimov, G. V.; Nogovitsin, E. A. *Europhysics Letters* **2006,** 75, (3), 378-384.

19. Ermoshkin, A. V.; Semenov, A. N. *Macromolecules* **1996,** 29, 6294-6300.

20. Kajiyama, T.; Tanaka, K.; Takahara, A. *Macromolecules* **1997,** 30, (2), 280-285.

21. Sperling, L. H., *Introduction to Physical Polymer Science*. 4th ed.; John Wiley & Sons: Hoboken, New Jersey, 2006; p 1-845.

22. Tuzar, Z., Overview of Polymer Micelles. In *Solvents and Self-Organization of Polymers*, Webber, S. E., Ed. Kluwer Academic Publishers: The Netherlands, 1996; Vol. 327, pp 1-17.

23. Chevalier, Y.; Zemb, T. *Rep. Prog. Phys.* **1990,** 53, 279-371.

24. Nose, T. *Polymer* **1995,** 36, (11), 2243-2248.

25. Soto Tellini, V. H.; Jover, A.; Garcia, J. C.; Galantini, L.; Meijide, F.; Tato, J. V. *Journal of the American Chemical Society* **2006,** 128, (17), 5728-5734.

26. Becheri, A.; Lo Nostro, P.; Ninham, B. W.; Baglioni, P. *The Journal of Physical Chemistry B* **2003,** 107, (16), 3979-3987.

27. Cameron, D.; Cooper, A. *Journal of Inclusion Phenomena and Macrocyclic Chemistry* **2002,** 44, (1), 279-282.

28. Okumura, H.; Kawaguchi, Y.; Harada, A. *Macromolecules* **2001,** 34, 6338-6343.

29. Ma, J.; Guo, C.; Tang, Y.; Xiang, J.; Chen, S.; Wang, J.; Liu, H. *Journal of Colloid and Interface Science* **2007,** 312, (2), 390-396.

30. Ma, J.-h.; Guo, C.; Tang, Y.-l.; Chen, L.; Bahadur, P.; Liu, H.-z. *Journal of Physical Chemistry B* **2007,** 111, 5155-5161.

31. Bovey, F. A.; Mirau, P. A., *NMR of Polymers*. Academic Press: San Diego CA, 1996; p 1-459.

32. Tellini, V. H. S.; Jover, A.; Garcia, J. C.; Galantini, L.; Meijide, F.; Tato, J. V. *Journal of the American Chemical Society* **2006,** 128, (17), 5728-5734.

33. Whang, H.; Vendeix, F.; Gracz, H.; Gadsby, J.; Tonelli, A. *Pharmaceutical Research* **2008,** 25, (5), 1142-1149.

34. Hasegawa, Y.; Miyauchi, M.; Takashima, Y.; Yamaguchi, H.; Harada, A. *Macromolecules* **2005,** 38, (9), 3724-3730.

35. Bergonzi, M. C.; Bilia, A. R.; Bari, L. D.; Mazzi, G.; Vincieri, F. F. *Bioorganic & Medicinal Chemistry Letters* **2007,** 17, (21), 5744-5748.

36. Krause, S., Polymner-polymer compatibility. In *Polymer Blends*, Paul, D. R.; Newman, S., Eds. Academic Press, Inc.: New York, 1978; Vol. 1, pp 15-113.

37. Tonelli, A. E.; Srinivasarao, M., *Polymers form the Inside Out: An Introduction to Macromolecules*. John Wiley & Sons: New York, New York, 2001; p 1-249.

38. Young, R. J.; Lovell, P. A., *Introduction to Polymers*. 2nd ed.; CRC Press: Boca Raton, FL, 1991; p 1-443.

39. Munk, P., *Solvents and Self-Organization of Polymers*. Kluwer Academic Publishers: Dordrecht, The Netherlands, 1996; p 1-509.

40. Mandema, W.; Zeldenrust, H.; Emeis, C. A. *Makromol. Chem.* **1979,** 180, 1521-1538.

41. Wesslén, B.; Wesslén, K. B. *Journal of Polymer Science Part A: Polymer Chemistry* **1992,** 30, (3), 355-362.

42. Tuzar, Z., *Solvents and Self-Organization of Polymers*. Kluwer Academic Publishers: Dordrecht, The Netherlands, 1996; Vol. 327, p 1-509.

43. Zushun, X.; Linxian, F.; Jian, J.; Shiyuan, C.; Yongchun, C.; Changfeng, Y. *European Polymer Journal* **1998,** 34, (10), 1499-1504.

44. Zushun, X.; Changfeng, Y.; Shiyuan, C.; Linxian, F. *Polymer Bulletin* **2000,** 44, 215-222.

45. Pitsikalis, M.; Woodward, J.; Mays, J. W.; Hadjichristidis, N. *Macromolecules* **1997,** 30, (18), 5384-5389.

46. Price, C.; Woods, D. *Polymer* **1974,** 15, (June), 389-392.

47. Antonietti, M.; Heinz, S.; Schmidt, M.; Rosenauer, C. *Macromolecules* **1994,** 27, 3276-3281.

48. Zamurovic, M.; Christodoulou, S.; Vazaios, A.; Iatrou, E.; Pitsikalis, M.; Hadjichristidis, N. *Macromolecules* **2007,** 40, (16), 5835-5849.

49. Zhang, L.; Eisenberg, A. *Journal of Polymer Science: Part B: Polymer Physics* **1999,** 37, 1469-1484.

50. Jiang, Z.; Zhu, Z.; Liu, C.; Hu, Y.; Wu, W.; Jiang, X. *Polymer* **2008,** 49, 5513-5519.

51. Canto, L. B.; Mantovani, G. L.; deAzevedo, E. R.; Bonagamba, T. J.; Hage, E.; Pessan, L. A. *Polymer Bulletin* **2006,** 57, (4), 513-524.

5. SOLID-STATE MORPHOLOGIES OF POLYMER BLENDS COMPATIBILIZED BY γ-CYCLODEXTRIN STARS

5.1. Background

As described previously in the Introduction (section 1.5), blending bulk polymers is a method used to engineer a final polymer material with properties more desirable than either homopolymer component. For blends of PDMS and PS, researchers have studied applications such as hydrophobic surfaces, membranes,[1] and tribology.[2] Mixing of PDMS and PS is challenging due to the negligible entropy gains, and a high degree of chemical incompatiblity. The phase diagram reported by Nose for PDMS/PS, with molecular weights of $M_{w,PS}$ = 1400-230,000g/mol and $M_{w,PDMS}$ = 600g/mol, essentially shows a two-phase morphology even when heating to 200° C.[3] For this blend in particular, stability problems arise with migration of the PDMS to the surface as well as inconsistent phase dispersion within the PS film.[4] It has been shown that when only 2wt% PDMS is incorporated into the blend, the surface behaves like pure PDMS.[4, 5]

Blend properties are often dictated by the exchange of properties between phase domains. Improvements in the mixing and stabilization of incompatible blends are typically accomplished in two ways.[6] First, reactive compatibilization can be used to physically trap the blended polymer into a networked microstructure by crosslinking the components to create an interpenetrating network (IPN). Second, a third component can be added to the blend that aids in the mixing of the two phases. This second approach describes our method for compatibilizing PDMS and PS using CD-stars. Other compatibilization additives commonly used for PDMS and PS blends include block copolymers of PS and PDMS (PS-b-PDMS).[7]

Monte Carlo simulations were used by Zhu *et al.*[8] to study homopolymer blend compatibilization with different graft copolymer architectures. This study revealed that the

most effective blend composition for compatibilizing an A and B homopolymer blend (with A as the dispersed phase) occured when a graft copolymer of A-g-B (A is the backbone) was used as the additive. This effect is illustrated in Figure 5.1 in which different graft copolymer architectures are explored. All copolymer architectures seen in this Figure appear to aid in compatibilization of the homopolymers, but it was found that (b) and (c) were the most effective for compatibilization. The resultant irregular structure of the blends containing A-g-B is a consequence of the decrease in interfacial energies between homopolymer A and B.[8] This composition mixture is similar to our system where the hybrid slip-ring graft copolymer of PDMS-g-(PS-CD-star) helps to compatibilize the minor component (PDMS) into the major component (PS).

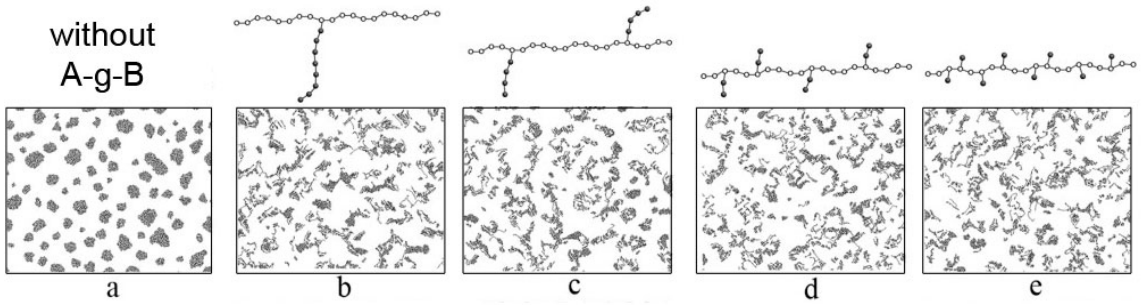

FIGURE 5.1. Monte Carlo simulations showing the effectiveness of A-g-B copolymers to compatibilize homopolymers A and B. Image (a) does not contain graft copolymer, whereas images (b-e) have graft copolymer. The volume fractions assigned for homopolymer A (○ and -), homopolymer B (● and open white area), and copolymer, are 0.243, 0.568, and 0.189, respectively. After reference [8].

Graft copolymers of PDMS-g-PS have not been studied a great deal, whereas studies of block copolymers of PDMS-b-PS are frequently found in the literature. Only a few researchers have synthesized graft copolymers of PDMS-g-PS. Graiver *et al.* reported successfully synthesizing block copolymers of PDMS-b-PS, but had difficulty synthesizing graft copolymers of PDMS-g-PS using free radical polymerization.[9] Difficulty arose when the PS grafts terminated by combination forming an insoluble network. However, Nakagawa

and coworkers performed a successful synthesis of PDMS-g-PS graft copolymers by using ATRP to polymerize uniform grafts.[10] However, studies using PDMS-g-PS for compatibilization of PDMS and PS, without creating an IPN, were not found in literature.

In this chapter we will explore the solid state morphology of films cast from the CD-star compatibilized solutions, studied in Chapter 4, to observe the effectiveness of the CD-star to act as a compatibilizer for PDMS and PS blends. As outlined previously in section 1.5.3, Rusa and Tonelli achieved solid-state blend compatibilization of PLLA/PCL after processing with pristine α-CD illustrating that physical confinement of polymers in CD-cores can overcome repulsive forces between two unlike polymers.[11] As a result of this finding, an impetus is established that gives the CD-stars similar potential to physically blend polymers through its CD-core. However, CD-stars have not been used as a compatibilization additive for homopolymer blends to date, but have been used by other researchers to create uniform porous films[12], or as crosslinkers to form IPNs[13]. Therefore, in this work, films will be prepared by spin casting and solution casting of the compatibilized solutions, and will be compared with films not containing CD-stars, to observe any differences in morphology.

5.2. Microstructure of Spun cast films

5.2.1 Spin Casting of Solutions

Boron doped silicon wafers (4 inch diameter), with an orientation of <100>, were purchased from WaferNet and cut into pieces measuring approximately 1.5cm x 1.5cm using a diamond tipped knife. Intense UV treatment was conducted on these cut wafer pieces for half an hour in order to break the Si-O-Si bonds on the surface. Immediately following the UV treatment, the wafer pieces were subjected to a series of 10-minute solution treatments to hydrolyze the surface. These treatment baths were administered in the order of (1) deionized water, (2) Baker-Clean® (JTB-111), (3) deionized water, and (4) isopropyl alcohol. Following the final solution treatment, all wafer pieces were then immediately dried under a nitrogen stream.

The treated wafers were examined by water contact angle to reveal a very hydrophilic surface, which was highly wettable, with a water contact angle that was essentially zero.

Blended solutions consisting of PS and PDMS with and without CD-stars in chloroform were examined. These solutions were previously prepared and characterized in Chapter 4 and shown in Figures 4.3 and 4.4 with concentrations of 10g/dl. Spin casting of these solutions onto the wafer pieces was conducted with a spin-coater under atmospheric conditions at 3000 rpm for 60 seconds. The spun-coated wafers were then dried overnight in a fume hood at room temperature followed by heat treatment at 60° C for 3 hours.

5.2.2 Morphologies of Spun Cast Films

The resultant spun cast films were examined using an optical microscope in reflectance mode to investigate the morphology. Additionally, profilometer measurements show that the spun cast films without CD-star had an average thickness of 1.8μm whereas films containing CD-star were on average 1.5μm in thickness.

Figures 5.2 and 5.3 show spun cast films containing *no star* and *with star* for varying PDMS compositions of 1 to 20 wt% PDMS-62 and PDMS-308, respectively. In both Figures it is observed that samples *without* CD-star generally had an increasing PDMS domain size with increasing PDMS content. On the other hand, the samples *with* CD-star seem to be void of larger PDMS domains and are seen to be rather homogeneous by comparison. Only when the CD-star containing samples reach 20 wt% PDMS do the domains begin to appear. By comparing images from Figures 5.2 and 5.3, it is noted that the difference in PDMS molecular weights between these samples produced no visual effect on domain size or degree of compatibilization for these spun cast films. Therefore, the resultant compatibility of these films seems to be independent of molecular weight.

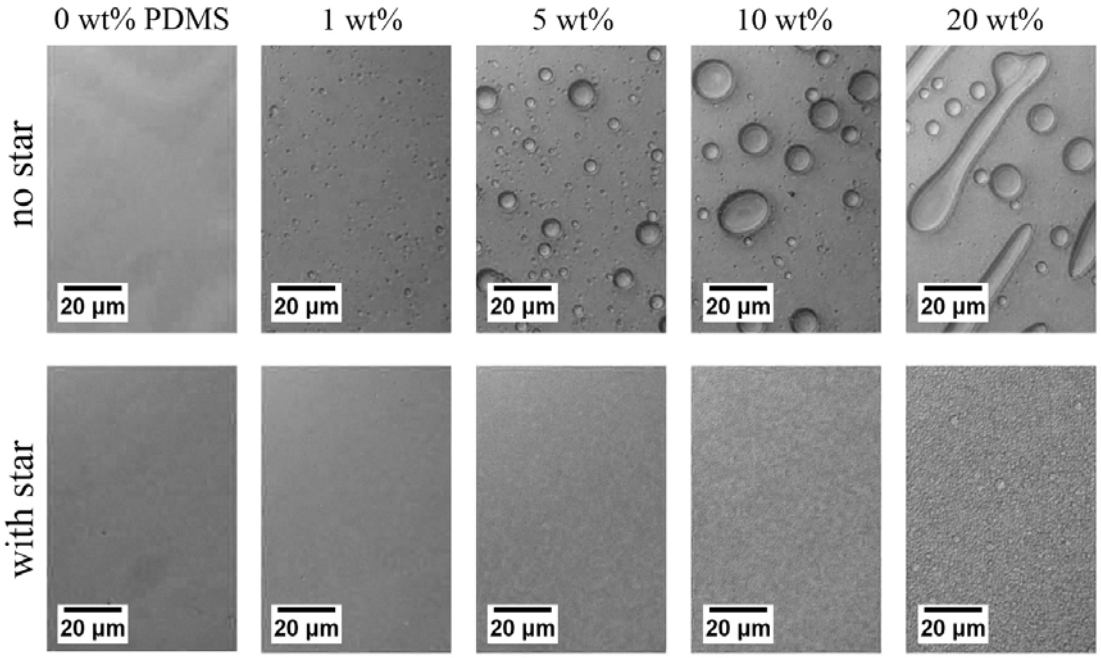

FIGURE 5.2. Comparison of spun cast films without star and with 1wt% CD-core with varying PDMS-62 content.

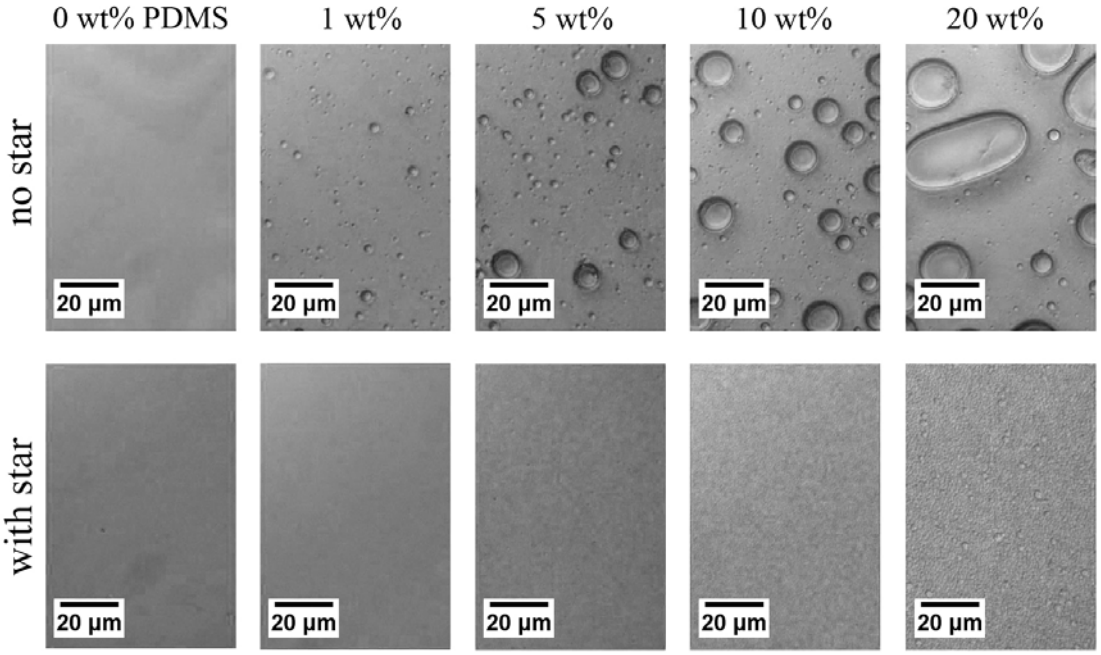

FIGURE 5.3. Comparison of spun cast films without star and with 1wt% CD-core with varying PDMS-308 content.

It is apparent from the optical micrographs in Figures 5.2 and 5.3 that the PDMS microstructure of the compatibilized films is very fine and generally much less than a micrometer. Therefore, atomic force microscopy (AFM) was conducted to characterize the morphology of the spun cast films on a finer scale. Figure 5.4 presents the images resulting from this characterization. All images were scanned in tapping mode with a dimensional area of 1μm x 1μm. Both the height and phase images are shown for each film tested.

AFM images of the compatibilized films in Figure 5.4 do not illustrate an ordered morphology, but do show a granular topology. As the PDMS content is increased, the height values seen on the film surface seem to fluctuate to a greater degree showing more surface heterogeneity. If the phase images in Figure 5.4 are carefully studied (whiter areas indicate softer PDMS regions on the film) it is observed that the PDMS phase morphology is fairly well dispersed down to the nanometer scale. However the observed phase-lag, seen in the phase images, does tend to increase with increasing PDMS content indicating a greater contrast between soft and hard regions. This may be a sign of decreased compatibilization. Overall, these films appear to be relatively well compatibilized.

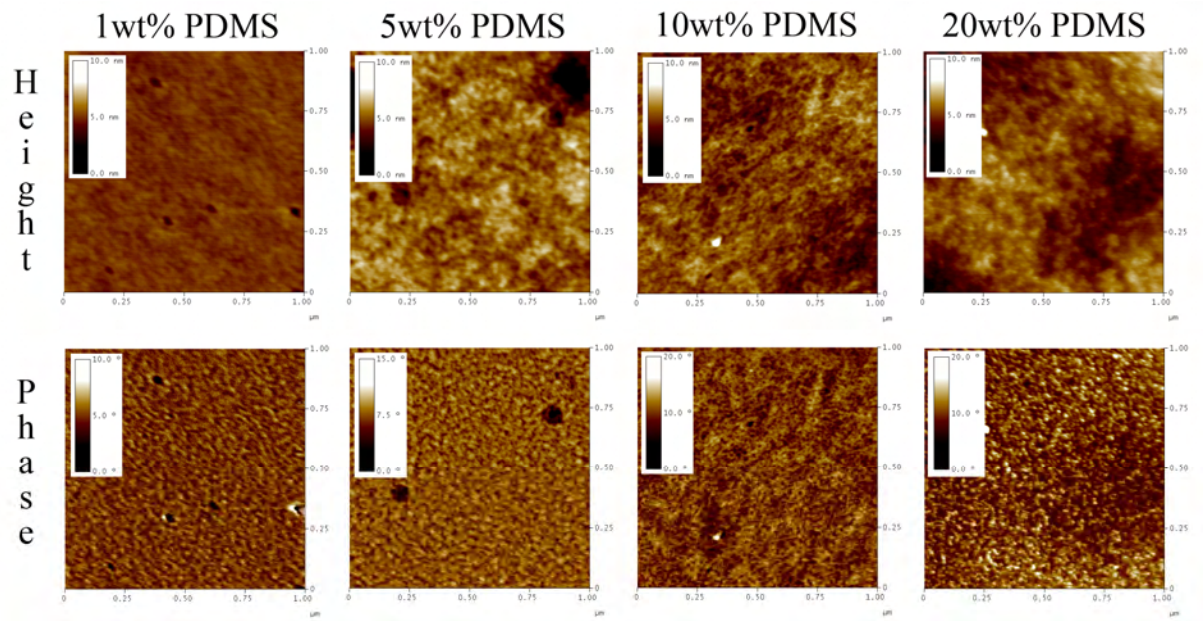

FIGURE 5.4. Atomic force microscope images of select spun cast films containing PDMS-308, where all samples incorporated 1wt% CD-core. The area scanned is 1µm x 1µm in all cases where the height and corresponding phase images and scales are shown.

The white domains seen in the phase images in Figure 5.4 appear to be roughly on the order of 50nm or less. Domains on this size scale correspond well with the characteristic size for a micelle and are within the range seen for the dynamic light scattering results in section 4.4.2. Therefore, since spin casting essentially flashes off the solvent through rapid evaporation, these images should be representative of what is observed in the compatibilized solution.

Further investigation of the surface morphology was carried out with scanning electron microscopy. The resultant images can be viewed in Figure 5.5, which show the spun cast films containing 10 wt% PDMS-308 with and without CD-star. The black phase regions in Figure 5.5(A) are caused by the electron density of silicon being higher than that of carbon, and therefore identify the PDMS phase. As can be observed in Figure 5.5(B), the CD-star compatibilized film has a granular morphology that is well compatibilized and without the distinct phase segregation seen for films with only PDMS and PS in (A). These images are

consistent with both the optical and AFM images and further confirm that if CD-star is incorporated into the blend, a significant increase in compatibilization does occur.

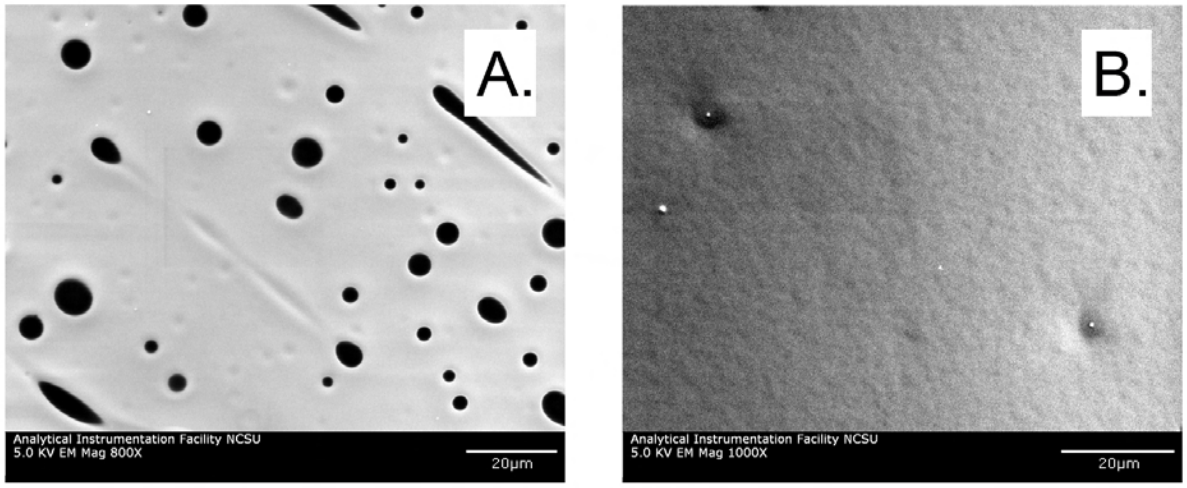

FIGURE 5.5. Scanning electron microscope images of spun coated films without (A) CD-star and with (B) CD-star. Both samples have 10wt% PDMS-308 incorporation. The CD-star sample (B) contains 1 wt% CD-core.

Additional investigation of the compatibilization effects of CD-star were conducted by varying the CD-star incorporation in the film, while leaving the PDMS amount constant. Figure 5.6 presents optical microscope images of the spun cast films containing 5 wt% PDMS (with both PDMS-62 and PDMS-308) and varying amounts of CD-star. It can be seen that the same general compatibilization trends are observed. Again the resultant compatibilization is independent of the blended PDMS molecular weight. Even with a small amount of CD-core (0.2 wt%), 5wt% PDMS can be effectively blended into the PS matrix. Here it is seen that with increasing amounts of CD-core, the surface appears to have a finer morphology, which may indicate an increased degree of compatibilization.

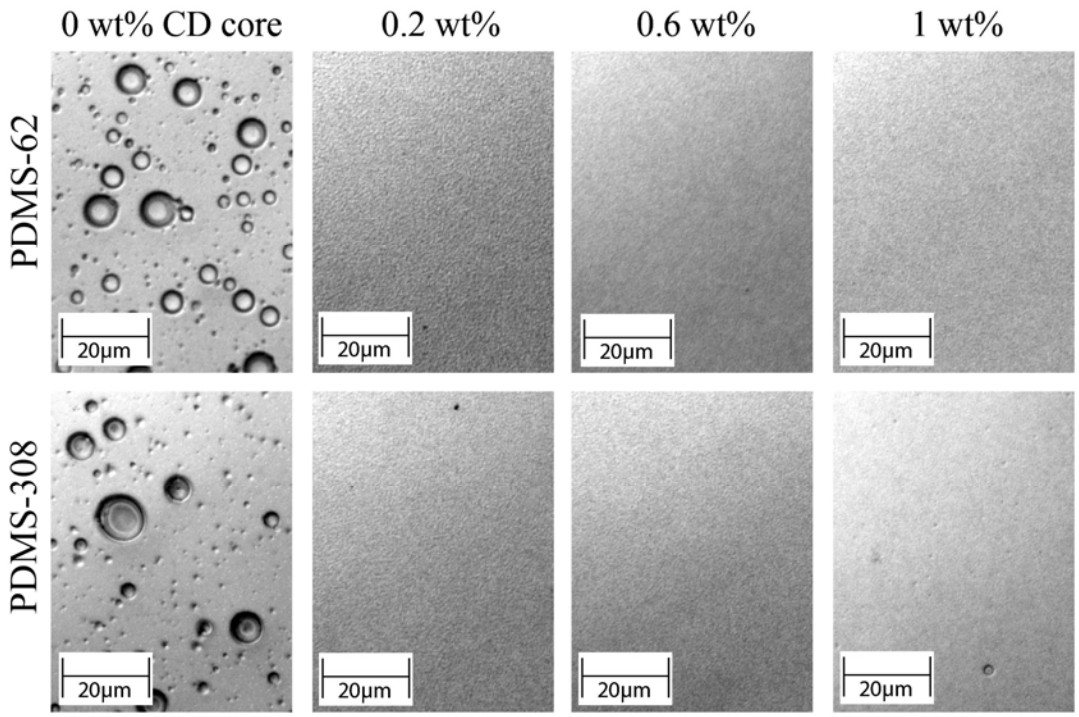

FIGURE 5.6. Optical microscope images of spun cast films containing 5wt% PDMS with varying amounts of CD-star.

Likewise, Figure 5.7 presents optical microscope images of the spun cast films containing 10 wt% PDMS (with both PDMS-62 and PDMS-308) and varying amounts of CD-star. In this case, the films containing 0.2 wt% CD-core have formed some larger domains, indicating a decrease in compatibilization. So for these samples, it appears that as long as 0.6wt% CD-core is present, a homogeneous morphology is found for 10 wt% PDMS. With that in mind, it seems if the ratio of PDMS to CD-star concentration is too high, larger PDMS domains form (as also seen for films with 20 wt% PDMS and 1 wt% CD-core in Figures 5.2 and 5.3). For the sample set in Figure 5.7, the films containing 0.2 wt% CD-core show a variance in the number of larger domains between the two PDMS molecular weights examined. The films containing PDMS-62 have slightly more large domains than the films containing PDMS-308. This is probably a result of PDMS-62 having less CD-star per PDMS chain (1

star *verses* 4.7 stars for PDMS-308) which decreases the hand-cuffing stabilization within the PS matrix.

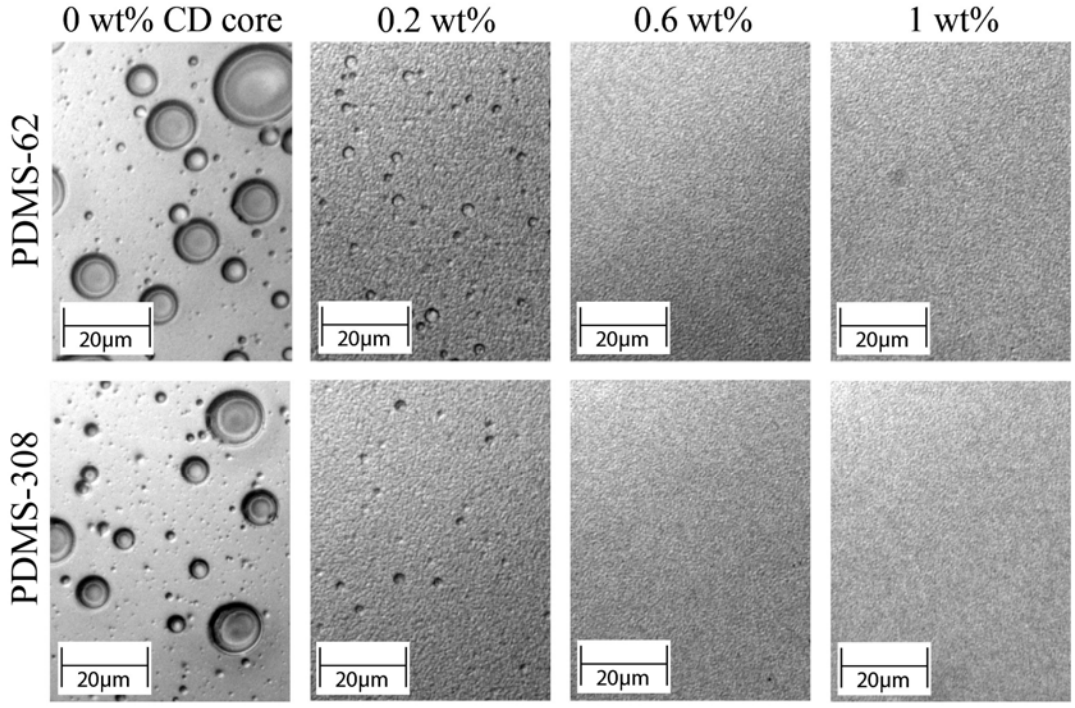

FIGURE 5.7. Optical microscope images of spun cast films containing a constant 10wt% PDMS with varying amounts of CD-core.

Tables 5.1 and 5.2 present the blend compositions and the PDMS/CD-star molar ratios between PDMS and CD-star for each spun cast sample film. The purpose of these tables is to examine if any of the increasingly "uncompatibilized" samples containing CD-star show any compositional similarities, particularly for samples of 20% PDMS in Figures 5.2 and 5.3, as well as 0.2 wt% CD-core samples in Figure 5.7. The samples of interest within these Tables are shown in bold type. The molecular weight values for PDMS-62 and PDMS-308 that were used in the molar ratio calculations are 62.7 kg/mol and 308 kg/mol, respectively, where the PDMS repeat unit was referenced to be 74.15 g/mol. Also, the CD-star (PS_6-γ-CD) used in these calculations had a molecular weight of 10,462 g/mol.

TABLE 5.1. Components making up the blends and the calculated molar ratios of PDMS/star.

Sample, (PDMS wt%)	CD-star: PS_6-γ-CD (mg)	PDMS (mg)	PS (mg)	repeats PDMS/star (mol/mol)	stars/PDMS chain (mol/mol)
PDMS-62					
(1)	40.3	5	454.7	17.5	48.3
(5)	40.3	25	434.7	87.5	9.7
(10)	40.3	50	409.7	175.1	4.8
(20)	**40.3**	**100**	**359.7**	**350.1**	**2.4**
PDMS-308					
(1)	40.3	5	454.7	17.5	237.3
(5)	40.3	25	434.7	87.5	47.5
(10)	40.3	50	409.7	175.1	23.7
(20)	**40.3**	**100**	**359.7**	**350.1**	**11.9**

From the ratios in Table 5.1, it appears that if a sample film has a molar ratio between 175 to 350 PDMS repeats/star then phase segregation starts to occur. When we compare this ratio range to the ratios found in Table 5.2 for the 10wt% PDMS with 0.2 wt% CD-core sample films (shown in bold), we find ratios that have values between 291 to 875 PDMS repeats/star before larger domains occur. So at first glance it would appear that compositions having ratios greater than 291 should exhibit reduced compatibilization. However in Table 5.2, the samples with 5 wt% PDMS and 0.2 wt% CD-star (shown in italic) were found to have a calculated ratio of 437 PDMS repeats/star yet they remain compatibilized. Therefore the degree of compatibilization cannot be simply predicted by the PDMS/CD-star molar ratio.

TABLE 5.2. Compositions of spun cast films with constant PDMS content and varying PDMS/star molar ratios.

Sample, (CD-core wt%)	CD-star: PS_6-γ-CD (mg)	PDMS (mg)	PS (mg)	repeats PDMS/star (mol/mol)	stars/PDMS chain (mol/mol)
5 wt% PDMS-62					
(0.2)	*8.06*	*25*	*466.94*	*437.6*	*1.9*
(0.6)	24.18	25	450.82	145.9	5.8
(1)	40.3	25	434.7	87.5	9.7
5 wt% PDMS-308					
(0.2)	*8.06*	*25*	*466.94*	*437.6*	*9.5*
(0.6)	24.18	25	450.82	145.9	28.5
(1)	40.3	25	434.7	87.5	47.5
10 wt% PDMS-62					
(0.2)	**8.06**	**50**	**441.94**	**875.3**	**1.0**
(0.6)	24.18	50	425.82	291.8	2.9
(1)	40.3	50	409.7	175.1	4.8
10 wt% PDMS-308					
(0.2)	**8.06**	**50**	**441.94**	**875.3**	**4.7**
(0.6)	24.18	50	425.82	291.8	14.2
(1)	40.3	50	409.7	175.1	23.7

This lack of correlation of the morphology with the molar ratios is puzzling. Perhaps this might be explained by some the CD-star not being threaded onto PDMS. In the ratio analysis, it was assumed that all of the PDMS and CD-star are interacting. However, this must not be an accurate assumption due to some ratios (and corresponding morphologies) not following the predicted trend and not showing a threshold ratio that represents incompatibility.

A second explanation might be based on the variation of PDMS droplet size with PDMS wt% in solution prior to spin coating. Two extreme cases must be considered for our CD-star system under constant stirring rate: (1) if the PDMS droplets are large, with a low surface area, and the interface becomes saturated with CD-star, then the excess CD-star does not participate in the PDMS threading, leading to insufficient compatibilization, or (2) if the PDMS droplets are small, with a larger surface area, less CD-star is available to saturate and compatibilize the domains, and the droplets will re-equilibrate to a larger size. Similar to case (1), Tolosa *et al.*[14] suggested in that in order to allow the surfactant to gain acceptable access to the interface, a decrease in droplet size (or increase in surface area) needs to be accomplished in an oil/water/surfactant emulsion. However, similar to case (2), they stated that if the surfactant inventory to stabilize the oil/water emulsion was insufficient to accommodate the increased surface area, then creation of smaller droplets by increasing the stirring rate would not be worthwhile.[14]

As hypothesized above, it is thought that the decrease in compatibilization observed for our sample films is a reflection of each extreme case outlined. For the samples in Table 5.1 containing 20 wt% PDMS with 1 wt% CD-core, the droplet size that was accomplished during stirring was large (with respect to lower wt% PDMS samples). This was caused by the large amount of PDMS in the composition (100mg verses 50 mg for the 10 wt% sample), therefore leading to similar issues as described in case (1). On the other hand, for the samples in Figure 5.2 with 0.2 wt% CD-core made with 10 wt% PDMS, these samples achieved a smaller initial droplet size from stirring but were unable to provide enough CD-star at the interface to aid in compatibilization, therefore acting similar to case (2). If these conditions hold true, then some conclusions can be drawn from these observations. When the ratio of PDMS repeats/star reaches a maximum value between 437 to 875, incompatibilization starts to occur for samples containing $\leq$ 10 wt% PDMS incorporation. Also, if a higher stirring rate could be accomplished for the 20 wt% PDMS sample solutions, then it is possible that further compatibilization could occur.

5.2.3 Water Contact Angle Analysis of Spun cast films

Figure 5.8 presents an illustration of a water contact angle measurement, including Young's equation, relating the surface tensions to the water droplet angle.[15] The angle θ seen in Young's equation is controlled by the three surface tension force vectors (γ) related to the liquid (L), surface (S), and vapor (V) phases of the system. For polymer blends, the resultant water contact angle is dependent on the film composition and water interactions with the blended film components. The water contact angles for several polymers have been tabulated by Owen where the homopolymers of PS and PDMS are listed as having angles of 91° and 101°, respectively.[16] Our measured water contact angle for PS has a value of 89°, in good agreement with Owen's value. Each measurement used a volume of 8μl of deionized water per drop. Sample films were measured three times and all of the recorded angles were averaged.

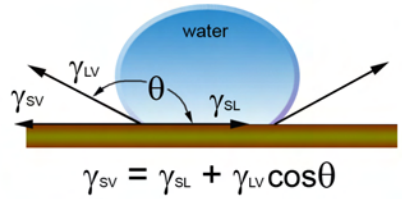

FIGURE 5.8. Illustration of a water contact angle measurement and the relation of surface tensions to Young's equation.

Miyata *et al.*[17] prepared an IPN of PDMS and PS for use in gas permeation membranes. They reported observing an increasing water contact angle with increasing PDMS weight fraction where at ~ 20wt% PDMS they observe a contact angle of ~102°. At approximately 40wt% PDMS (or greater mass) the films gave a constant contact angle of ~107°. Wu *et al.*[18] spun cast films of PS-b-PDMS copolymers with varying compositions of PS and PDMS on mica (hydrophilic surface). They reported a water contact angle of 107° at 20 mol% PDMS, whereas an angle of 112° is seen for a sample with 40 mol% PDMS. Also, they saw a constant angle of 112° for PDMS amounts in excess of 40 mol% for the PS-b-PDMS spun cast films.

Figure 5.9 presents the measured water contact angles for our spun cast films with varying amounts of PDMS and constant 1wt% CD-core. In general it can be seen that as the PDMS content increases, the water contact angle increases. The sample film with 20 wt% PDMS-308 *without* CD-star shows a contact angle of ~102° which may imply that the surface interactions are essentially PDMS-like. The differences observed between PDMS-62 and PDMS-308 for the sample films *without* CD-star are within the experimental error. This is also true for the sample films *with* CD-star. However, the sample sets containing star and without star seem to parallel each other. This observed trend seems to be explained by the overall composition of the samples, which is an increasing water contact angle with increasing PDMS content.

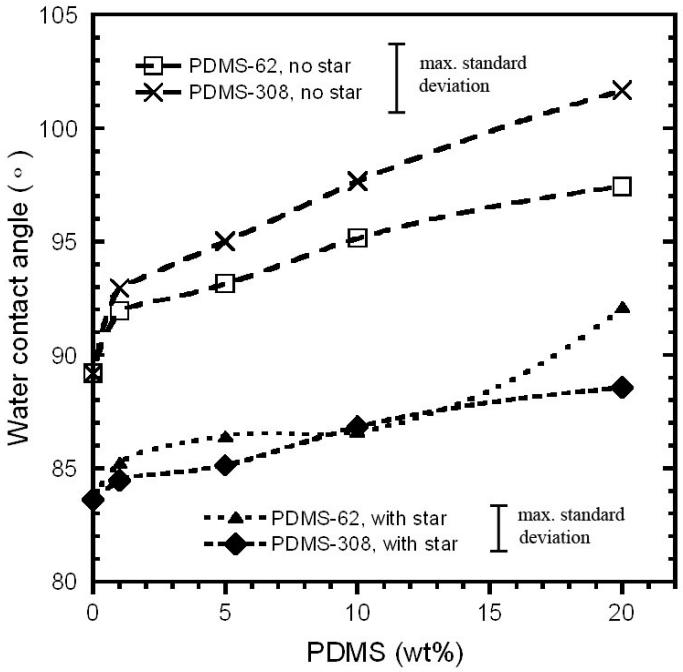

FIGURE 5.9. Water contact angle of films with constant 1 wt% CD-core and varying PDMS content. The maximum standard deviation for each data set is shown.

Likewise, Figure 5.10 presents the measured water contact angles for the spun cast films containing constant amounts of PDMS, (A) 5 and (B) 10 wt%, with varying amounts of CD-core. For the sample sets in (A), it can be seen that a rapid decrease in contact angle is observed for a small addition of CD-core, after which the contact angles are similar to the sample set without PDMS. Similar behavior is observed in (B), although the contact angle remains above the line for samples with PDMS. Again the trends seen in both (A) and (B) appear to be explained by the composition of the spun cast films.

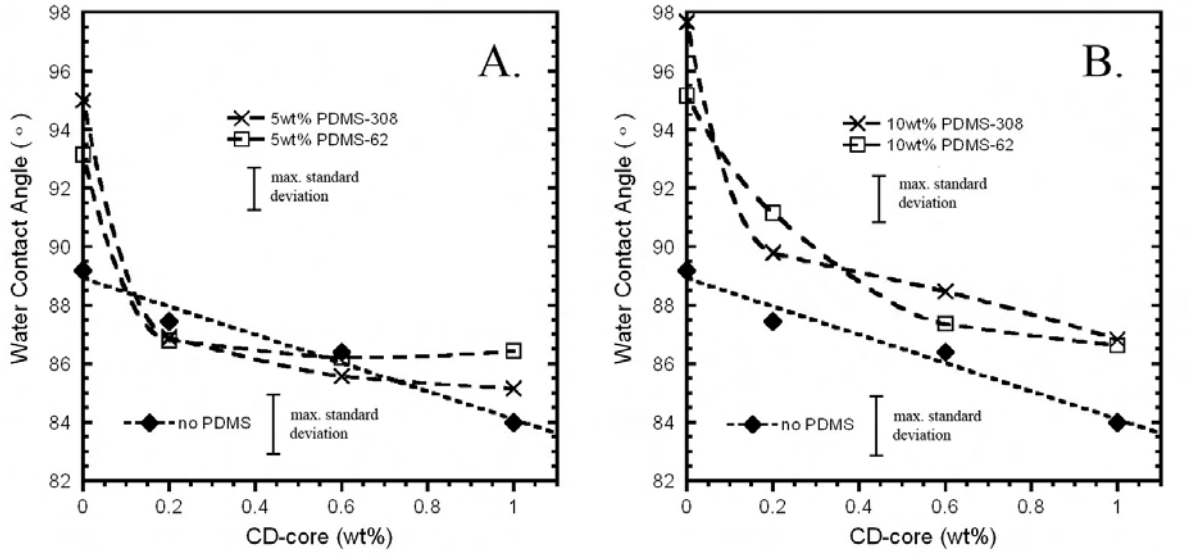

FIGURE 5.10. Water contact angle for samples with A.) 5 wt% PDMS, and B.) 10 wt % PDMS. The maximum standard deviation for each data set is shown.

5.2.4 Aging and stability of spun cast films

Thermal aging of polymer blends is a method used to inquire about the stability of the blend and to show whether coarsening of the morphology may occur. This method relieves stresses incurred during initial casting of the films and allows the blend to move toward equilibrium. Spun cast films with constant CD-star and increasing PDMS (same films as seen in Figures 5.2 and 5.3) were placed into a vacuum oven, which was evacuated three times with subsequent nitrogen gas back-filling before heating to 125° C. Thermal aging was conducted

on the spun cast films at a temperature of 125° C for 3 days under a stream of dry nitrogen. This aging temperature is well above the T_g of PS (~100° C). After 3 days, the heat was terminated and the films were allowed to cool over the duration of 4 hours to room temperature, while remaining under nitrogen. These films were then removed from the oven and examined with an optical microscope in reflectance mode.

Comparision of the unaged films in Figures 5.2 and 5.3 can be made with the aged films in Figures 5.11 and 5.12 containing increasing amounts of PDMS-62 and PDMS-308, respectively. When comparing the unaged films to the aged films *without* CD-star, some coarsening was observed to occur for all of the PDMS domains. Visual identification of coarsening was observed as “fish-eye” domains and coarsening ridges within the PDMS domains.

Likewise, by comparing unaged and aged films *containing* CD-star, the aged films appear to have a notable stability to thermal aging (at this magnification) especially with 1 and 5 wt% PDMS incorporation. However when comparing the aged 20 wt% films containing CD-star (in Figures 5.10 and 5.11) to the non-aged films containing CD-star (in Figures 5.2 and 5.3), these films show the highest degree of coarsening, while the 10 wt% samples exhibit a much lower degree of coarsening. The largest domains that were formed during aging for the 20 wt% PDMS films *with CD-star* now have a characteristic size that is on the order of the smaller PDMS domains for the 20 wt% PDMS *without* CD-star. Therefore it is apparent that for decreased amounts of PDMS, while leaving the CD-star content constant, that increased compatibilization and stability occur.

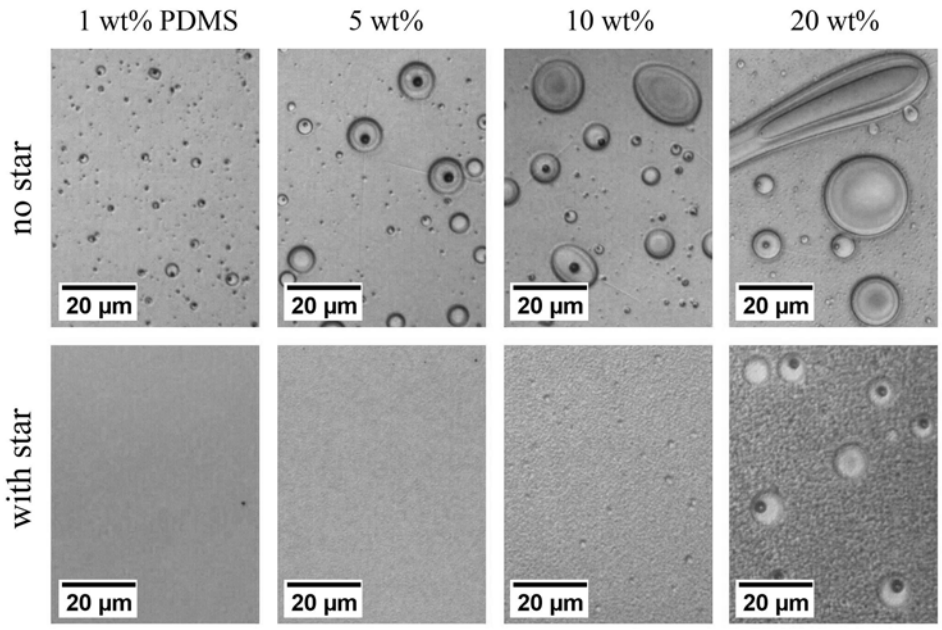

FIGURE 5.11. Spun cast films containing PDMS-62 aged at 125° C for 3 days.

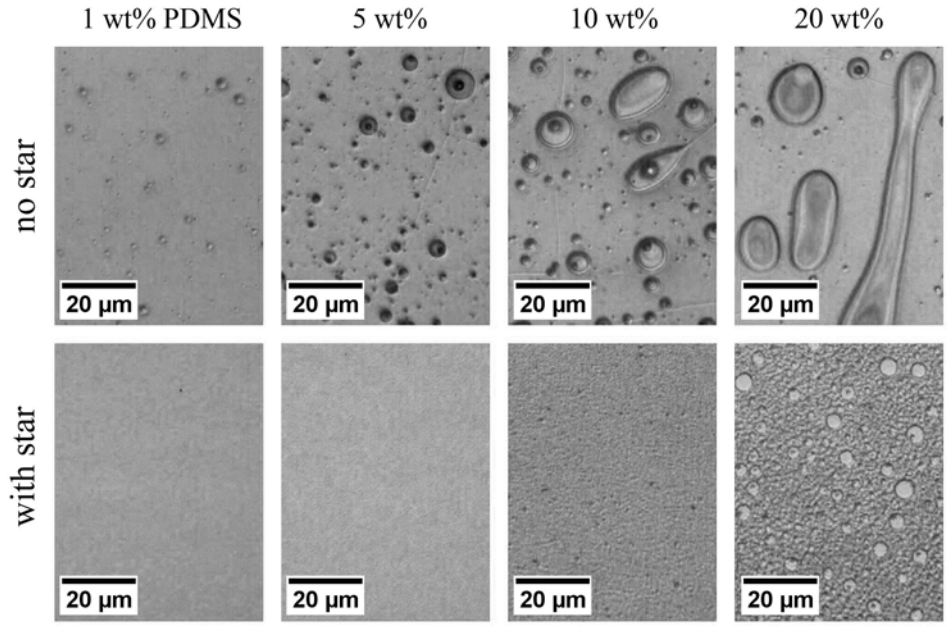

FIGURE 5.12. Spun cast films containing PDMS-308 aged at 125 °C for 3 days.

Maric and Macosko[19] observed that melt blending at 200° C with PDMS/PS (20/80 w/w) with 1 to 3% PS-b-PDMS copolymer produced micelles of the copolymer in the PS phase. They observed that the M_n of the copolymer had a large impact on the PDMS domain size, where small PDMS domains were observed when a smaller block copolymer (M_n = 16kg/mol) was used. However these smaller domains seemed to be unstable to annealing, whereas when higher molecular weight copolymers (>M_n = 83 kg/mol) were used, they proved to be more stable to annealing. Likewise, Petitjean et al.[20] reported that blends of PS-b-PDMS and PS showed that their surfaces became like PDMS when 0.2-2.0wt% PS-b-PDMS is added, and that upon annealing the film remained stable.

5.3. Microstructure of Solution Cast Films

5.3.1. Solvent Casting of Solutions

Solution casting was performed in polytetrafluoroethylene (PTFE) molds to ensure that the films could be retrieved easily. Films were cast from the same solutions used in the spin casting experiments and which were reported in Chapter 4. A few of the resultant cast films can be seen in Figure 5.13. A two day controlled evaporation of the solutions was established by placing a glass dish over the cast films. This glass dish was sealed along the edge by a paper towel in order to slow film drying and reduce bubble formation. All films tended to bow during formation, but bubble development was virtually nonexistent. Following the controlled evaporation, the cast films were allowed to air dry for up to two weeks in the fume hood.

It was found that all films with PDMS displayed some cloudiness and visually had a two-phase morphology. These films were observed to contain a non-uniform PDMS phase distribution and clearly showed a layer of PDMS remaining in the PTFE casting molds after film retrieval. This observation is especially true for films *without* CD-star. However, when

the films *with* CD-star were cast, a large reduction in the amount of residual PDMS left behind in the casting molds was observed.

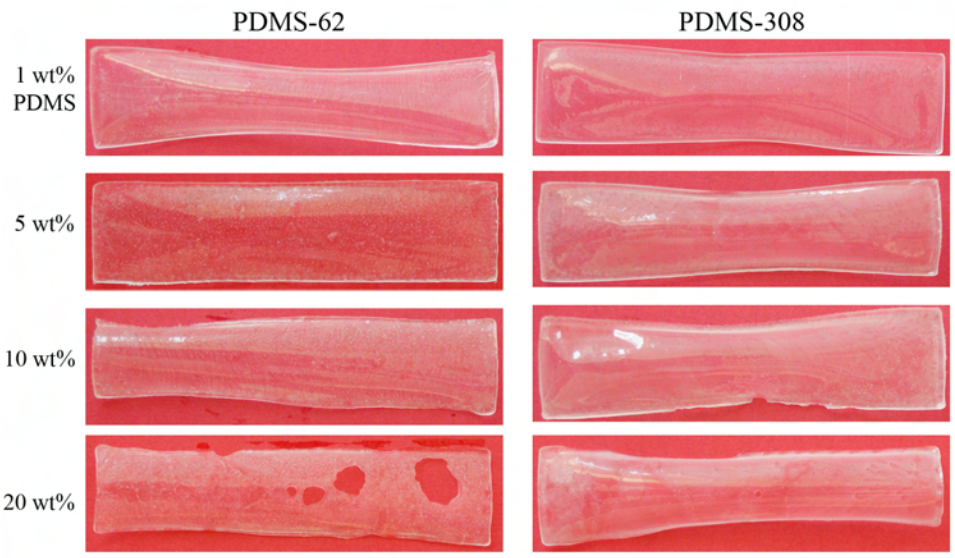

FIGURE 5.13. Shown are cast films of PDMS and PS blends without star. These films are also representative for the cast films containing CD-star.

5.3.2. Compression Molding of Films

Cast films were additionally processed by compression molding. This was done to flatten the bowed films so that mechanical testing could be conducted (mechanical properties are examined in Chapter 6). All films were processed in parallel to assure identical histories. First the solution cast films were placed into an oven at 60° C under vacuum for 4 days in order to remove the majority of solvent remaining in the films. Afterwards, these films were compression molded at 120° C for 5 minutes at 5,000 psi between polyimide mold-release films and polished steel plates. Rapid cooling was then performed on the film by removing them from the heated platens into room temperature. Additional heat treatment was conducted on the sample films at 90° C for 14 days, while under vacuum in order to remove any residual solvent remaining in the films as well as relax any residual stresses from compression molding. Determination of complete solvent removal was conducted by DSC.

The films were considered to be sufficiently dry when the PS cast film showed a T_g similar to that of the original PS pellets used to prepare the films.

Two primary problems arose with this film processing. First, PDMS remained in the PTFE casting mold, and second, PDMS was squeezed out of the sample films during compression molding. The PDMS residue observed after compression molding can be seen in Figure 5.14 on the polyimide mold-release film for a solution cast film containing 20 wt% PDMS-308. Thus it is obvious that the amount of PDMS remaining in each sample is less than the initial amount added.

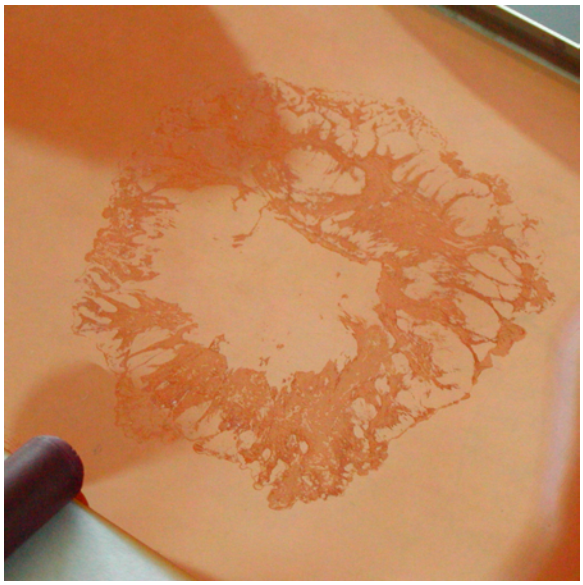

FIGURE 5.14. PDMS residue remaining on mold-release film after compression molding the 20 wt% PDMS-308 cast film (without CD-star).

5.3.3. Determination of PDMS Remaining in Films after Processing

Loss of PDMS from solution casting and subsequent compression molding of the films has been shown to be a significant problem. So it is important to quantitatively determine how much PDMS remains in the films after these processing steps. Therefore, compositional

analysis was conducted on the post-processed films using ^{1}H-NMR. As presented earlier, Tables 5.1 and 5.2 show the initial mass compositions for the solution cast films. These initial compositions can be used to determine the expected molar ratios between PDMS and PS if no PDMS were lost. The difference between the expected ratio from the initial blend compositions and the ratios found from ^{1}H-NMR after pressing the films can be used to find the amount of PDMS remaining in the film.

For ^{1}H-NMR analysis, ~55mg of each compression molded film was dissolved in 1ml of $CDCl_3$. These solutions were allowed to fully dissolve over the course of 2 hours. Each sample was observed to be clear without any undissolved particles. From the collected ^{1}H-NMR spectra, all peaks were then integrated to determine the areas in order to quantitatively examine the composition of the blend.

Figure 5.15 shows a representative ^{1}H-NMR spectrum of a blended film that contains a dissolved sample of PS/PDMS/CD-star with 5wt% PDMS-308 and 1wt% CD-core in $CDCl_3$. Peaks in Figure 5.15 for area (1) are due to the hydrogens on the PS phenyl groups, where area (2) is primarily due to the backbone hydrogens on the PS (-CH_2- and -CH-) and, to a lesser degree, the hydrogens on the CD-core, whereas area (3) is due to the methyl hydrogens on the PDMS (-CH_3). Since area (1) peaks contain the $CDCl_3$ peak, this renders them unusable for comparing with peak (3) to quantitatively determine PDMS molar quantities. Therefore, areas (2) and (3) were ratioed to find the residual PDMS remaining in the films.

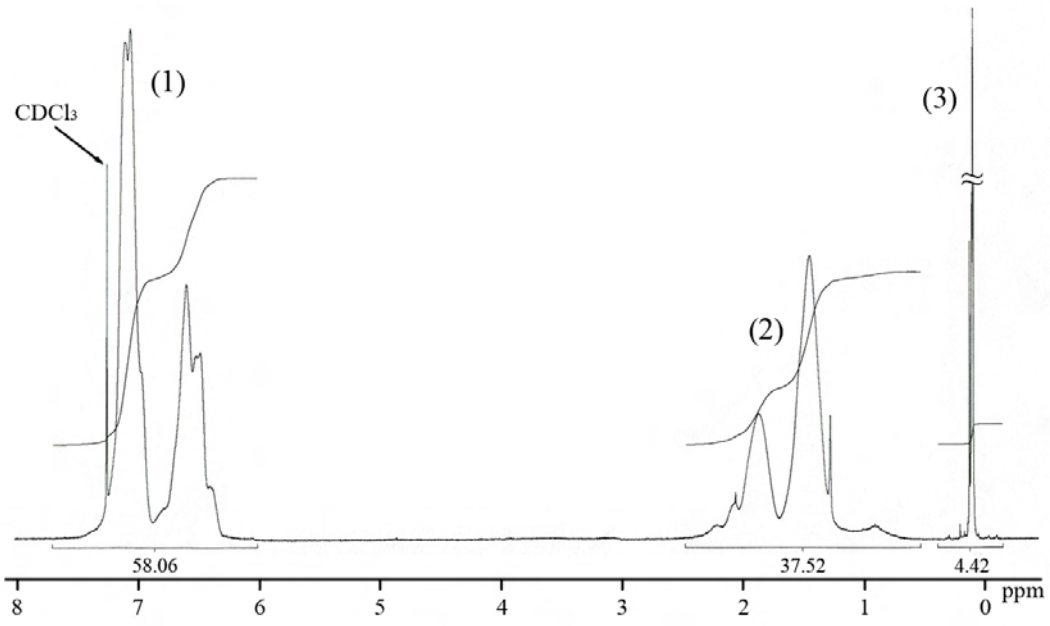

FIGURE 5.15. Representative ^{1}H-NMR spectrum showing integrated areas used to determine PDMS retained from the dissolved PS/PDMS/CD-star film with 5 wt% PDMS-308. Set of peaks in area (1) are due to PS phenyl groups, set (2) peaks are due to PS backbone groups and the CD-core, and (3) peak is due to PDMS.

These results are plotted in Figure 5.16, along with the initial PDMS contents. Two data sets are shown in this Figure where (1) contains CD-star and (2) has no CD-star. It can be observed that if CD-star is present, then considerably more PDMS is retained within the film. It should be highlighted that generally *80% PDMS retention* is accomplished for films *with CD-star* up to 10wt% PDMS incorporation, compared to only *20% PDMS retention* for films *without CD-star*. It appears that the ability of 1 wt% CD-core to retain PDMS in the samples levels off beyond 10 wt% initially added PDMS. This is further evidence of complexation of PDMS with CD-star, and subsequent compatibilization with PS.

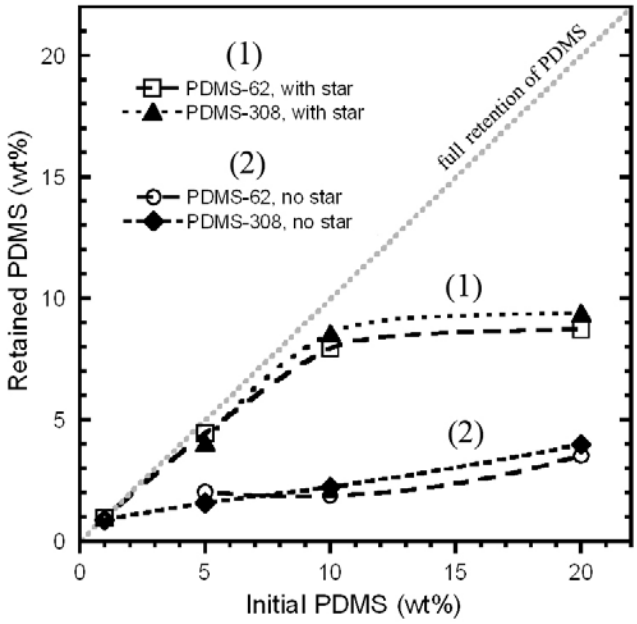

FIGURE 5.16. Initial PDMS wt% *vs* actual retained PDMS wt% obtained by ^{1}H-NMR. The CD-core content in data set (1) is constant at 1 wt%.

Likewise, Figure 5.17 shows samples with constant amounts of PDMS in the films and varying amounts of CD-core. This figure shows that when the amount of CD-core is increased in the films, the amount of PDMS retained within the films is increased as well. Again, this indicates that the CD-star is interacting with the PDMS causing it to be physically complexed in the PS matrix reducing its mobility. It is interesting to note that for both the 5 or 10 wt% PDMS sample sets, PDMS retention is found at approximately 80% of the initial amount introduced. For the 5 wt% PDMS sample set, the amount of retention appears to be independent of PDMS molecular weight used.

It also appears that for data set (1) in Figure 5.17 most of the PDMS is retained after 0.2wt% CD-core incorporation, indicating that perhaps no more than 0.2 wt% is needed for ~4 wt% PDMS compatibilization. This equates to 350 repeats PDMS/CD-star. Moreover, for data set (2) with 10 wt% initial PDMS, most of the PDMS is retained after 0.6 wt% CD-core addition, indicating that this is the minimum amount of CD-core needed to successfully retain 8 wt%

PDMS in PS. This equates to 248 repeats PDMS/CD-star. If more data points had been collected for data set (2), in particular for samples between 0.2 to 0.6 wt% CD-core, then the PDMS/CD-core ratio may be closer to the value of 350 found for data set (1).

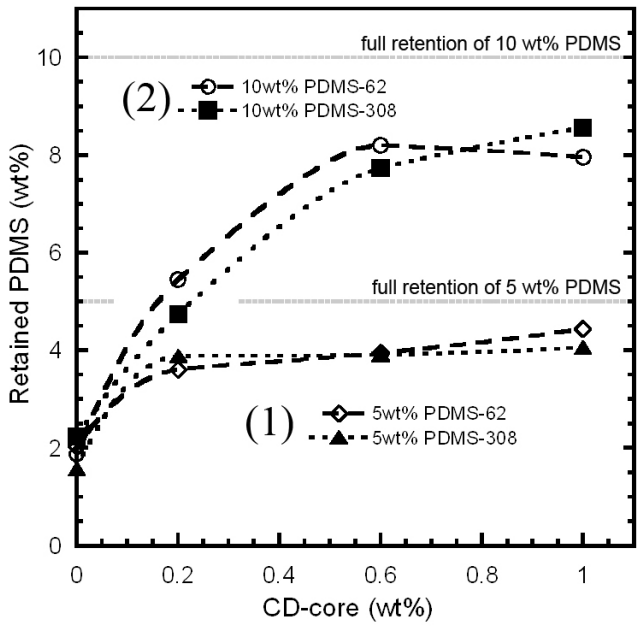

FIGURE 5.17. Amount of PDMS remaining in compression molded films initially containing (1) 5 wt% and (2) 10 wt% PDMS with varying amounts of CD-core.

5.3.4. Compression Molded Film Morphology

Small sample films were cut from the compression molded films having dimensions of 6 mm x 25 mm. The thicknesses of the films were found to be ~200 μm. Figures 5.18 and 5.19 show the compression molded films made with PDMS-62 and PDMS-308, respectively. In these Figures, the compression molded films are laid over the words "NC-State" for the purpose of helping to show the clarity of the films. In addition, below each film image, transmission optical micrographs show the morphology of each film, with the focal plane somewhere inside the film.

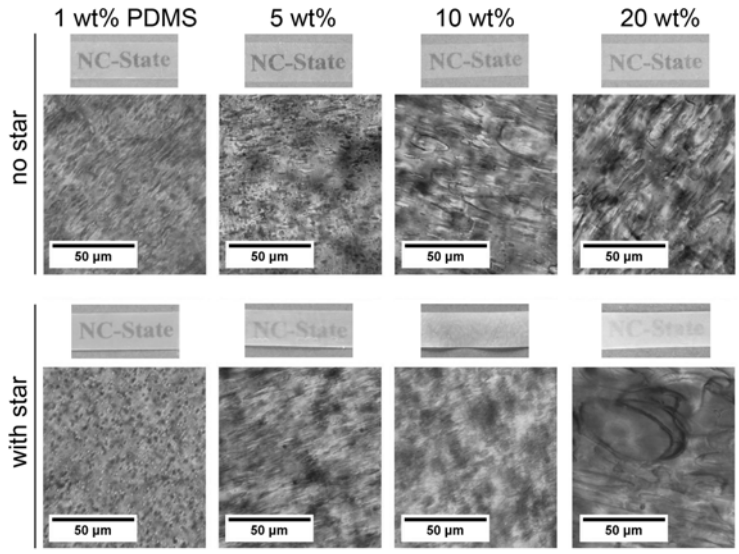

FIGURE 5.18. Transmission optical micrographs for films with PDMS-62. Sample films containing star all have 1 wt% CD-core. Presented above these images are the compression molded films illustrating film opacity, as judged by the ability to read the "NC-State" text.

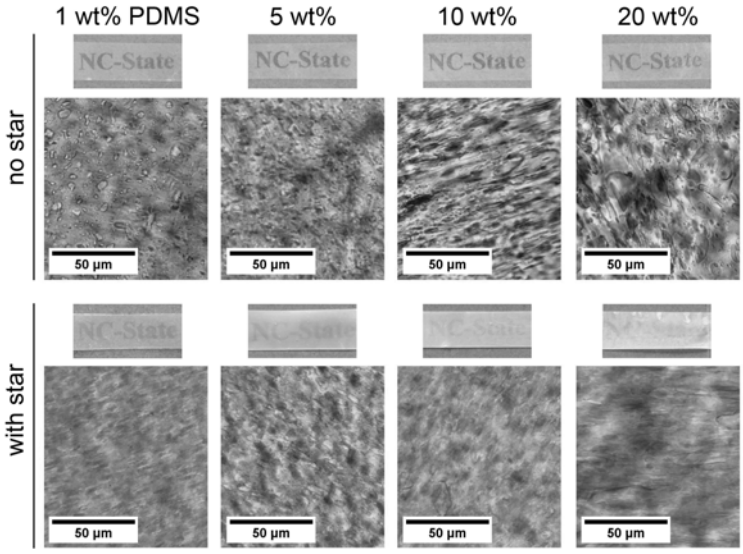

FIGURE 5.19. Transmission optical micrographs for films with PDMS-308. Sample films containing star all have 1 wt% CD-core. Presented above these images are the compression molded films illustrating film opacity, as judged by the ability to read the "NC-State" text.

If the compression molded films in Figure 5.18 and 5.19 are studied carefully, then a trend starts to emerge. It can be seen that for all films *without CD-star* the transparency is relatively high and does not seem to change much with increasing PDMS content. On the other hand, for the sample films *with CD-star* the films appear to get increasingly cloudier as the PDMS amount increases. This effect is a direct consequence of the results noted in Figure 5.16 where increased PDMS retention occurs with CD-star incorporation. Therefore the clarity of the films inversely correlates with the amount of PDMS found within each film.

Likewise, if we now examine the films in Figures 5.20 and 5.21 which have 5 and 10 wt% PDMS, respectively, with varying amounts of CD-core, a similar trend emerges. In both Figures, the films without CD-core tend to be clearer. For the sample films in Figure 5.20 with 5wt% PDMS and CD-core, the opacity of these films seems to be generally constant, which correlates well with the retained amount of PDMS found for these films (all have ~ 4wt% PDMS retained). However, for the sample films in Figure 5.21 containing 10 wt% PDMS and CD-core, the films appear to be getting increasingly cloudy with increased CD-core content, which again correlates with the final amounts of PDMS found for these samples.

In summary, the solution cast films exhibit a trend of increased cloudiness with increased PDMS retention. PDMS retention increases with increasing CD-star content, thus films *without* CD-core show more transparency than films *with* CD-core.

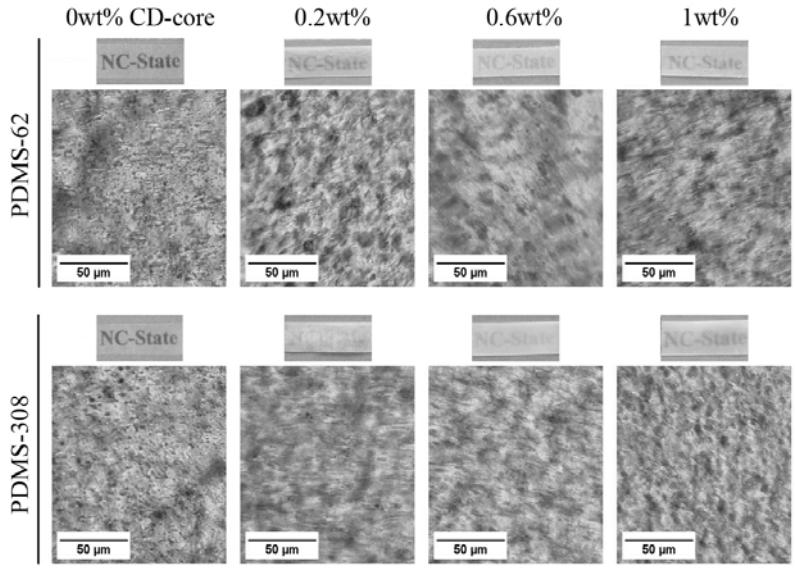

FIGURE 5.20. Transmission optical micrographs for films with constant 5wt% PDMS and varying amounts of CD-core. Presented above these images are the compression molded films illustrating film opacity, as judged by the ability to read the "NC-State" text.

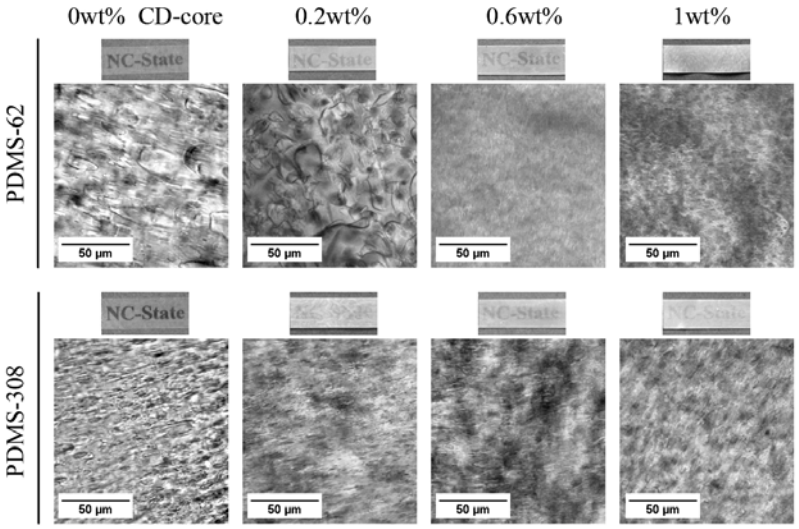

FIGURE 5.21. Transmission micrographs for films with constant 10wt% PDMS and varying amounts of CD-core. Presented above these images are the compression molded films illustrating film opacity, as judged by the ability to read the "NC-State" text.

The morphology in the transmittance micrographs for all samples presented in Figures 5.18 to 5.21 seems to be independent of composition and the presence of CD-star. PDMS domains can be clearly seen and appear to have a distribution of sizes. However, it is difficult to see if domain size changes with increasing PDMS content. This could be due to the fact that these micrographs contain superimposed images from focused and unfocused planes within the 200μm thick sample. Difficulty arises when attempting to identify trends in domain size since it is unclear whether individual or superimposed domains are being observed.

These results raise an important question. Why are the films containing CD-core not clear if the compatibilized casting solutions were initially stable and clear? This outcome is probably caused by coalescence of the micelles as the solvent evaporates and concentration increases. At higher concentrations (tending toward the solid-state), the micelle structure is no longer stable. Therefore even though we do not see micelle sized domains in the solid films, the fact remains that CD-star still helps to stabilize and compatibilize PDMS into PS. This is evidenced by PDMS being retained to a much greater degree when CD-star is present then when it is not. Since we see larger domains than expected for the cast and compression molded films, coalescence of PDMS does occur, but the complexation or physical hand-cuffing of the PDMS into the CD-star remains.

5.4. Conclusions

Film formation from PDMS/PS/CD-star solutions was explored two ways: (1) by spin casting the solutions, and (2) by solution casting and sebsequent compression molding. Spin casting of films showed that compatibilization of PDMS into PS was accomplished with CD-stars as evidenced by a reduction in PDMS domain size to nanoscale levels. Compatibilization of PDMS up to a weight fraction of 20 wt% was largely achieved with 1 wt% CD-core addition, as evidenced by the spin cast film images. Experiments holding the PDMS fraction constant showed that a 5 wt% PDMS sample can be relatively compatibilized with only 0.2 wt% CD-

core, whereas 10 wt% PDMS can be satisfactorily compatibilized by 0.6 wt% CD-core. AFM analysis showed that spun cast films with CD-star are nanophase separated. Additionally, the spun cast films appear to be generally stable to coarsening after 3 days at 125° C.

Empirical evidence shows that when blends of PDMS and PS are solution cast and compression molded, PDMS has a tendency to migrate out of the film, changing the composition of the blend. It has also been shown that compression molded films are not as intimately compatibilized as the spun cast films as evidenced by optical microscopy. However, blend films show a large increase in PDMS retention when CD-star is present as revealed by quantitative ^{1}H-NMR compositional analysis. This demonstrates that PDMS can be incorporated to a much larger degree into PS when CD-stars are used as compatibilizers. PDMS retention was also shown to be dependent on the amount of CD-star incorporation.

5.5. References

1. Kim, H.-J.; Jeong, Y.-S.; Lee, Y.-S. *Journal of Industrial and Engineering Chemistry* **1999,** 5, (1), 69-73.

2. Ndoni, S.; Jannasch, P.; Larsen, N. B.; Almdal, K. *Langmuir* **1999,** 15, 3859-3865.

3. Nose, T. *Polymer* **1995,** 36, (11), 2243-2248.

4. Lucas, P.; Robin, J.-J. *Advanced Polymer Science* **2007,** 209, 111-147.

5. Selby, C. E.; Stuart, J. O.; Clarson, S. J.; Smith, S. D.; Sabata, A.; Ooij, W. J. v.; Cave, N. G. *Journal of Inorganic and Organometallic Polymers* **1994,** 4, (1), 85-93.

6. Utracki, L. A. *Canadian Journal of Chemical Engineering* **2002,** 80, (6), 1008-1016.

7. Shelby, C. E.; Stuart, J. O.; Clarson, S. J.; Smith, S. D.; Sabata, A.; Ooij, W. J. v.; Cave, N. G. *Journal of Inorganic and Organometallic Polymers* **1994,** 4, (1), 85-93.

8. Zhu, Y.; Ma, Z.; Li, Y.; Cui, J.; Jiang, W. *Journal of Applied Polymer Science* **2007,** 105, 1591-1596.

9. Graiver, D.; Decker, G. T.; Kim, Y.; Hamilton, F. J.; Harwood, H. J. *Silicon Chemistry* **2002,** 1, 107-120.

10. Nakagawa, Y.; Miller, P. J.; Matyjaszewski, K. *Polymer* **1998,** 39, (21), 5163-5170.

11. Rusa, C. C.; Tonelli, A. E. *Macromolecules* **2000,** 33, (15), 5321-5324.

12. Stenzel, M. H.; Davis, T. P.; Fane, A. G. *Journal of Materials Chemistry* **2003,** 13, 2090-2097.

13. Du-Chesne, A.; Wenke, K.; Lieser, G.; Wenz, G. *Acta Polymer* **1997,** 48, 142-148.

14. Tolosa, L.-I.; Forgiarini, A.; Moreno, P.; Salager, J.-L. *Ind. Eng. Chem. Res.* **2006,** 45, 3810-3814.

15. Sperling, L. H., *Introduction to Physical Polymer Science*. 4th ed.; John Wiley & Sons: Hoboken, New Jersey, 2006; p 1-845.

16. Owen, M. J., In *Physical Properties of Polymers Handbook, Ch. 48*, Mark, J. E., Ed. AIP Press: New York, 1996.

17. Miyata, T.; Higuchi, J.-I.; Okuno, H.; Uragami, T. *Journal of Applied Polymer Science* **1996,** 61, 1315-1324.

18. Wu, N. J.; Zheng, A.; Huang, Y. M.; Liu, H. L. *Journal of Applied Polymer Science* **2007,** 104, (2), 1010-1018.

19. Maric, M.; Macosko, C. W. *Journal of Polymer Science Part B-Polymer Physics* **2002,** 40, (4), 346-357.

20. Petitjean, S.; Ghitti, G.; Jerome, R.; Teyssie, P.; Marien, J.; Riga, J.; Verbist, J. *Macromolecules* **1994,** 27, 4127-4133.

6. THERMAL AND MECHANICAL PROPERTIES OF BLENDED FILMS CONTAINING γ-CYCLODEXTRIN STARS

6.1. Background

Bridging of blend interfaces with compatibilizing copolymers is a practical method for efficiently combining the properties of the two phases. A classic example is high impact PS (HIPS). When a small amount of polybutadiene (PB) containing PS grafts is imbedded into PS, significant increases in impact toughness are observed through dissipation of energy into the PB rubbery phase.[1] This additional impact toughness is a direct result of the increased interfacial mixing caused by the copolymer grafts. However, not only does the interfacial cohesiveness affect properties, but the size of the rubbery domains also proves important for energy dissipation. For PB in HIPS, a domain size of ~2.5μm was found to be optimal in dispersing impact energies when PS is partially grafted onto PB by reactive compatibilization.[2]

Typically, as a consequence of using copolymers for compatibilization, a reduction in the dispersed phase size occurs due to the lowering the interfacial energy between blend phases, and this in turn alters the mechanical properties of the blend. These altered properties are most importantly a reflection of the ability of the copolymer segment length to create a cohesive interface. Penetrative interactions within the interface can be described by whether or not copolymer segments will form a wet or dry brush into the respective polymer domains as explained by Leibler for a block copolymer.[3] If a block copolymer forms a wet brush ($N_i > P_i^{3/2}$), where N_i is the DP of copolymer with repeats of species *i*, and P_i is the DP of a blended homopolymer of species *i*, then the copolymer species intermingle with the intended homopolymer to extend into and entangle with the bulk polymer. If a dry brush ($N_i < P_i^{3/2}$) is formed, then mixing of the block copolymer into the intended homopolymer is not accomplished and the interface is weakly bridged for transferring energy between domains. Assuming these concepts can be applied to our case with the CD star arms having a DP = 6

and the PS homopolymer having a molecular weight of 325,000 g/mol, this corresponds to N_i = 6 and P_i = 3120, which lies firmly within the dry brush regime since $N_i << P_i^{3/2}$. This implies that the threaded CD-star probably does not have long enough arms to sufficiently be wet by the PS homopolymer leading to poor combined properties.

Whatever the outcome of the wet or dry interfacial interactions, the area between domains gives rise to an additionally developed "interphase". This interphase forms when the interfacial components start to mix into each other leading to a material that has different properties than the individual homopolymers. Interphase thicknesses for immiscible polymer pairs typically are on the order of ~2nm whereas a polymer/copolymer interphase shows thicknesses on the order of ~30nm.[4] This gives insight as to the intermingling of the blend phases and the need to accomplish a thicker interphase region as seen for copolymers. It has been shown that a copolymer segment used for compatibilization should be on the order of the entanglement molecular weight of that particular homopolymer.[4] This knowledge helps support the necessity of the copolymer to be of a length to entangle with the homopolymer matrix giving added emphasis to Leibler's wet brush theory. However, even if a thick interface is accomplished with a copolymer (typically with 0.5 to 2 wt% incorporation), it sometimes has minimal effect on the solid-state behavior of the blend.[4]

Examination of PS and PDMS blended films *with* and *without* CD-star will consist of an assessment of the thermal properties *via* differential scanning calorimetry and thermal gravimeteric analysis, followed by an evaluation of the mechanical properties by dynamic mechanical analysis. These characterization techniques will give us a general idea as to the degree of compatibilization that was accomplished for these blends and what properties may have been enhanced as a result of adding the CD-star compatibilizer to a blend of PDMS and PS.

6.2. Thermal Properties of Blended Films

6.2.1 Differential Scanning Calorimetry

Observation of the softening and melting temperatures of polymer components within a blend is commonly done using a differential scanning calorimeter (DSC). An indication of partial blend compatibilization can be seen when DSC thermograms show the homopolymer T_gs beginning to shift toward each other.[5, 6] Furthermore, fully miscible blends are indicated when a single T_g is observed that lies between the blended homopolymer T_gs (eg. PS and poly(phenylene ether)).[2] All thermogram traces presented in this work display the second heating cycle at a ramp rate of 10°C/min under helium (after cooling from 130 °C with a cooling rate of 10°C/min).

In Figure 6.1, the DSC thermograms are presented for (A) the individual components making up the blends, and (B) blended films with varying CD-star and PS compositions. It can be observed in (A) that PDMS (both PDMS-62 and PDMS-308) has a T_g at -125 °C, a cold crystallization temperature (T_c) at approximately -85 °C, and a T_m between -47 °C and -38 °C. It has been reported that the crystal structure of PDMS is monoclinic with a T_m of -40 °C which agrees well with the T_m we observe.[7, 8] Also in (A) we see the pure CD-star T_g at 90 °C is notably below the pure PS T_g of 102 °C. The effect on $T_{g,PS}$ of mixing the CD-star into PS can be observed in (B). This figure shows that as an increased amount of CD-star is incorporated into PS, the $T_{g,PS}$ of the blend decreases, which points to miscibility between CD-star and PS blends. All blended films of CD-star and PS were transparent.

Figure 6.2 contains DSC traces for films with various CD-star amounts. Graphs (A & B) initially were made with 5 wt% PDMS, whereas (C & D) initially had 10 wt% PDMS, and the intent was to keep the PDMS amount constant. However, some PDMS is lost in the processing (recall section 5.3.3), and the actual amount of PDMS varies in these films. Therefore both the CD-star *and* PDMS contents vary within these films, making them more difficult to interpret. For reference, the amount of retained PDMS within the films is shown

in parentheses for each thermogram. With variances in composition in mind, a few minor trends can still be seen in Figure 6.2(A & B) by comparing solely the samples *with* CD-star which all contain roughly 4 wt% retained PDMS. Sample films with 10 wt% PDMS are also shown in Figure 6.2(C & D) but only as an additional reference, due to their larger variance in retained PDMS.

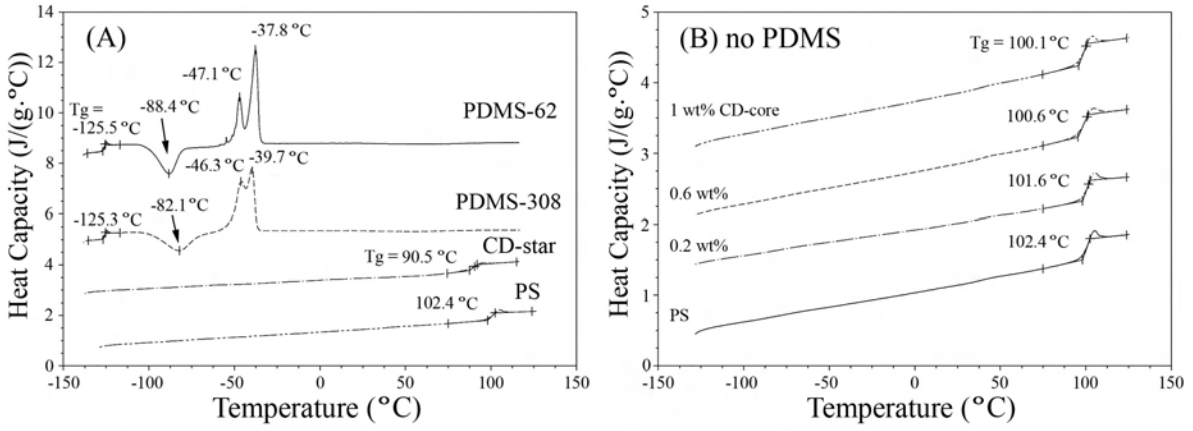

FIGURE 6.1. DSC thermograms of (A) individual components making up the blends, and (B) blends of PS and CD-star with varying amounts of CD-star. Traces have been shifted vertically for clarity.

Trends in the DSC data for these films are best identified by plotting the measured T_gs with respect to the CD-core amount initially blended. This plot is shown in Figure 6.3 in order to aid in identifying T_g trends to show compatibilization more clearly than the data sets in Figure 6.2. In addition, this plot includes calculated T_g values that were found using the Fox relationship, shown as equation (6.1).[9] The variables within equation (6.1) are described as the weight fraction of each blended component w_1 and w_2, the glass transition temperatures of the blend components $T_{g,1}$ and $T_{g,2}$, and the resultant glass transition temperature of the blend $T_{g,B}$. This equation predicts the resultant T_g of miscible blends. In this case, the blended components used in these calculations are the CD-star (T_g = 90.5 °C) and PS (T_g =

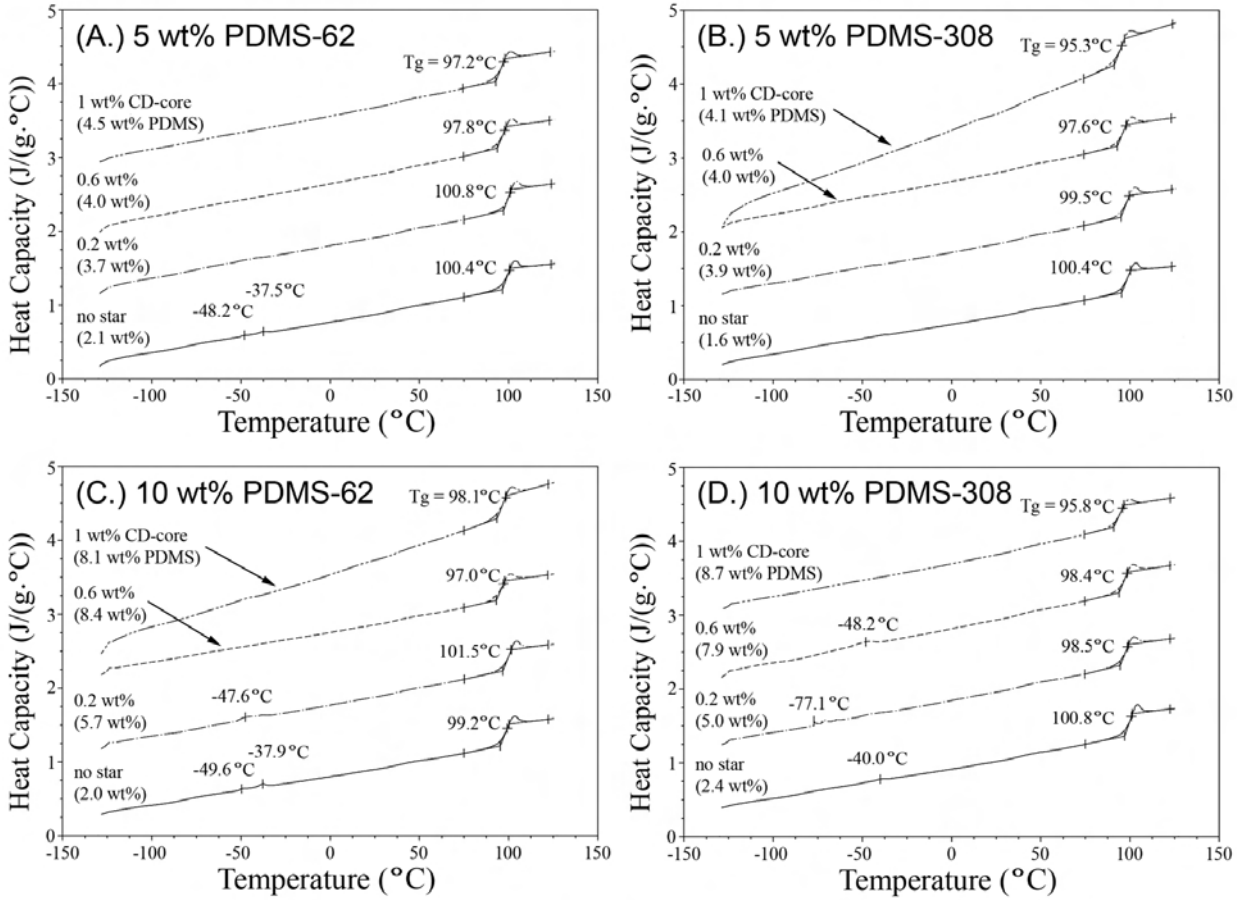

FIGURE 6.2. DSC thermograms for films with initially 5wt% PDMS (A and B), and 10 wt% PDMS (C and D) with varying amounts of CD-core. Retained values of PDMS wt% are shown in parentheses as found by ^{1}H-NMR after film processing. Traces have been shifted vertically for clarity.

102.4 °C), which were proven to produce a miscible blend as we saw in Figure 6.1(B). All masses used to calculate the weight fractions for the CD-star and PS were taken from Table 5.2.

$$\frac{1}{T_{g,B}} = \frac{w_1}{T_{g,1}} + \frac{w_2}{T_{g,2}} \quad \text{---------- (6.1)}$$

In Figure 6.3, T_g values are plotted for sample sets with relatively constant amounts of PDMS. Each data set in this plot corresponds to the set of thermograms shown in Figure 6.2(A–D) and is labeled as such in the sample legend.

We can see that for sample set (A) in Figure 6.3, a decrease in T_g is observed with increasing CD-core content. Likewise, for sample set (B), we see that with increasing CD-core content there is a larger decrease in $T_{g,PS}$ (compared to PDMS-62 samples). However, for data sets (C & D) there are not enough data points with constant PDMS content to discern any trends. The observed decreases in $T_{g,PS}$ for sample set (A) could be due to the increased CD-star content within these films which has been shown to lower $T_{g,PS}$ (Figure 6.1(B)).

When we compare the $T_{g,PS}$ trends in Figure 6.3(A & B) to the "no PDMS" sample set, an obvious decrease in $T_{g,PS}$ is observed with increasing CD-core. Since we observe a larger decrease in T_g value with PDMS incorporation for this data set, then this gives some basis to conclude that PDMS is being compatibilized within these films which facilitates lower $T_{g,PS}$ values. Comparision of sample films containing only 4 wt% or 8 wt% PDMS/PS (without CD-star), cannot be made since the amount of retained PDMS in these samples is below 2.4 wt%.

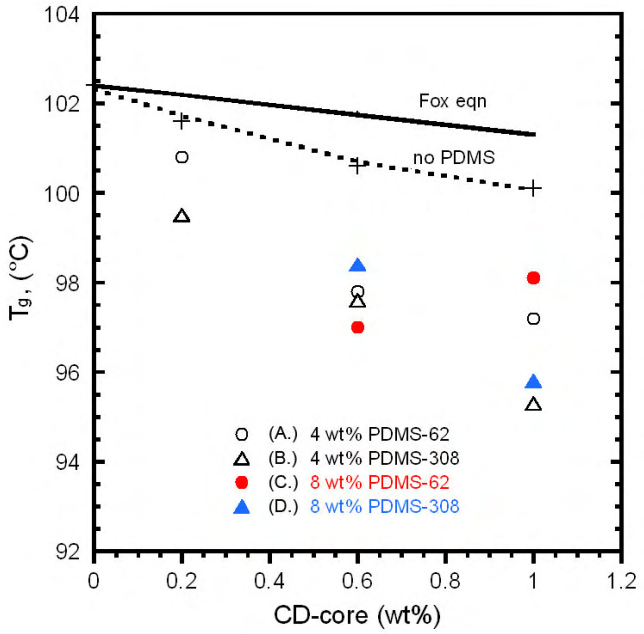

FIGURE 6.3. Plot showing T_g trends of the blended films. Sample assignments (A-D) should be referenced as the thermogram sets from Figure 6.2. The sample set with "no PDMS" can be referenced in Figure 6.1(B). The Fox equation line is described in the text.

DSC thermograms of sample films containing constant 1 wt% CD-core with varying amounts of PDMS can be seen in Figure 6.4. Within this figure, data sets (A and B) are *without* CD-star whereas data sets (C & D) are *with* CD-star. Again the retained PDMS amounts for each sample film, as found by ^{1}H-NMR in section 5.3.3, are given in parentheses. It is interesting to note in (A) that a very small amount of PDMS incorporation affects the $T_{g,PS}$ by a few degrees giving a value of 99°C for the ~1wt% PDMS-62 blend whereas for pure PS the T_g is 102°C. This observation of PDMS influencing the T_g of PS in Figure 6.4(A & B) will be important for evaluating data sets (C & D) with 1 wt% CD-star present. Thus, the initial decrease in T_g seen in (C & D) might be simply caused by PDMS incorporation rather than compatibilization of PDMS within the CD-core.

As before, it is beneficial to plot the T_gs of these sample films from Figure 6.4 with respect to *retained* PDMS in order to identify any relevant trends in the data sets. This plot can be seen

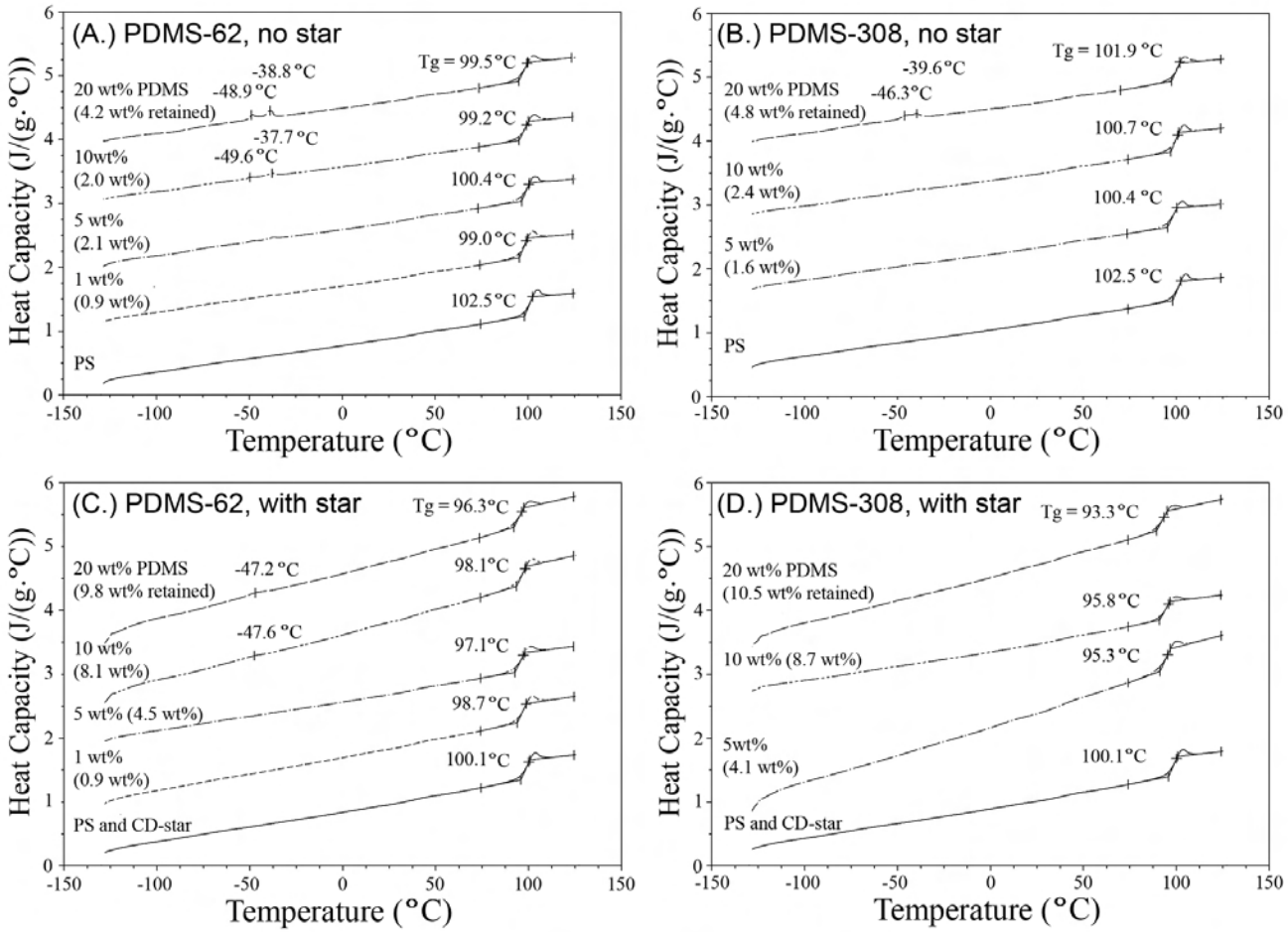

FIGURE 6.4. DSC thermograms for films with constant CD-star (1wt% CD-core) and varying amounts of PDMS-308. Retained values of PDMS wt% values are shown in parentheses as found by ^{1}H-NMR after film processing. Traces have been shifted vertically for clarity.

in Figure 6.5. The data in Figure 6.5 comes from the DSC traces in Figure 6.4. The Fox relationship is also plotted in Figure 6.5. The sample masses used in the Fox equation were previously listed in Table 5.2 in Chapter 5, and again only include the CD-star and PS masses.

In Figure 6.5, sample sets (A & B) *without* CD-star seem to have T_gs that do not follow much of a trend. Technically these sample sets should exhibit two very well separated phases resulting in the $T_{g,PS}$ not being affected by the PDMS and measuring around 102 °C. However these sample sets do show that the $T_{g,PS}$ is affected by the presence of PDMS, which generally lowers the $T_{g,PS}$ by a few degrees. All of the T_g values from these samples seem to cluster between 99 °C to 101 °C with no trend seen. Since these samples did not retain more than 4.8 wt% PDMS, we do not have T_gs for sample films with higher PDMS amounts.

On the other hand, if we examine sample sets of (C & D) *with* CD-star in Figure 6.5, these films exhibit a trend of decreasing $T_{g,PS}$ values with increasing amounts of retained PDMS. It is observed that sample set (D) shows slightly lower T_gs overall than for sample set (C). Apparently, this is a molecular weight effect. This may indicate that sample films with PDMS-308 have achieved a higher degree of compatibilization than sample films with PDMS-62, possibly because a larger number of CD-stars are found on each chain. Compatibilization is thought to be occurring for sample sets (C & D) due to the fact that the $T_{g,PS}$ values are lower than samples without CD-star. This is evidenced by the inconsistent and fluctuating T_gs in (A & B). If compatibilization was not occurring for (C & D) then it would be expected that T_g trends would parallel the Fox equation. With that said, since we are unable to make sample films containing larger amounts of PDMS without CD-star, it is difficult to discern whether or not the decrease in T_gs for (C & D) are entirely due to CD-star compatibilization and not partially due to the presence of increased amounts of PDMS.

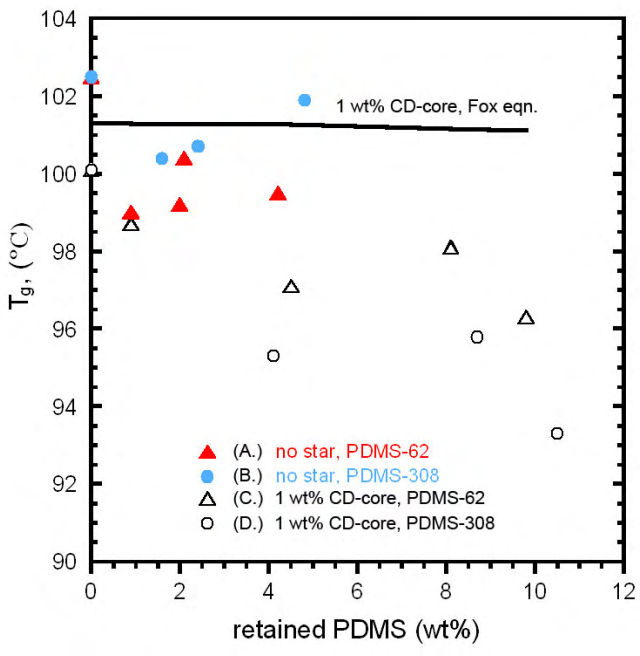

FIGURE 6.5. Plot showing trends of T_g for blended films. Sample assignments (A-D) should be referenced as the thermogram sets from Figure 6.4. The Fox equation data set is described in the text.

Overall the DSC data seems to point to increased compatibilization with samples containing CD-star which is identified as a shift in the PS T_g values to lower temperatures. This is consistent with what would be expected if compatibilization was occurring, as seen when the T_gs of the homopolymer blends shift in values towards each other. However since the T_g of the PDMS at -125 °C is so weak and unidentifiable, then it is difficult to confirm whether both T_gs move in toward each other using DSC. Wang and Krause also had difficulty seeing the $T_{g,PDMS}$ for a PDMS-b-PS with 14 wt% PDMS using DSC.[6] These results are still significant considering that (1) PDMS is highly immiscible with PS, and (2) the fact that a small amount of PDMS can influence the T_g of the PS (the majority of the mass) when compatibilized by CD-star.

6.2.2 Thermal Gravimetric Analysis

Thermal stability of the compression molded films was investigated using thermal gravimetric analysis (TGA). Individual components making up the blends and the blended films with CD-stars where heated from room temperature to 600°C under nitrogen at a ramp rate of 5 °C/min. The derivative weight loss curves are shown to emphasize rates of degradation.

Figure 6.6 shows the derivative weight loss curves for films initially containing 10 wt% PDMS-308 with varying CD-core content. Insets of (A) show a magnification of the lower temperature CD-core degradation region, whereas (B) shows a magnification of the PDMS degradation region. Within the insets (A) and (B), the actual compositional values for the individual components of CD-core and PDMS are shown, respectively.

It can be observed in Figure 6.6(A) that the degradation temperature (T_d) for the blended films containing CD-star molecules are higher than for the pure CD-star core. However, for the CD-star films in (A), small peaks for the blends are present under the pure CD-star core degradation peak. This indicates that some of the CD-star may remain unthreaded, thereby pointing to some CD-star being uncomplexed in the PS matrix of the films. As expected in Figure 6.6(A), the magnitudes of the T_d peaks for the films are observed to increase with increasing CD-core amounts.

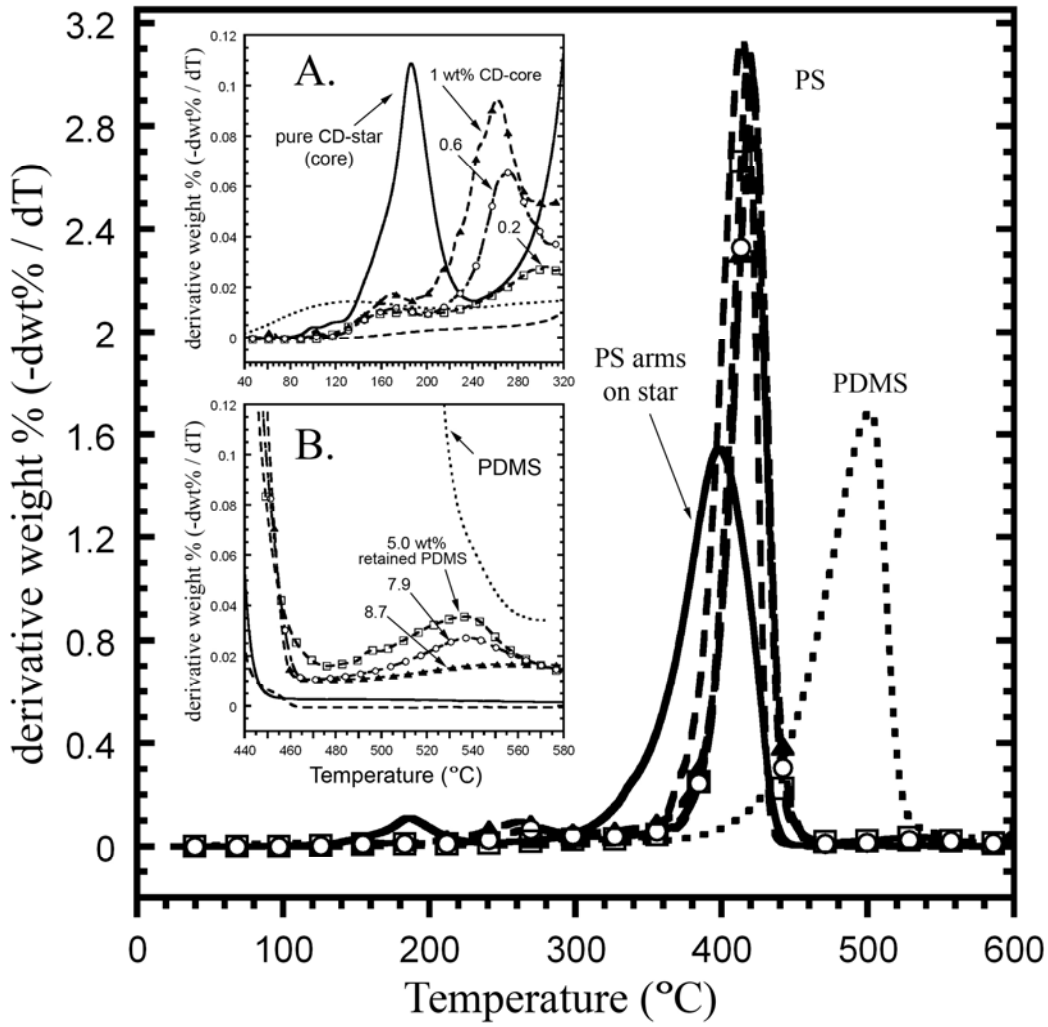

FIGURE 6.6. Comparitive TGA derivative plots of films containing PS and PDMS blends with 1 wt% CD-core (-▲-), 0.6 wt% CD-core (-○-), 0.2 wt% CD-core (-□-), along with the individual components of PDMS-308 (- - -), PS (— —), and CD-star (——). Insets show (A.) expansion of lower temperature region, and (B.) expansion of higher temperature region.

However within the PDMS degradation region, seen in Figure 6.6(B), an interesting trend emerges. Shown are the compositional values for the actual amounts of retained PDMS in the films. The peak trend in this region shows an increasing amount of PDMS for decreasing peak height, which is opposite to the expected trend. If we take into consideration the

amount of CD-core within each film blend, then a trend of decreasing PDMS peak height with increasing CD-core amount is observed. This suggests that the PDMS degradation in this temperature range is effectively reduced by it being threaded into the CD-core.

Similar trends have been observed for CD-ICs in which CD remains on the polymer. These CD-ICs have been shown to exhibit slightly higher than normal T_ds.[10] Huang *et al.* observed that for a physical mixture of PEO/α-CD the T_d was found to be 315 °C, whereas when a PEO-(CD-IC) is examined it had a T_d of 334 °C.[11] Therefore it appears that polymers in the CD complex are slightly more stable and have greater protection against thermal degradation.

An increase in T_d was also observed if the CD is washed from the CD-IC and the polymer is coalesced. Physical blends, such as those reported by Uyar *et al.*, of PVAc/PC show two degradation temperatures with values of 369 °C and 538 °C which correspond to the two homopolymers. [12] For coalesced PVAc/PC from CD-ICs, the T_ds where found to be 377 °C and 551 °C, a several degree increase in T_d.[12] PDMS T_d values for the films in Figure 6.6 show similar trends as CD-ICs *or* coalesced polymers from CD-ICs, which suggests that inclusion of polymer within the CD-core helps to stabilize the polymer against thermal degradation.

6.3. Dynamic Mechanical Analysis

Dynamic mechanical analysis (DMA) is a very sensitive technique that probes the viscoelastic properties of polymers to yield their elastic and loss moduli. This method can show various molecular motions within a polymer such as long-range chain motions (T_g = α-relaxation), polymer side-group torsional motions (β-relaxation), or polymer back-bone motions (γ-relaxations).[9] The observed relaxations are a direct consequence of the polymer structure and its environment. This leads to the notion that DMA can be effectively used to probe molecular movements and compatibilization effects in a blend.[13]

The essential DMA relationships are described in equations 6.2 – 6.7, where the variables are defined as the complex modulus E^*, stress σ, strain e, angular frequency ω (= $2\pi f$), frequency in Hz f, storage modulus E', loss modulus E'', and phase angle δ. Figure 6.7 illustrates the basis for these relationships.[14]

$$e = e_0 \exp(i\omega t) \text{ --------(6.2)}$$

$$\sigma = \sigma_0 \exp i(\omega t + \delta) \text{ ---------(6.3)}$$

$$E^* = \frac{\sigma_0}{e_0}\exp(i\delta) = \frac{\sigma_0}{e_0}(\cos\delta + i\sin\delta) \text{ -------(6.4)}$$

$$E' = \frac{\sigma_0}{e_0}\cos\delta \text{ ----------(6.5)}$$

$$E'' = \frac{\sigma_0}{e_0}\sin\delta \text{ ----------(6.6)}$$

$$\tan\delta = \frac{E''}{E'} \text{ ----------(6.7)}$$

The storage modulus E' can be viewed as the ability of the material to store energy without permanent deformation, whereas the loss modulus E'' can be described as the ability of a material to lose energy through molecular motions or viscous response of the polymer chains.[15] The ratio E''/E', as seen in equation 6.6, is known as the *tan* δ term and is independent of geometry effects. This quantity measures dampening of the material and its effectiveness to lose energy to molecular rearrangements and internal friction.[15] It should be noted that these sub-T_g transitions of T_β and T_γ are generally too weak to be detected using DSC.[15]

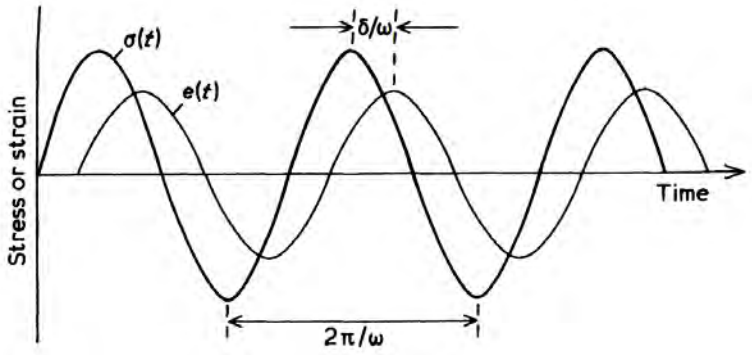

FIGURE 6.7. Sinusoidal oscillation and response of a linear viscoelastic material. From reference [14].

Sinusoidal oscillations were applied at a strain amplitude of 0.1% and a frequency of 1Hz to probe the viscoelastic chain motions of the compression molded films seen in Chapter 5. The temperature was equilibrated at -130 °C for 5 minutes before ramping to 130 °C at 2 °C/min.

6.3.1. Evaluation of E', E'', and Tan δ for Blended Films

The sample films examined by DMA all had varying PDMS contents and were compression molded as stated in section 5.3.2. Sample sets containing PDMS-62 or PDMS-308 were tested *without* and *with* CD-star. Almost all sample films with an initial 20 wt% PDMS content failed in the DMA due to sample grip slippage. However, one sample made with an initial composition of 20 wt% PDMS-308 and 1 wt% CD-star was successfully examined without grip slippage occuring.

For Figures 6.8 – 6.10, the data sets are labeled as (A) PDMS-62 without CD-star, (B) PDMS-308 without CD-star, (C) PDMS-62 with CD-star, and (D) PDMS-308 with CD-star. For all legends within these Figures, sample curves are labeled with the initial wt% of PDMS present, as well as, in parentheses, the retained amount of PDMS as found in section 5.3.3. Additionally, all comparable samples within these curve composites have been identified with the same line pattern assignments and symbols.

Figure 6.8 shows the E' curves as a function of temperature for all films examined. For all blended films containing PDMS in Figure 6.8, three changes in slope for E' are discernable. The first slope change is due to the T_g of the PDMS at -123 °C, whereas the second is due to melting of PDMS crystals (T_m) at approximately -40 °C. The third and largest slope change is due to the T_g of the PS at around 100 °C. All of these thermal events cause the storage modulus to change. These events mostly cause a decrease in E' due to an increase in the thermal mobility of the polymer chains.

One noteworthy variation between films *without* CD-star in Figure 6.8(A and B) and films *with* CD-star (C and D) is the magnitude of the PDMS T_g step at -123 °C. Since the samples containing CD-star retained more PDMS during processing, a much larger $T_{g,PDMS}$ peak is seen. In addition, a broad peak is observed (primarily in (D)) between -110 °C to -40 °C for films with PDMS which is due to the cold crystallization event PDMS undergoes before reaching its T_m at -40 °C. This event is seen to slightly increase E' of the films as crystallization takes place inferring an increase in strength. This broad cold crystallization peak in E' was also reported by Clark and coworkers for blends of PDMS and PS.[16] Finally, after heating above the T_m of PDMS, a steeper decrease in E' is observed until reaching $T_{g,PS}$ where the mechanical integrity of the film dissolves.

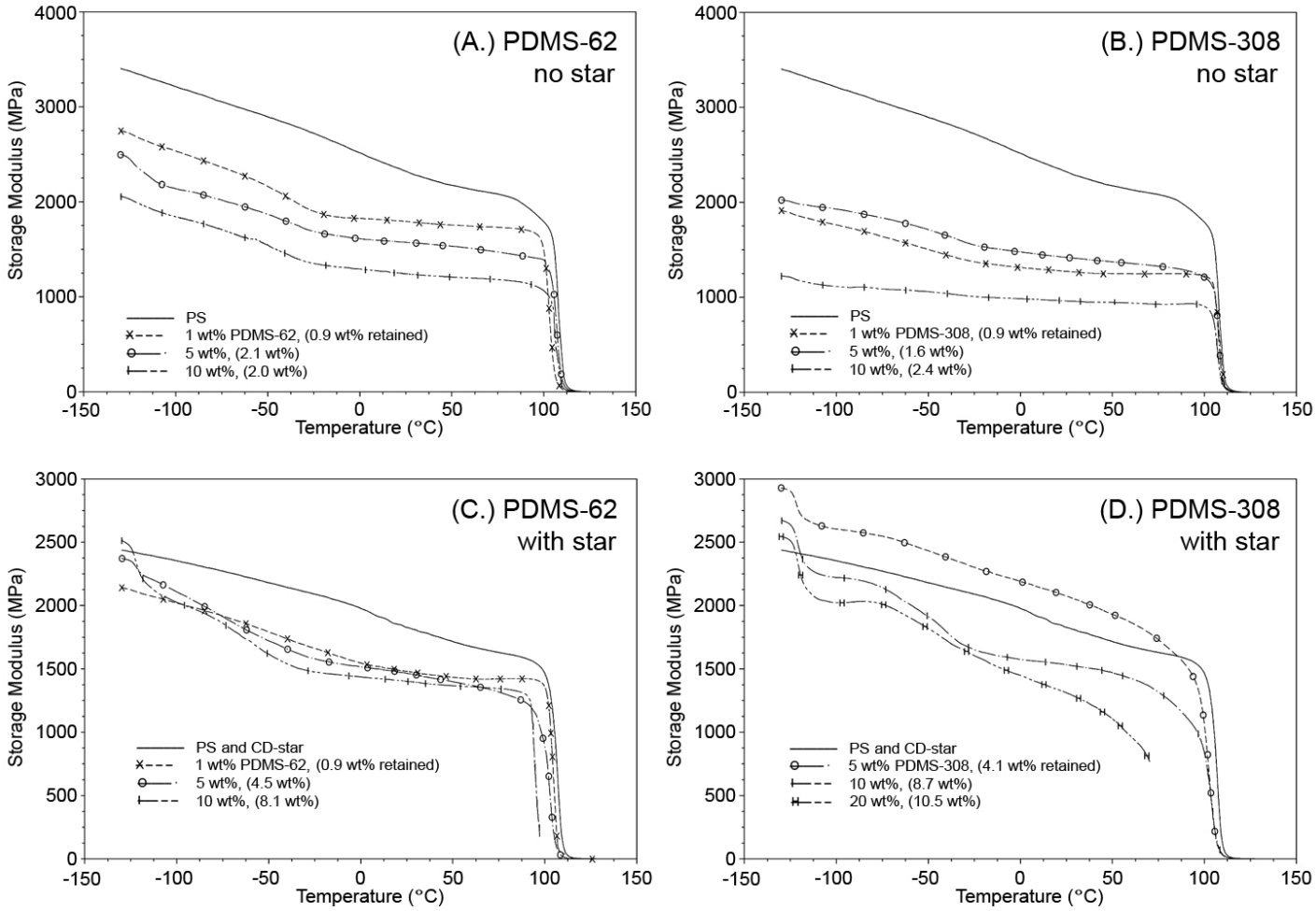

FIGURE 6.8. Storage Modulus (E') curves for PDMS-308 films with constant 1wt% CD-core.

Likewise in Figure 6.9, data curves of E'' show samples *with* and *without* CD-star. Data sets of E'' in Figure 6.9 give an indicator of how the molecular motions of the polymers behave as temperature is increasing. Several thermal events happen within these curves. Therefore, in order to aid the discussion of these curves, four regions are specified and shown in Figure 6.9(A) as (I.) PDMS T_g region, (II.) PDMS cold crystallization region, (III.) PS T_β region, and (IV.) PS T_g region. These regions will be referenced when analyzing all of the sample sets in Figure 6.9.

Within region (I), there is a large variance in the $T_{g,PDMS}$ peak heights between samples *with* and *without* CD-star. It can be seen in the curve sets (A & B) *without* CD-star that only very faint peaks emerge for these samples. On the other hand, sample sets (C & D) *with* CD-star show much larger peaks indicating a greater amount of PDMS within these sample films. This trend corresponds well with the amount of retained PDMS that we have seen earlier for all films. It is noteworthy to point out that the sample curves *without* CD-star show $T_{g,PDMS}$ values of -123 °C, whereas the sample films *with* CD-star show $T_{g,PDMS}$ values of -121 °C. This may indicate that the CD-star films are becoming partially compatibilized as evidenced by the $T_{g,PDMS}$ peak shifting towards the $T_{g,PS}$ peak. As a reference, pure PDMS rubber also has been shown to have a $T_{g,PDMS}$ at -123 °C.[17]

Cold crystallization of PDMS can be observed in region (II). The peaks that develop here point to the PDMS chains being in motion and rearranging themselves into the crystal structure. Peak maxima occur when most of the chains have rearranged into the crystal structure, indicating a decrease in the rate of crystal formation is occuring. Most sample films containing PDMS exhibit a cold crystallization peak. However sample set (D) shows an interesting behavior in this region. Here we see a large broad peak that initiates in region (II) and expands into (III) without showing a definitive maximum. This may indicate a higher degree of compatibilization is being observed in these films which possibly indicates a higher degree of homogeneity within the film.

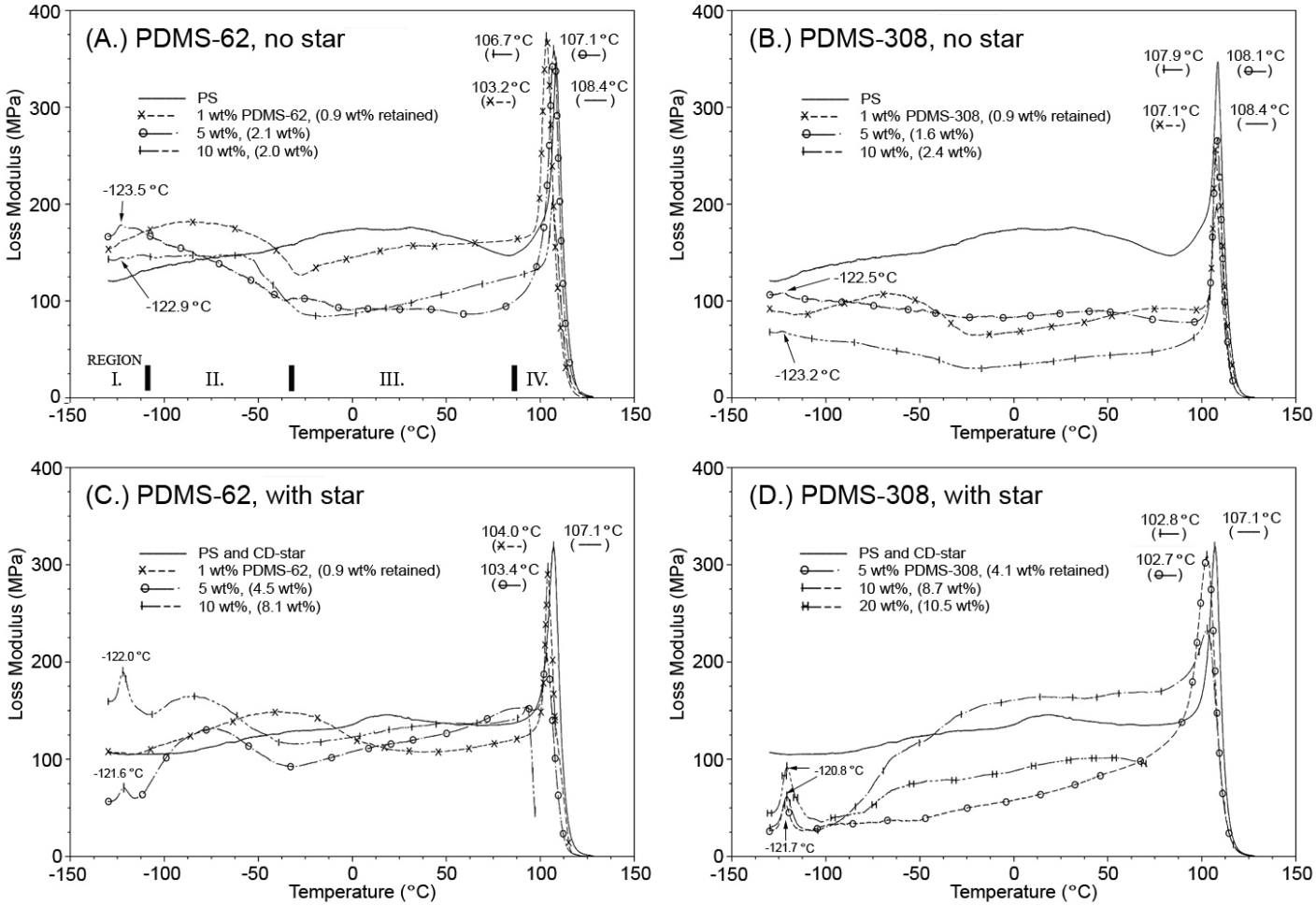

FIGURE 6.9. Loss Modulus (E'') for PDMS-308 films with constant 1 wt% CD-core.

In region (III) we are able to observe the T_β transition for PS which is where the torsional vibrations of the PS phenyl group occur. Within this temperature range, a large broad peak at 50°C should be observable.[9] In fact this peak is seen for the pure PS films in A and B. This peak remains identifiable (without much variation) for most samples which contain CD-star especially in (D). For the CD-star containing films in (D), this peak is exaggerated and broad which may identify an increased film compatibility with PDMS by affecting the T_β PS transition lending more molecular movement to the phenyl side-chains.

Region (IV) presents the area of the $T_{g,PS}$ transition. When CD-star is present in PS, as for samples in (C & D), the $T_{g,PS}$ is lowered to 107 °C from a value of 108 °C observed for pure PS. As seen in the DSC data for films *without* CD-star in (A & B), a slight decrease in $T_{g,PS}$ is observed when PDMS is present. However the magnitude of this decrease depends on the molecular weight of the PDMS. For varying amounts of PDMS-62 in (A) the $T_{g,PS}$ is between 103 to 108 °C, whereas for PDMS-308 in (B) the $T_{g,PS}$ is between 107 to 108 °C. This indicates that sample films in (A) have a higher degree of PDMS mixing and increased contact area with PS, leading to a lowing of the $T_{g,PS}$. On the other hand, in (B), these sample films have a higher degree of phase segregation resulting in $T_{g,PS}$ values that are on the order of pure PS.

Small subtleties are observed within region (IV) between samples *without* and *with* CD-star. In sample set (C) we see values of $T_{g,PS}$ that are similar to the films without CD-star in (A). However for sample set (D), we see $T_{g,PS}$ values that are much lower than the values observed for the sample films without CD-star seen in (B). Here we observe an approximate 5 degree decrease in $T_{g,PS}$ for films with CD-star, perhaps indicating an increase in compatibilization. Since shifts in $T_{g,PS}$ are seen to move toward the $T_{g,PDMS}$ peaks, and visa versa, then this tends to indicate partial compatibilization occuring in this sample set.

In Figure 6.10, the tan δ curves are presented. These curves do not show any variances in the data when compared to the E'' data set in Figure 6.9. Therefore, the trends seen for

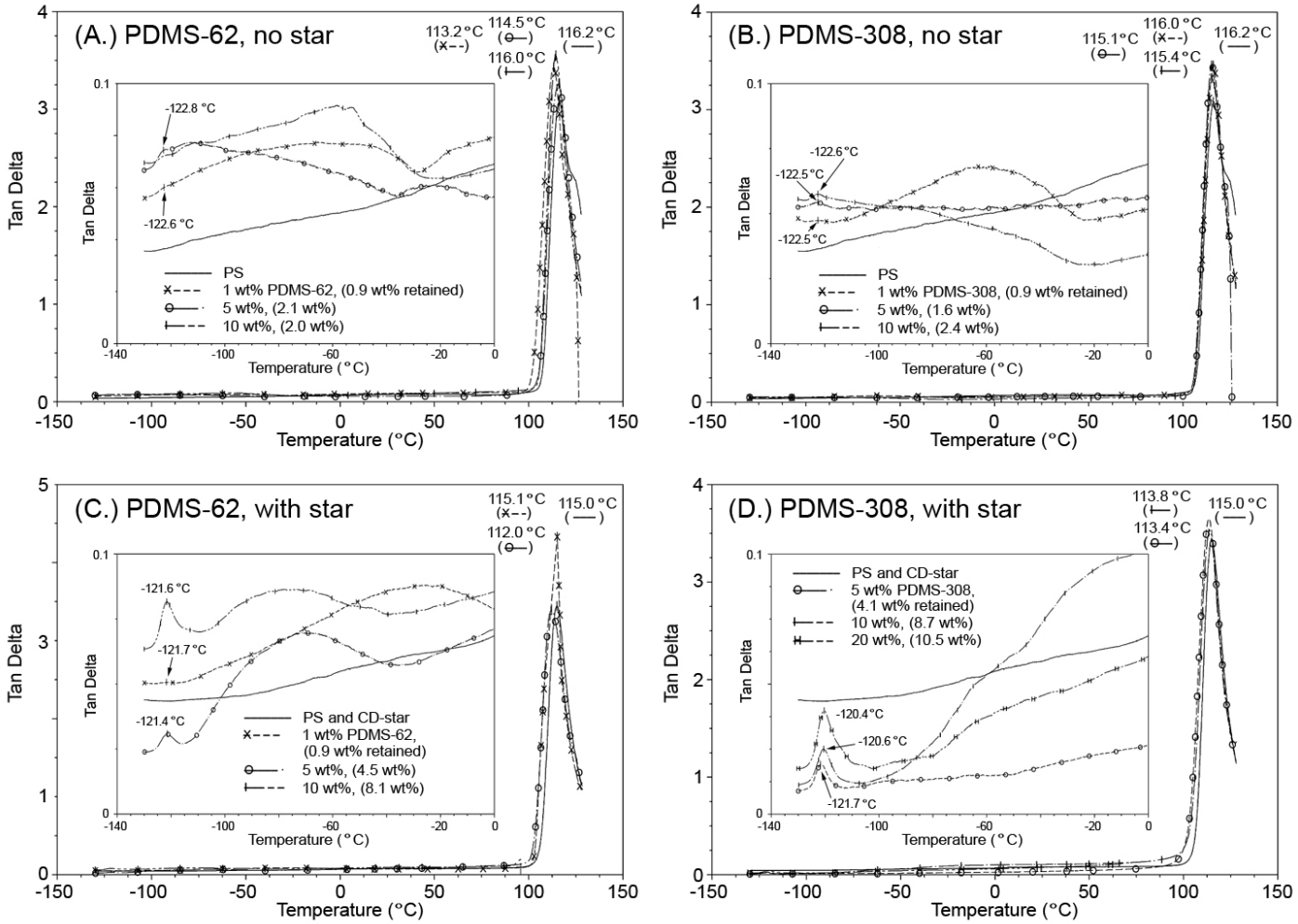

FIGURE 6.10. Tan delta (δ) for samples with varying PDMS and constant 1wt% CD-core.

E'' are also seen for tan δ curves, resulting in identical conclusions. Ebdron *et al.* also saw similar PDMS transitions for tan δ, E'', and E' when studying polyurethane/PDMS IPNs.[18]

The area under the tan δ curve for T_β is said to indicate the toughness of the polymer although it is an indirect measurement.[15, 19] Several researchers have seen this relationship, however, this is not entirely accepted by all. For our sample films, the area for $T_{\beta,PS}$ is eclipsed by the E' values that dominate the denominator causing the values to be very small. This indicates, when studying the $T_{\beta,PS}$ areas, that no considerable toughness increase was obtained as analyzed by DMA. However, actual impact toughness measurements using a Charpy impact test ideally need to be conducted in order to confirm this conclusion.[1]

6.4. Conclusions

Partial compatibilization appears to be occurring for the CD-star containing films as evidenced by shifts to lower $T_{g,PS}$ values in the DSC and DMA data. This can be seen when viewing the overall $T_{g,PS}$ trends in the these data sets that show a decrease in T_g with increasing PDMS content. However this trend cannot be completely verified without being able to compare films with similar amounts of PDMS incorporated without CD-star. For films with only PDMS/PS the $T_{g,PS}$ is slightly altered and does not follow a definite trend. In these blends the $T_{g,PS}$ fluctuates between 99 and 102 °C for PDMS contents up to 4.5 wt% in PS. Therefore this gives reason to believe that the larger $T_{g,PS}$ reduction we observe for films *with* CD-star having values between 93 and 101°C are real compatibilization effects. For the films with CD-star, a trend of decreasing $T_{g,PS}$ is seen for increasing amounts of PDMS.

Magnitudes of the degradation temperature peaks for the PDMS compatibilized films containing CD-star decrease with increasing CD-core incorporation. This suggests that when PDMS is threaded into CD-star, a decrease in thermal degradation occurs. Furthermore, when PDMS is present, CD-star core degrades at a higher temperature than seen for pure

CD-star. Likewise, this suggests that thermal degradation of the CD-core is stabilized by the presence of a threaded PDMS guest molecule.

Mechanical properties of the films compatibilized with CD-star did not show much improvement as measured by DMA. The short arms used in the CD-star compatibilization studies must have formed a thin interphase, thereby not improving the integrity of the film. This is thought to be due to the arm length being only DP = 6 and not being of entanglement length (the M_w of the arm would need to be 19,000 g/mol) which is DP $\geq$ 185 for linear PS.[7] Greater phase compatibilization may have been accomplished if longer arms on the CD-star were used in this study, possibly resulting in an alteration of mechanical properties with more entanglements formed with the matrix. However, one issue with using longer armed stars is the dilution of the CD-core, which necessitates the addition of more CD-star to accomplish the same degree of PDMS threading.

6.5 References

1. Bucknall, C. B.; Cote, F. F. P.; Partridge, I. K. *Journal of Materials Science* **1986,** 21, 301-306.

2. Akkapeddi, M. K., Commercial Polymer Blends. In *Polymer Blends Handbook,* Utracki, L. A., Ed. Kluwer Academic Publishers: Netherlands, 2003; Vol. 2, pp 1023-1115.

3. Leibler, L. *Makromol. Chem., Macromol. Symp.* **1988,** 16, 1-17.

4. Utracki, L. A. *Canadian Journal of Chemical Engineering* **2002,** 80, (6), 1008-1016.

5. Roslaniec, Z., Two Multiblock copolymer blends. In *Block Copolymers*, Balta-Calleja, F. J.; Roslaniec, Z., Eds. Macel Dekker, Inc.: New York, 2000; pp 311-346.

6. Wang, B.; Krause, S. *Journal of Polymer Science: Part B: Polymer Physics* **1988,** 26, 2237-2246.

7. Brandrup, J.; Immergut, E. H.; Grulke, A., *Polymer Handbook*. 4th ed.; A Wiley-Interscience Publication: Toronto, Canada, 1999.

8. Schilling, F. C.; Gomez, M. A.; Tonelli, A. E. *Macromolecules* **1991,** 24, 6552-6553.

9. Sperling, L. H., *Introduction to Physical Polymer Science*. 4th ed.; John Wiley & Sons: Hoboken, New Jersey, 2006; p 1-845.

10. Uyar, T.; Rusa, C. C.; Hunt, M. A.; Aslan, E.; Hacaloglu, J.; Tonelli, A. E. *Polymer* **2005,** 46, (13), 4762-4775.

11. Huang, L.; Allen, E.; Tonelli, A. E. *Polymer* **1998,** 39, (20), 4857-4865.

12. Uyar, T.; Rusa, C. C.; Wang, X. W.; Rusa, M.; Hacaloglu, J.; Tonelli, A. E. *Journal of Polymer Science Part B-Polymer Physics* **2005,** 43, (18), 2578-2593.

13. Scobbo-Jr., J. J. *Polymer Testing* **1991,** 10, 279-290.

14. Young, R. J.; Lovell, P. A., *Introduction to Polymers*. 2nd ed.; CRC Press: Boca Raton, FL, 1991; p 1-443.

15. Menard, K. P., *Dynamic Mechanical Analysis*. CRC Press: Boca Raton, FL, 1999.

16. Clark, A. J. F.; Shaver, A.; Eisenberg, A. *Polymer Engineering and Science* **1981,** 21, (11), 707-711.

17. Santra, R. N.; Samantaray, B. K.; Bhowmick, A. K.; Nando, G. B. *Journal of Applied Polymer Science* **1993,** 49, 1145-1158.

18. Ebdon, J. R.; Hourston, D. J.; Klein, P. G. *Polymer* **1984,** 25, 1633-1639.

19. Arranz-Andres, J.; Benavente, R.; Pena, B.; Perez, E.; Cerrada, M. L. *Journal of Polymer Science: Part B: Polymer Physics* **2002,** 40, 1869-1880.

7. CONCLUSIONS AND FUTURE WORK

7.1. Conclusions

Star polymers containing a γ-cyclodextrin core and PS arms were successfully synthesized and used to compatibilize PDMS into PS. Compatibilization was first recognized when the turbid PDMS/PS emulsion formed a clear, stable solution upon addition of the star. Clearing is a consequence of the ability of the CD-star to migrate and concentrate at the PDMS interface thereby placing the CD-star and PDMS in close proximity to form a threaded complex. Characterization of these clear solutions by ^{1}H-NMR revealed that CD-star was threaded onto PDMS. It has been shown that a solvent selective for PS, and poor for PDMS, is chloroform, which was chosen as the solvent. This selective environment will tend to form micelles with the CD-star and PDMS complex. These micelles are a result of the PDMS threading into CD-star, which in turn, creates a hybrid slip-ring graft copolymer of PDMS-g-(PS-γ-CD). Characterization of the cleared solutions *via* dilute solution viscometery, dynamic light scattering, and gel permeation chromatography show property traits similar to traditional graft copolymers in selective solvents.

The compatibilized and incompatibilized solutions were spun cast into films in order to investigate the solid-state morphology. Films containing CD-star were found to have homogeneous morphologies, whereas films without CD-star show a distinct phase separation. AFM and SEM images for the compatibilized films point to PDMS domain sizes being on the order of 50nm or less, which is silimar to the characteristic size expected for a micelle. Either increasing PDMS with constant CD-star *or* decreasing CD-star with constant PDMS caused a variation in the degree of compatibilization within these films. Ratios of 437 to 875 PDMS repeats/CD-star were shown to be within the range at which incompatibility starts to occur.

In addition, the blended solutions were quiescently solution cast and then compression molded to yield free-standing films. However, PDMS diffused out of the films during these processes. Solution ^{1}H-NMR was conducted to determined the amount of PDMS retained in these films. It was found that when CD-star was present ~80% of the initial PDMS was retained, whereas if the blend did not contain CD-star, then ~20% PDMS was retained. This presents evidence that the PS arms on the CD-stars are anchoring the PDMS into the PS matrix and keeping it from migrating out of the film.

Properties of the compression molded films were investigated by DSC, DMA and TGA. DSC showed a small decrease in the PS T_g which may indicate partial compatibilization. DMA revealed T_g shifts for the PS and PDMS homopolymers toward each other when CD-star was present in the films, which supports the notion of partial compatibilization. DMA also revealed that the mechanical properties were not significantly different for films *with* or *without* CD-stars. TGA analysis found that the magnitude of the PDMS degradation decreased when increasing amounts of CD-star were found in the films.

A few additional conclusions can be made when considering all of the summarized results. As the length of the CD-star arms increases, two opposing effects occur. On the one hand, shorter arms are necessary in order to induce migration of the CD-star to the PDMS/PS interface by PS interactions. On the other hand, the mechanical properties of the cast films are adversely affected by star arms being shorter than the entanglement molecular weight. This results in reduced interactions with the PS matrix, thereby causing poor property blending between phases. Therefore, star arm length directly affects the kinetics of compatibilization in solution as well as the solid-state compatibilization with CD-stars.

Conditions for solution compatibilization with CD-stars appear to occur when the concentration is neither excessively high nor low. If the concentration is reduced to a dilute state below the coil overlap concentration, then the micelles become unstable and

dethreading of the CD-star is presumed to occur, as shown in the dynamic light scattering results. However, if the solvent is slowly removed to result in very high concentrations, then micelles become destabilized causing coalescence to occur that form large PDMS domains, as seen in the solution cast films. The concentration choosen (10g/dl) was found to produce good conditions for micelle stability.

Finally, films spun cast from compatibilized solutions were shown to have a homogeneous nanoscale morphology. However, if the same compatibilized solution was slowly cast by solvent evaporation, biphasic morphology with micron sized domains developed. The difference between these casting methods lies in the solvent evaporation rate. For spin casting, the solvent is essentially flashed off, which prevents the micelles from coalescing. For solution casting, the solvent slowly evaporates giving the polymer micelles time to rearrange and phase segregate. Phase segregation in the solution cast films occurs during casting and clearly happens before compression molding.

7.2. Future Work

The future work described within this section provides some interesting avenues that could be used to further develop the compatibilization aspects of the CD-star or answer some interesting questions about the CD-star threading/dethreading conditions.

7.2.1 Gamma-Irradiation of Blends Before Solution Casting

One interesting avenue that could be very fruitful in retaining the compatibilization within the solution is to irradiate the PDMS while the solution is stabilized. Irradiation has been shown to crosslink PDMS chains by dissociation of a proton from a methyl group to form a radical that induces crosslinking.[1] This method does not require any special chemical functionality on the PDMS to accomplish crosslinking but does require a gamma radiation source. Therefore if the PDMS micelles in the blend were crosslinked before being solution

cast, this may aid in preserving the micelle structure. This may also help to decrease the amount of coalescence between micelles and prevent the CD-star from dethreading during solution evaporation.

Irradiated oils of PDMS were researched by Charlesby and Garratt by examining resultant gelation times during periods of irradiation, in which they reported a value of 21.4eV per crosslink point.[2] It was also found that oxygen played a large role by inhibiting the crosslinking reaction. They found if oxygen was present, then twice as much gamma radiation was needed in order to obtain a gel. However PS is also known to crosslink when irradiated. For comparison, the radiation yield stated by Senake-Perera and Hill for PDMS was 2.48 crosslinks/100eV, whereas for PS it was 0.043 crosslinks/100eV.[3] This indicates that PDMS is much more susceptible to crosslinking *via* gamma irradiation than PS. This will favorably target PDMS for crosslinking which may prevent larger domain sizes from forming when casting from compatibilized solutions.

Aromatic molecules such as benzene are very stable in gamma radiation.[4, 5] Therefore benzene is an ideal solvent for CD-star solution compatibilization. An additional experiment was conducted in which solutions were made containing varying amounts of PDMS and 1 wt% CD-core in benzene. Composition fractions for these samples are identical to the solutions described in section 4.3. All solutions were prepared at a concentration of 10g/dl in benzene. The solutions were observed to be clear and compatibilized before irradiation. In addition, the vial head-space was purged by nitrogen in an attempt to remove the oxygen. The amount of radiation needed to crosslink a total of 100mg of PDMS-308 (i.e. all of the PDMS) was calculated to be 0.67 Mrads using a value of 21.4eV per crosslink. Theoretically this will give one crosslink per PDMS chain. However, in order to compensate for the possible presence of oxygen within the system, a final dose of 1.6Mrads was administered to the sample solutions. The gamma radiation source used for these irradiation studies was cobalt-60.

Uncompatibilized blends *without* CD-star require stirring in order to maintain an emulsion to prevent bilayer phase separation, whereas solutions *with* CD-star were compatibilized and stable. Therefore, only the CD-star compatibilized solutions were irradiated due to the lack of stirring facilities in the irradiation chamber. Figure 7.1 shows spun cast films of the post-irradiated solutions *with* 1 wt% CD-core, as well as spun cast films of the unradiated solutions *without* CD-star. All the solutions post-radiation remained clear with no color change observed.

As can be seen in Figure 7.1, the films do not appear to be much different than those observed in Chapter 5. If anything, the 20wt% PDMS samples look to be less compatibilized than sample films spun cast from chloroform seen in Figure 5.3. However, when the irradiated solutions were solution cast (films not shown) using the same methods described before in section 5.3, phase segregation within these cast films was apparent. Therefore this particular experiment was determined to be unsuccessful. It is thought that compatibilization by crosslinking the PDMS micelles did not occur to the desired degree as evidenced by the biphasic morphology of the solution cast films.

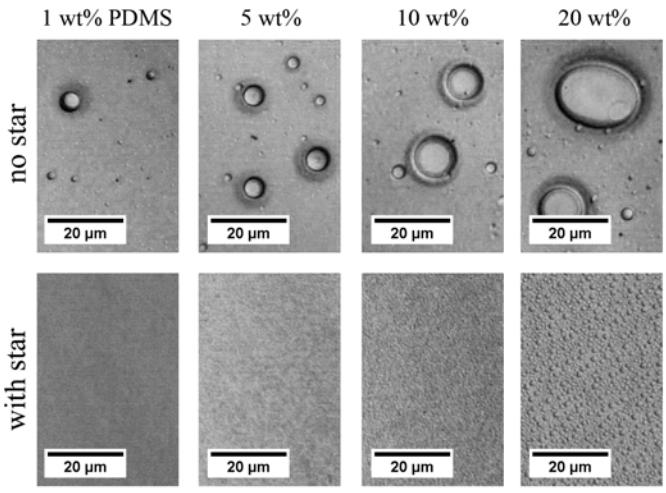

FIGURE 7.1. **Comparision of spun cast films with and without CD-star. Solutions *with* CD-star were irradiated before spin casting.**

A hypothesis was developed to help explain why the films did not show the effects of PDMS crosslinking after being irradiated. Since the major components of these solutions are benzene and PS, these components are thought to be essentially shielding the PDMS micelles from the gamma radiation. This caused the amount of radiation being delivered to the PDMS to be insufficient for crosslinking the micelles. Thus an experiment that irradiates the solutions for an extended time needs to be performed. Since the sample preparation procedure outlined in Chapter 4 does not need to be changed, this method could be very promising if the appropriate amount of gamma radiation can be determined.

7.2.2 PDMS End-Capping After Threading of CD-star

Since it has been predicted that CD-stars may be sliding off the PDMS chain in either dilute solutions or when solution cast, then it might be interesting to examine what effect PDMS end-capping might have on final properties. In addition, this might be a route for isolating the threaded complex by selective precipitation which separates it from the PS homopolymer. If isolation was possible with the hybrid slip-ring threaded complex, then we can more definitively examine the characteristics of this complex molecule in various environments.

To prevent CDs from dethreading from a polymer, the ends of the polymer chain can be end-capped with a large functional species, such as a 4-tritylphenyl or dinitrophenyl group.[6, 7] An illustration of this concept can be seen in Figure 7.2 below. There are several chemical reactions that can accomplish this. Typically, researchers use polymers with either hydroxyl or amine groups terminated at the ends which easily react with end-capping species.[8, 9] However when hydroxyl groups are found at the chain end, then a permethylated CD must be used to form the polyrotaxane in order to prevent the CD hydroxyl groups from participating in the end-capping reaction.[6] An aminopropyl-terminated PDMS can be purchased from Gelest Inc. that would work well for end-capping the CD-star compatibilization system.

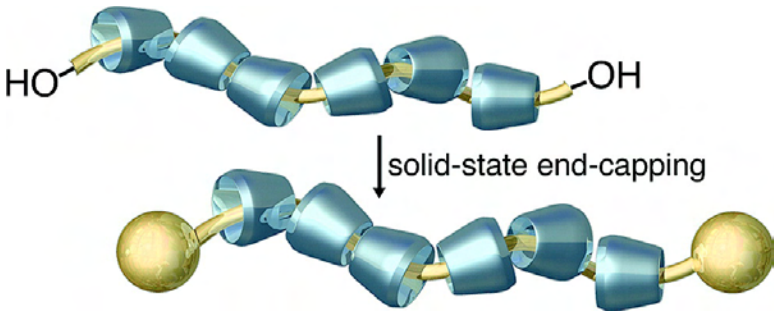

FIGURE 7.2. End capping of a formed cyclodextrin polyrotaxane. After reference [6].

Whether we can or cannot isolate the CD-star/PDMS complex, this method should give us a better fundamental grasp as to the interactions in various environments. Additionally this will provide an idea of whether or not the dethreading of the CD-star is the cause for instabilities in dilute solutions. Furthermore, end-capping of compatibilized samples may help to reduce micelle aggregation and larger domain formation in samples slowly cast from solution.

7.2.3 Continued Polymerization of PS Arms on Threaded Complexes

In Chapter 6, mechanical properties of the compatibilized films were examined. It was pointed out that an improvement in the mechanical properties might result if interfacial bridging could be accomplished to a higher degree. This requires longer arms on the CD-stars in order to be at the desirable entanglement length of DP ~ 185. However, it was also noted that threading of larger armed CD-stars on PDMS was difficult to accomplish to any great extent. This was due to a decreased interactions between the PS homopolymer and CD-star which reduced the CD-star driving force to the interface, as seen in section 4.3.4. Therefore since the bromine atoms on the ends of the CD-star PS arms are not removed, they

are still available for additional ATRP reactions. This gives us the option to extend the PS arms on the CD-star.

Since styrene monomer is a solvent for polystyrene, then it is quite possible that styrene could be used as the solvent for blend compatibilization before polymerizing longer arms.[10] One foreseen caveat within this method would be removing the copper catalyst from the reaction mixture after polymerization. Filtering the blended solution through the basic alumina column in order to remove the copper may disrupt the micelle formation or dethread the CD-stars from the PDMS. Therefore it might be necessary to end-cap the PDMS beforehand to prevent dethreading of the CD-star. If the star arms could be successfully extended this way, then this may help in bridging the interface sufficiently so that the mechanical properties of the blended polymers could be better combined.

7.3 References

1. Palsule, A. S.; Clarson, S. J.; Widenhouse, C. W. *J. Inorg. Organomet. Polym.* **2008,** 18, 207-221.

2. Charlesby, A.; Garratt, P. G. *Proceedings of the Royal Society of London. Series A, Mathematical and Physical Sciences* **1963,** 273, (1352), 117-132.

3. Senake-Perera, M. C.; Hill, D. J. T., Radiation Chemical Yields: G Values. In *Polymer Handbook*, 4th ed.; Brandrup, J.; Immergut, E. H.; Grulke, A.; Abe, A.; Bloch, D. R., Eds. John Wiley & Sons: 2005; pp II/481-II/497.

4. Jedináková, V.; Novák, J. *Journal of Radioanalytical and Nuclear Chemistry* **1980,** 60, (1), 141-148.

5. Charlesby, A. *Proceedings of the Royal Society of London. Series A, Mathematical and Physical Sciences* **1955,** 230, (1180), 120-135.

6. Kihara, N.; Hinoue, K.; Takata, T. *Macromoleculaes* **2005,** 38, (2), 223-226.

7. Harada, A. *Coordination Chemistry Reviews* **1996,** 148, 115-133.

8. Ooya, T.; Akutsu, M.; Kumashiro, Y.; Yui, N. *Science and Technology of Advanced Materials* **2005,** 6, 447-451.

9. Araki, J.; Ito, K. *Soft Matter* **2007,** 3, 1456-1473.

10. Choi, K. Y., Overview of Polymerization Reactor Technology. In *Handbook of Polymer Science and Technology*, Cheremisinoff, N. P., Ed. CRC Press: 1989; Vol. 1, pp 67-102.